Scaling Effects on the Hydrodynamics and Performance of Current Turbines

Hannah Ross

A dissertation
submitted in partial fulfillment of the
requirements for the degree of

Doctor of Philosophy

University of Washington

2020

Reading Committee:

Brian Polagye, Chair

Alberto Aliseda

James Riley

Program Authorized to Offer Degree:
Mechanical Engineering

University of Washington

Abstract

Scaling Effects on the Hydrodynamics and
Performance of Current Turbines

Hannah Ross

Chair of the Supervisory Committee:
Associate Professor Brian Polagye
Mechanical Engineering

The performance of a current turbine is influenced by numerous variables related to the geometry of the turbine and channel, the fluid properties, and the external forces acting on the system. These variables can be non-dimensionalized to form parameters that affect the dimensionless performance of a turbine. If these parameters are held constant between geometric scales, a smaller turbine model can exactly represent a much larger prototype. This method of testing scale models is frequently used to reduce the time and costs associated with the early stages of design. However, not all parameters can be easily matched between scales or maintained within experiments. These limitations prevent models from achieving complete similarity with full-scale prototypes and make it challenging to isolate the effects of individual parameters on turbine performance. Furthermore, the influence of certain parameters on turbine hydrodynamics and performance is not fully understood. Therefore, the aim of this work is to investigate the effects of certain scaling parameters on the hydrodynamics and performance of laboratory-scale current turbines. Three specific objectives are addressed. The first objective is to characterize the effects of the blockage ratio, Reynolds number, and Froude number on turbine performance and flow dynamics with the goals of better understanding the relative influence of these parameters and improving the quality of laboratory-scale testing. The second objective is to assess several analytical corrections

intended to account for the influence of blockage on turbine performance. A better understanding of the effectiveness of these corrections will enable data collected under confined conditions to be accurately extrapolated to other environments. The third objective is to investigate the effects of blockage on the wake of a cross-flow current turbine. Better understanding these effects will inform the design of arrays that can exploit blockage to augment turbine performance.

To characterize the effects of the blockage ratio, Reynolds number, and Froude number on turbine performance, a cross-flow current turbine was tested in a laboratory flume. The turbine's power and thrust coefficients were measured under a set of baseline operating conditions, then each parameter was increased while the others were maintained at their baseline values. We additionally measured the local channel depth directly upstream and downstream of the turbine to quantify the deformation of the free surface. We found that all three parameters significantly influenced turbine performance, with the power coefficient most sensitive to changes in the Reynolds number and least sensitive to changes in the Froude number. Furthermore, free surface deformation was affected by the Froude number but remained relatively unchanged from baseline values when the blockage ratio and Reynolds number were varied. Because all three parameters significantly affected the turbine's power and thrust coefficients, they should be carefully controlled in experiments where scale similarity is desired. In addition, further research is needed to determine the underlying fluid mechanisms that cause the observed change in turbine performance with Froude number.

Because scale models are frequently tested at relatively high blockage ratios, it is desirable to correct measured performance for blockage effects. However, there has been limited experimental validation of the analytical blockage corrections presented in the literature. This work evaluated corrections against experimental data to recommend one or more for future use. For this investigation, we tested a cross-flow turbine and an axial-flow turbine under conditions of varying blockage with other dimensionless parameters, such as the Reynolds

and Froude numbers, held approximately constant. Increasing blockage improved turbine performance, resulting in higher thrust and power coefficients over a larger range of tip-speed ratios. Of the analytical corrections evaluated, the two based on measured thrust performed best. Unexpectedly, these corrections were more effective for the cross-flow turbine than the axial-flow turbine. We attribute this result to changes in the local Reynolds number caused by increasing blockage, an effect not captured by the analytical theory. For both turbines, the corrections performed better for thrust than power, which is consistent with the assumptions that underlie the analytical theory.

The potential to increase turbine performance through the use of high blockage arrays has inspired recent interest in array design. Arrays are typically composed of multiple rows of turbines, with downstream turbines operating in the wake of upstream turbines. To inform the design of arrays, the effects of blockage on the wake of a cross-flow current turbine were evaluated. Velocity data were collected downstream of the turbine under two different blockage conditions. As before, to isolate blockage effects, other dimensionless parameters that affect turbine performance were held approximately constant. The turbine was operated at the tip-speed ratio corresponding to peak power for each blockage ratio. Increasing the blockage caused faster streamwise flow speeds through and around the turbine, a decreased overall wake size, elevated turbulent kinetic energy, and an increased viscous dissipation rate. These results suggest that higher blockage could increase the power output and reduce the physical footprint of current turbine arrays due to faster wake mixing. However, these benefits must be weighed against the potential for high blockage arrays to reduce a turbine's "basin efficiency", which is an important ecological parameter. Furthermore, we observed that decreasing the width of the experimental channel while holding the depth constant decreased the extent of the wake in the lateral direction only. The wake was unaffected in the vertical direction, which suggests that lateral and vertical blockage have independent effects on turbine wakes. Consistent with prior studies, we also observed significant wake

mixing in the vertical (i.e., spanwise) direction and negligible wake mixing in the lateral direction for both blockage conditions.

TABLE OF CONTENTS

LIST OF FIGURES

LIST OF TABLES

NOMENCLATURE

b	channel width
c	blade chord length
d	local channel depth
d_ℓ	turbine offset from lateral boundary
d_t	turbine submergence depth
d_0	channel free-stream depth
f	range of frequencies in the inertial subrange
g	acceleration of gravity
u	streamwise velocity component
u_t	streamwise velocity through the turbine rotor
u_1	streamwise velocity in the core flow
u_2	streamwise velocity in the bypass flow
v	lateral velocity component
w	vertical velocity component

A_c	channel cross-sectional area
A_r	turbine aspect ratio
A_s	support structure projected area
A_t	turbine projected area
A_1	wake cross-sectional area
ADV	acoustic Doppler velocimeter
BMSC	Bamfield Marine Sciences Centre
C_P	power coefficient
$C_\mathrm{P,blade}$	blade power coefficient
C_T	thrust coefficient
CA	confinement asymmetry
D	turbine rotor diameter
Fr	Froude number
H	turbine rotor height
N	number of blades
P	mechanical power produced by the turbine

P_{tot}	total mechanical power removed from the flow
R	turbine rotor radius
Re	chord-based Reynolds number
Re_ℓ	local Reynolds number
S	frequency spectrum in the inertial subrange
T	thrust produced by the turbine
TI	turbulence intensity
TKE	turbulent kinetic energy
UNH	University of New Hampshire
UW	University of Washington
V_0	free-stream velocity
We	Weber number
X	streamwise direction
Y	lateral direction
Z	vertical direction
α	constant scaling factor

α_{p} blade preset pitch angle

α_{t} blade twist or helix angle

β blockage ratio

β_{ℓ} lateral blockage ratio

β_{v} vertical blockage ratio

ε rate of viscous dissipation of turbulent kinetic energy per unit mass

ε_{c} channel surface roughness height

ε_{t} turbine surface roughness height

η basin efficiency

λ tip-speed ratio

μ dynamic viscosity

ν kinematic viscosity

ρ fluid density

σ solidity

σ_{s} fluid surface tension

τ torque

ω	turbine angular velocity
$\mathcal{T}$	temperature
$\square_{\mathrm{b}}$	value in bluff body theory
$\square_{\mathrm{m}}$	model scale
$\square_{\mathrm{max}}$	value at the point of theoretical maximum power
$\square_{\mathrm{p}}$	prototype scale
$\square'$	equivalent unconfined value

ACKNOWLEDGMENTS

This dissertation is the culmination of almost six years spent researching the hydrodynamics of current turbines. Throughout this time, I have been supported and encouraged by numerous people, and I own them all a massive thank you. I would especially like to acknowledge my advisor, Brian Polagye. Brian's dedication to his students and to his work is inspiring, and the willingness with which he shares his time, knowledge, and resources make him an exceptional mentor. Thank you for everything you have taught me.

I would also like to acknowledge my committee members, James Riley, Alberto Aliseda, and Alex Horner-Devine, who have answered my questions and guided my research. Their insights have pushed my work in new and interesting directions. And to John Kramlich, thank you for being my teaching mentor and role model. Furthermore, as anyone who has passed through the UW Mechanical Engineering Department knows, we would not be the same without Wanwisa Kisalang. Her positivity and ability to fix just about every problem has lifted my spirits on more than one occasion.

Finishing a Ph.D. was made much easier by the continual support of my husband, Mike West. Thank you for following me to the other side of the country, for motivating me to get outdoors and step out of my comfort zone and, most of all, for always cooking me dinner.

Adjusting to living thousands of miles from home was made much easier by my Aunt Ruth and Uncle Dale Hultengren, who welcomed us into their home when we moved to Seattle and gave us a place to live for over 2 years. Thank you to the entire Hultengren family for taking us in.

Experiments are not easily done alone, and the contributions of Ben Strom, Kate Van Ness, Dom Forbush, Noah Johnson, Carl Stringer, Corey Crisp, Aidan Hunt, Craig Hill,

Michelle Hickner, Eamon McQuaide, and Reggie Rocamora were critical in establishing the experimental infrastructure I used to complete my work. Many of these people also helped me set up for and run experiments, and I am grateful for their willingness to pitch in.

Work is made better by the company of friends, and I was lucky to find a group of friends in my co-workers at the Marine Renewable Energy Lab. Thanks to Emma Cotter for being my default adventure buddy for 5 years, to Curty Rusch for all of the skiing adventures, to Isabel Scherl for always being willing to go for a run or bake a cake, to Trevor Harrison for being a solid roommate and conversationalist, and to Ben Maurer for serving as an academic mentor and unofficial mountain bike instructor, sometimes simultaneously. And to everyone who has ventured into the mountains with me, thank you for making grad school about much more than just work.

To my best friends, Jesse Nance and Amber Kapoor, thanks for being my family in undergrad and inspiring me to work just as hard as you do.

I would also like to acknowledge several people who served as mentors early on in my academic career and helped me on my path to graduate school. Thank you to David Huddleston, Steve Anton, Gerhard Kramm, David Mascareñas, and Jaione Ortega Gómez.

Thank you to my mom, Kathryn Ross, for teaching me to always finish what I start and to my dad, Sidney Jones, for encouraging my love of math and science from a young age.

This work was supported by the National Science Foundation Graduate Research Fellowship Program and the Department of Defense Naval Facilities Engineering Command. Eric Clelland is acknowledged for his role facilitating experiments at the Bamfield Marine Sciences Centre, and Martin Wosnik and John Ahern are acknowledged for supporting experiments at the Center for Ocean Renewable Energy at the University of New Hampshire. An additional thank you goes to Martin for sharing his expertise on blockage effects and turbine dynamics. Finally, I would like to thank the Alice C. Tyler Charitable Trust for enabling significant upgrades to the experimental facilities at the University of Washington.

Chapter 1
INTRODUCTION

Concerns about the negative environmental impacts of fossil fuel emissions continue to drive research on innovative methods of power generation, including harnessing energy from moving water. The relatively young field of marine renewable energy includes tidal current, ocean current, and riverine energy. These three types of current energy employ turbines that convert the energy of flowing water into mechanical, rotational energy and, ultimately, electricity. Historically, the majority of research on turbines designed to capture the power of a moving fluid has been conducted to support the wind energy industry. Unlike wind turbines, current turbines operate in flows that are naturally confined by channel walls and a free surface. This confinement alters the dynamics of the flow around a turbine, impacting the performance of the turbine, the nature of the wake, the mechanisms of wake recovery, and the flow energetics [23, 30, 37]. These unique operating conditions must be considered to optimize current turbine designs. Therefore, although prior work in the wind energy field has informed the development of current turbines, new research is needed to support the growth of the marine energy industry [43].

1.1 Scale Model Similarity

To optimize individual turbine and array designs, explore new control schemes, and investigate environmental effects, researchers frequently use numerical and experimental models. Because numerical methods do not require the fabrication of physical models, they can more easily be used for large parameter sweeps, full-scale analysis, and array design. However, experimental models may be preferable if the dynamics of a system are too complicated to accurately model numerically. Furthermore, experimental data are essential for the valida-

tion of numerical models. Due to constraints on computational capabilities and experimental facilities, both numerical and experimental modeling is often conducted at reduced geometric scales. A scale model can exactly represent a larger prototype if certain dimensionless parameters are identical between the model and prototype [51]. Holding these parameters constant guarantees geometric and dynamic similarity between scales. Geometric similarity requires that all lengths be scaled by the same factor, and dynamic similarity indicates that relevant force ratios are constant between the model and prototype. If both geometric and dynamic similarity are achieved, velocity and acceleration ratios will be constant as well, and the pattern of streamlines in the two flows will be identical. These conditions indicate that kinematic similarity has been achieved. If geometric, dynamic, and kinematic similarity exist between a model and a prototype, the dimensionless performance of the prototype will equal the dimensionless performance of the model. For example, turbine performance is often characterized by the power coefficient (C_{P}), a dimensionless parameter defined as

$$C_{\mathrm{P}} = \frac{P}{\frac{1}{2}\rho A_{\mathrm{t}} V_0^3}, \tag{1.1}$$

where P is the mechanical power produced by the turbine, ρ is the fluid density, A_{t} is the projected area of the turbine rotor, and V_0 is the free-stream velocity. Note that $P = \tau\omega$, where τ is the measured torque and ω is the angular velocity of the turbine. If complete similarity exists between a model and prototype turbine,

$$C_{\mathrm{P,m}} = C_{\mathrm{P,p}}, \tag{1.2}$$

where the subscript 'm' denotes the model and the subscript 'p' denotes the prototype. Therefore,

$$P_{\mathrm{p}} = \frac{1}{2} C_{\mathrm{P,m}} \rho_{\mathrm{p}} A_{\mathrm{t,p}} V_{0,\mathrm{p}}^3. \tag{1.3}$$

Assuming the power coefficient of the model has been measured and the prototype fluid density, turbine area, and free-stream velocity are known, the power output of the prototype can be calculated from Equation (1.3).

1.2 Objectives

The use of scale-similar models is a powerful technique, as it allows the behavior of a full-scale system to be determined from a smaller model, reducing the time and costs associated with the early stages of design. Researchers in the marine energy field frequently use scale models of current turbines to predict the behavior of full-scale systems. However, as further detailed in Section 2.4, it can be difficult to achieve complete similarity between a model turbine and a full-scale prototype [4, 50]. Furthermore, due to physical or numerical constraints, certain dimensionless parameters are often varied within experiments [4, 15, 41, 47]. The influence of some parameters on turbine performance is not fully understood, creating uncertainty in interpreting scale model results. Therefore, the primary objective of this work is to experimentally quantify the effects of specific scaling parameters on the hydrodynamics and performance of current turbines. A better understanding of these parameters will improve the quality of model testing and inform the intentional use of scaling effects to increase turbine performance.

This work focuses on three dimensionless parameters: the blockage ratio, Reynolds number, and Froude number. A physical interpretation of these parameters and their relevance to turbine performance is detailed in Chapter 2. The methods used in our experiments are discussed in Chapter 3, and the primary objectives of this work are addressed in Chapters 4-6. Chapter 4 experimentally characterizes the effects of the blockage ratio, Reynolds number, and Froude number on the hydrodynamics and performance of a cross-flow current turbine, illustrating the importance of all three parameters. Chapter 5 assesses the effectiveness of multiple analytical models designed to correct for the effects of blockage, improving the extrapolation of model results to larger scales. Finally, Chapter 6 evaluates the effects of blockage on the wake of a current turbine, informing the use of this scaling effect to improve turbine performance.

Chapter 2
BACKGROUND

Investigating the effects of dimensionless scaling parameters on turbine performance requires knowledge of the form of these parameters. To determine relevant parameters, a Buckingham pi analysis [51] is performed in Section 2.2. This analysis requires knowledge of the geometry of the systems under consideration. Therefore, before the Buckingham pi analysis is presented, an overview of the two most common current turbine designs is given in Section 2.1.

2.1 Current Turbine Designs

Most current turbines are either an axial-flow (i.e., horizontal-axis) or cross-flow (i.e., vertical-axis) type [43]. An example of both turbine designs is given in Figure 2.1. Axial-flow turbines are characterized by blades that rotate about an axis parallel to the direction of incoming flow, and their rotors typically have circular profiles. Cross-flow turbine blades rotate about an axis perpendicular to the flow and have rotors with rectangular or elliptical profiles. The number of blades, blade geometry, and support structure configurations for both turbine types can vary significantly. Furthermore, cross-flow turbines can be oriented either vertically, with their axes of rotation perpendicular to the free surface, or horizontally, with their axes of rotation parallel to the free surface. For the Buckingham pi analysis conducted in Section 2.2, a vertical orientation is considered.

2.2 Buckingham Pi Analysis

When analyzing current turbine designs, researchers are often interested in power output and structural loading, particularly thrust (T) in the streamwise direction. Ideally, all di-

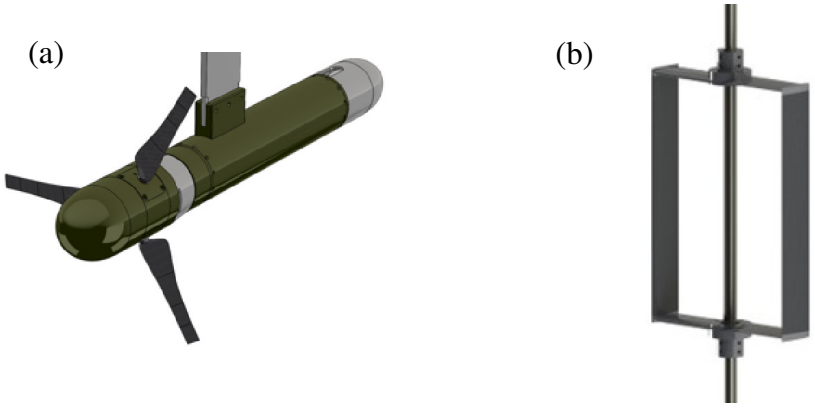

Figure 2.1: Illustrations of an axial-flow (a) and cross-flow (b) turbine. The axial-flow turbine illustration is courtesy of Justin Burnett.

mensionless parameters that affect P and T are held constant within individual experiments and between a model and full-scale prototype. To determine the parameters relevant to current turbine performance, a Buckingham pi analysis [51] is conducted. The first step in this analysis involves listing all of the relevant variables and their units, expressed in reference dimensions (i.e., mass [M], length [L], and time [T]). Current turbines operate in channels, and the channel boundaries can affect performance [30]. Therefore, the Buckingham pi analysis must include the geometry of both the turbine and channel. Although experimental water tunnels can have circular cross-sections, most water tunnels, flumes, tow tanks, and natural channels are rectangular in aspect. This analysis considers an open channel flow with a rectangular cross-section. Because the flow is assumed to have a free surface, the effects of gravity and surface tension must be considered as well. Variables relevant to the Buckingham pi analysis are listed in Table 2.1. These variables apply to both cross-flow and axial-flow turbines, although the height of an axial-flow turbine rotor is equal to its diameter. This list is not necessarily exhaustive but attempts to capture the primary geometric, material, and external variables that can affect the power and thrust of a turbine. Several of these variables are illustrated visually for both a cross-flow turbine and an axial-flow turbine in

Variable	**Description**	**Dimension**
D	turbine rotor diameter	L
H	turbine rotor height (i.e., blade span)	L
c	blade chord length	L
α_{p}	blade preset pitch angle	-
α_{t}	blade twist or helix angle	-
-	blade section profile	-
-	support structure configuration	-
N	number of blades	-
b	channel width	L
d_0	channel free-stream depth	L
d_{t}	turbine submergence depth	L
d_ℓ	turbine offset from lateral boundary	L
ε_{t}	blade surface roughness height	L
ε_{c}	channel surface roughness height	L
ρ	fluid density	ML^{-3}
μ	fluid dynamic viscosity	$\mathrm{ML}^{-1}\mathrm{T}^{-1}$
σ_{s}	fluid surface tension	MT^{-2}
V_0	free-stream velocity	LT^{-1}
TI	turbulence intensity	-
ω	turbine angular velocity	T^{-1}
g	acceleration of gravity	LT^{-2}

Table 2.1: Geometric, material, and external variables that can affect the power and thrust of a turbine.

Figures 2.2 and 2.3.

The second step in the Buckingham pi analysis involves selecting a set of "repeating" variables that are used to non-dimensionalize the remaining variables. The number of repeating variables is equal to the number of reference dimensions used. In this case, mass, length, and time are all used, so three repeating variables are selected. The repeating variables must collectively include all reference dimensions and be dimensionally independent, i.e., one repeating variable cannot be made dimensionless using the other two. Therefore, the variables D, V_0, and ρ are selected. The remaining variables, including P and T, are non-dimensionalized by D, V_0, and ρ, yielding a set of dimensionless "pi terms". The pi terms are not unique and can multiplied with each other or scaled by constants to yield parameters that are more physically meaningful. The pi terms resulting from this analysis are listed in Table 2.2. The dependent pi terms are the dimensionless power and thrust coefficients, and the independent terms are the dimensionless parameters that affect power and thrust. The turbine radius (R), defined as

$$R = \frac{D}{2} \tag{2.1}$$

and fluid kinematic viscosity (ν), defined as

$$\nu = \frac{\mu}{\rho} \tag{2.2}$$

are used in Table 2.2 for convenience. Note that ν is a function of fluid temperature ($\mathcal{T}$).

2.3 Relevant Dimensionless Parameters

The Buckingham pi analysis indicates that the parameters listed in Table 2.2 should be held constant between scales for a model to accurately represent a prototype. However, if certain parameters are "large" (or "small") enough at both scales, changes in these parameters can have insignificant effects, and their influence on turbine performance can be neglected. For the work considered herein, we assume that the dimensionless roughness heights remain approximately constant, and these parameters can be neglected. Furthermore, at the scales

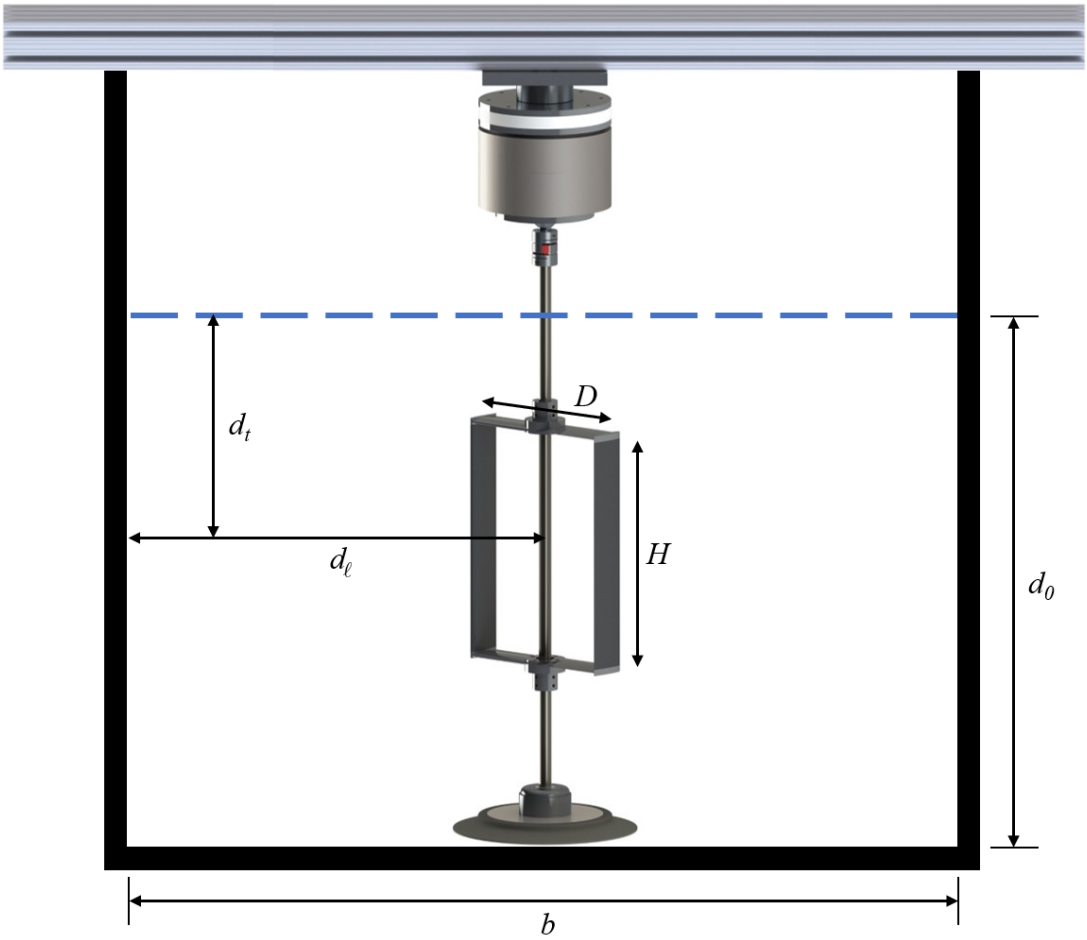

Figure 2.2: Dimensional variables related to the geometry of a cross-flow turbine and channel. The blue dashed line indicates the free surface of the flow.

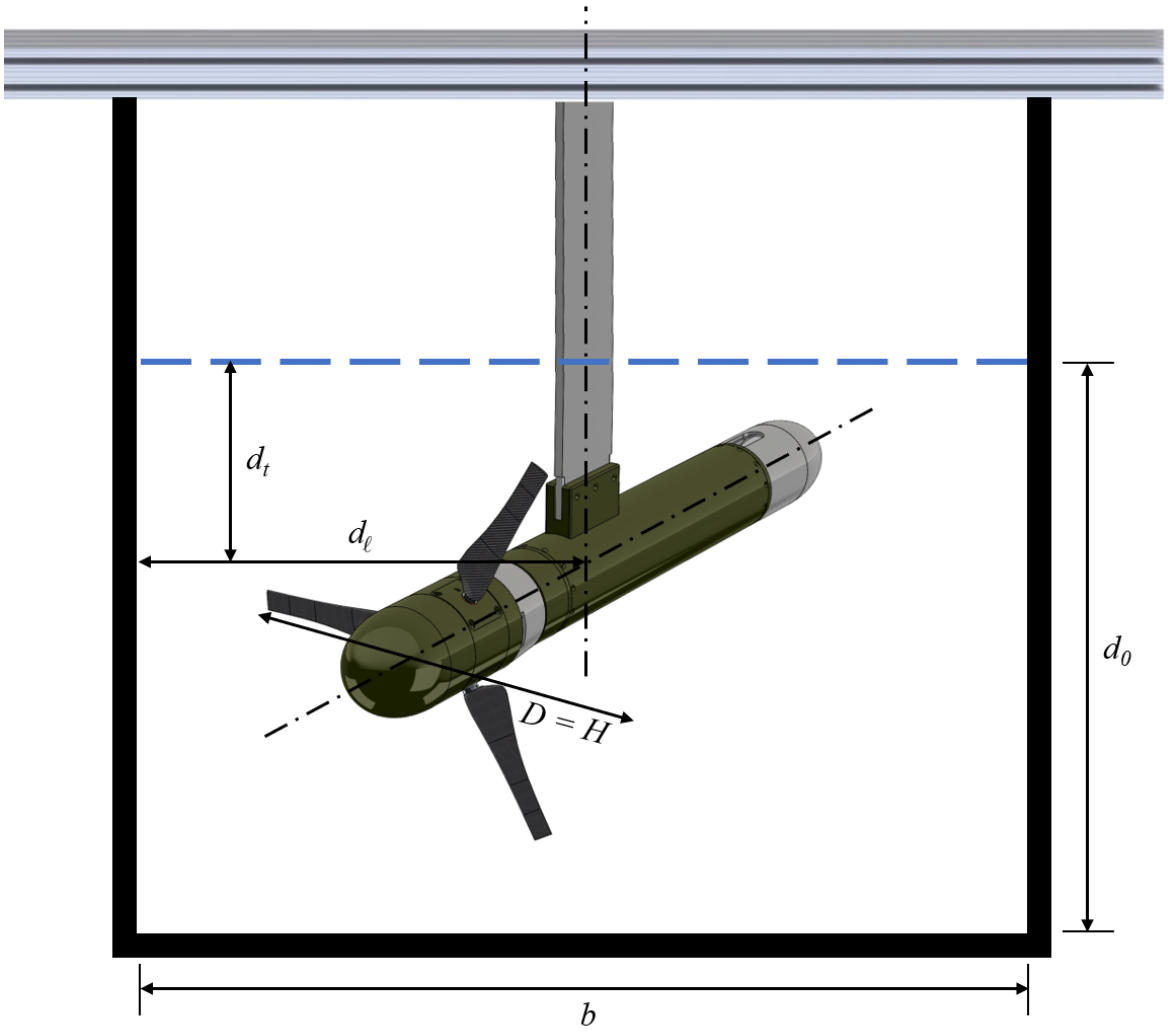

Figure 2.3: Dimensional variables related to the geometry of an axial-flow turbine and channel. The blue dashed line indicates the free surface of the flow.

Pi Term	**Symbol**	**Description**
$\frac{\tau\omega}{\frac{1}{2}\rho A_\mathrm{t} V_0^3}$	C_P	power coefficient
$\frac{T}{\frac{1}{2}\rho A_\mathrm{t} V_0^2}$	C_T	thrust coefficient
$\frac{H}{D}$	A_r	turbine aspect ratio
$\frac{c}{R}$	-	chord-to-radius ratio
α_p	-	blade preset pitch angle
α_t	-	blade twist or helix angle
-	-	blade profile
-	-	support structure configuration
$\frac{Nc}{2\pi R}$	σ	solidity
$\frac{D}{b}$	β_ℓ	lateral blockage ratio
$\frac{H}{d_0}$	β_v	vertical blockage ratio
$\frac{d_\mathrm{t}}{d_0}$	-	dimensionless submergence depth
$\frac{d_\ell}{b}$	-	dimensionless lateral offset
$\frac{\varepsilon_\mathrm{t}}{c}$	-	dimensionless turbine roughness height
$\frac{\varepsilon_\mathrm{c}}{d_0}$	-	dimensionless channel roughness height
$\frac{V_0 c}{\nu}$	Re	chord-based Reynolds number
$\frac{\rho V_0^2 d_0}{\sigma_\mathrm{s}}$	We	Weber number
TI	-	turbulence intensity
$\frac{\omega R}{V_0}$	λ	tip-speed ratio
$\frac{V_0}{\sqrt{g d_0}}$	Fr	Froude number

Table 2.2: Dimensionless parameters relevant to the power output and thrust of a current turbine.

considered in this work, it is expected that the fluid's surface tension will be small relative to its inertia and, therefore, the Weber number can be neglected as well. Many of the parameters listed in Table 2.2 are related to turbine geometry. Specifically, the aspect ratio, chord-to-radius ratio, blade preset pitch angle, blade twist or helix angle, blade profile, support structure configuration, and solidity involve only turbine geometric variables. The effects of these parameters on turbine performance have been investigated in the archival literature [12, 20, 27, 28, 39, 57, 61, 68, 74, 75]. Although geometric optimization remains an active area of research [73], these parameters are not the focus of this body of work. For the studies described herein, the turbine geometry is either held constant, or changes in geometric parameters are shown to have a negligible effect on turbine performance.

All other pi terms involve fluid and channel properties in addition to turbine geometry. Consistent with the definition of turbulent kinetic energy, the turbulence intensity is defined as

$$\mathrm{TI} = \frac{\sqrt{\frac{1}{3}[(u - \langle u \rangle)^2 + (v - \langle v \rangle)^2 + (w - \langle w \rangle)^2]}}{\langle \sqrt{u^2 + v^2 + w^2} \rangle}, \tag{2.3}$$

where u, v, and w are the streamwise, lateral, and vertical velocity components, respectively, and the angle brackets represent a time average. The turbulence intensity represents the strength of turbulent fluctuations relative to the magnitude of the mean flow and has been shown to affect turbine performance [16, 53]. Therefore, turbulence intensity is held approximately constant in this work. The dimensionless submergence depth and lateral offset are related to the effects of boundary proximity, which is a topic of potential future work and is beyond the scope of the experiments presented herein. Boundary proximity is discussed further in Appendix A. The turbine tip-speed ratio represents the blade tangential velocity relative to the free-stream velocity. Tip-speed ratio has a significant impact on the power and thrust coefficients. Typically, C_P and C_T are characterized over a range of tip-speed ratios.

The remaining dimensionless parameters are the lateral and vertical blockage ratios, the Reynolds number, and the Froude number. The blockage ratios represent the relative size of

the turbine and channel cross-sections in the lateral and vertical directions. Higher blockage ratios indicate the flow is more confined around the turbine, which can affect performance [23, 30, 34, 37, 70]. If the lateral and vertical blockage ratios are unequal, flow confinement is asymmetric. Kinsey and Dumas [40] defined the confinement asymmetry (CA) as

$$\mathrm{CA} = \max\left(\frac{\beta_\ell}{\beta_\mathrm{v}}, \frac{\beta_\mathrm{v}}{\beta_\ell}\right). \tag{2.4}$$

They concluded that a confinement asymmetry exceeding unity affects turbine performance, relative to a turbine operating with symmetric confinement at the same overall blockage ratio (β), defined as

$$\beta = \beta_\ell \beta_\mathrm{v} = \left(\frac{D}{b}\right)\left(\frac{H}{d_0}\right) = \frac{A_\mathrm{t}}{A_\mathrm{c}}, \tag{2.5}$$

where A_c is the cross-sectional area of the channel. However, they also found that the effects of confinement asymmetry are negligible for $\mathrm{CA} < 3$. Since $\mathrm{CA} < 3$ in all of our experiments, we consider only the overall blockage ratio, and the subtly of confinement asymmetry is largely left as a topic of potential future work.

These assumptions and simplifications reduce the list of dimensionless parameters to the blockage ratio, Reynolds number, and Froude number. The blockage ratio denotes the projected area of the turbine relative to the channel cross-sectional area, the Reynolds number represents the ratio of inertial to viscous forces in a fluid, and the Froude number, which is only relevant to flows with a free surface, gives the ratio of inertial to gravitational forces in a fluid. As discussed in Section 1.2, the blockage ratio, Reynolds number, and Froude number are the primary dimensionless parameters considered in this work.

2.4 Limitations of Scale Models

To achieve complete similarity, all relevant dimensionless parameters must be held constant between a model and full-scale prototype. However, for current turbines, it is difficult to match the full-scale values of all parameters using a geometrically smaller model. The Reynolds number is particularly challenging to maintain. Specifically, if kinematic viscosity is held constant, the test velocity for a model is inversely proportional to the geometric

scale (e.g., at a 10:1 geometric scale, an experimental facility would require a 20 m/s inflow velocity to match the Reynolds number of a full-scale prototype in 2 m/s flow). Such velocities are practically impossible to achieve in experimental facilities. As a result of these limitations, testing of current turbine models often occurs at reduced Reynolds numbers [4]. Typically, model Reynolds numbers are below the threshold where turbine performance can be considered independent of Reynolds number [4, 50]. Therefore, changes in the Reynolds number will affect model results.

Limitations on the size of experimental facilities also prevent model testing from occurring at full-scale blockage ratios. Blockage ratio matching is best achieved with smaller models. However, reducing model scale compounds the difficulty of matching Reynolds number. These conflicting requirements often result in models that match neither the Reynolds number nor the blockage ratio of the full-scale system. These limitations highlight the need to better understand the effects of these parameters on turbine performance to more accurately extrapolate model results to larger scales.

In addition to holding relevant dimensionless parameters constant between scales, these parameters should be maintained within experiments that investigate the effects of changing dimensionless turbine geometry. However, this can be difficult to achieve. For example, an experiment investigating the effects of changing the turbine aspect ratio requires varying either the diameter or height of the rotor, which affects the blockage ratio. To maintain a constant blockage ratio, the channel width or depth must change. Most flumes and tow tanks are a fixed width, but the depth can vary. However, changing the channel depth alters the Froude number, so the free-stream velocity must be adjusted accordingly. Changing the free-stream velocity impacts the Reynolds number. This can be compensated for by adjusting the water temperature, which varies its viscosity. Although this makes for a complicated experimental procedure, failing to hold the blockage ratio, Reynolds number, and Froude number constant will alter the results of the experiment [39], making it challenging to differentiate performance effects caused by the aspect ratio from the performance effects of other parameters. Furthermore, as detailed in Section 4.1, changing either the blockage

ratio, Reynolds number, or Froude number can inadvertently impact the other parameters, producing a hybrid effect. The difficulty of holding these parameters constant within experiments reinforces the importance of understanding their influence on turbine performance in order to inform the design of better experiments.

Chapter 3

METHODS

Common materials and methods used in this body of work are detailed in this chapter. Methods unique to a specific experiment are described in the chapter dedicated to that experiment. Details of the experimental turbines, test rigs, facilities, performance characterization methods, and wake measurement techniques are included here.

3.1 Turbines and Test Rigs

The experiments described in this work employed a total of three laboratory-scale turbines: two cross-flow turbines and an axial-flow turbine. Renderings of the turbines and test rigs are shown in Figure 3.1. The cross-flow turbine shown in Figure 3.1 (a) has two straight blades connected to a central shaft by thin struts. The aluminum blades and struts are NACA 0018 and NACA 0008 airfoils, respectively, with a chord length of 0.0405 m. The blades are mounted with a 6° preset pitch angle. The turbine has a diameter of 0.1720 m and a variable height that ranges between 0.1638 m and 0.2340 m. During testing, the turbine's rotational speed was regulated by a servomotor (Yaskawa SGMCS-05B3C41) equipped with a 2^{18} count rotary encoder. Two six-axis load cells mounted above and below the rotor (ATI Industrial Automation Mini45 and Mini40) measured the forces and torque. The top load cell was separated from the servomotor by ceramic stand-offs to minimize thermal drift in the cell. The free-stream velocity was measured $5D$ upstream of the turbine's axis of rotation with an acoustic Doppler velocimeter (ADV, Nortek Vector). Both the turbine and ADV measurement volumes were centered laterally and vertically in the channel. The water temperature was monitored with a submersible temperature probe (NovaLynx 270-WQ101). All instruments were sampled at a frequency of 1 kHz, with the exception of the ADV, which

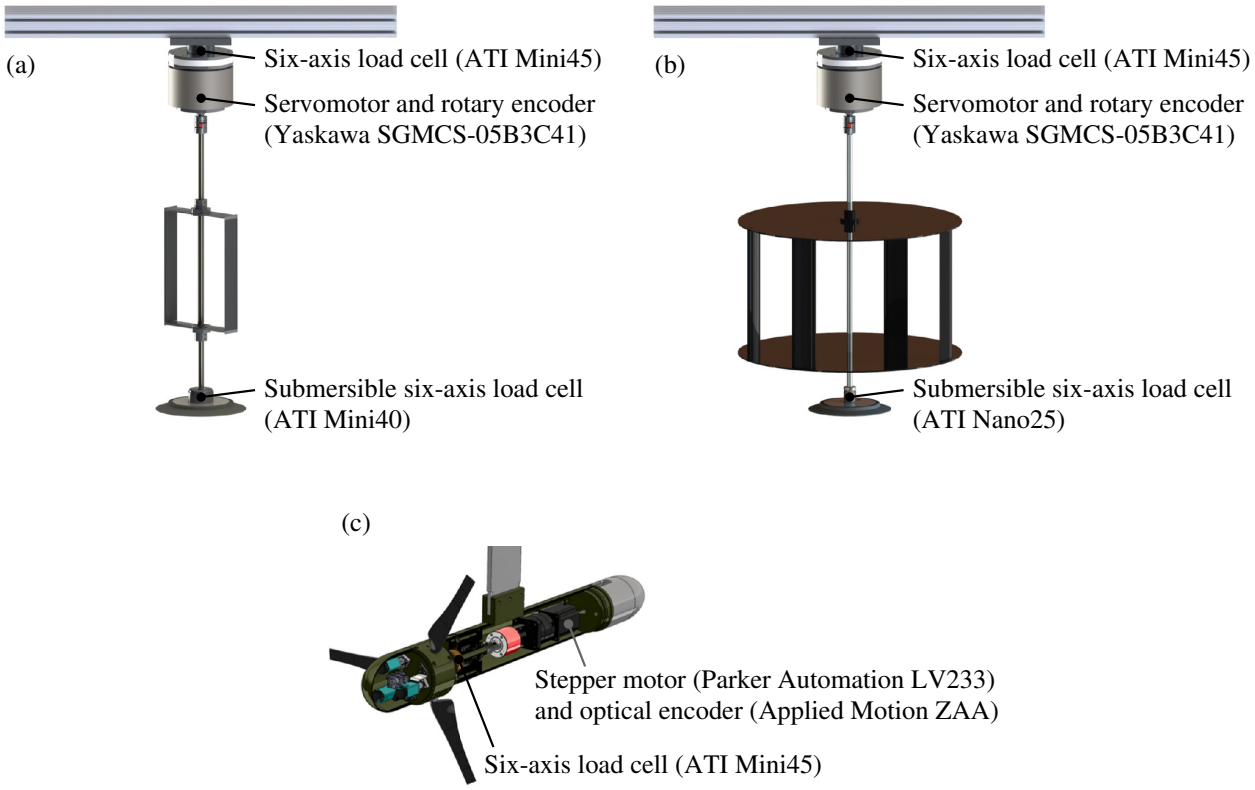

Figure 3.1: Renderings of the cross-flow (a, b) and axial-flow (c) turbines used in this work. The axial-flow turbine rendering is courtesy of Justin Burnett.

was sampled at 64 Hz. Custom scripts implemented in Matlab and Simulink (Mathworks) were used to control the instruments and collect data.

The cross-flow turbine shown in Figure 3.1 (b) was designed primarily to produce a substantial blockage ratio and is not an optimized design. The turbine has four straight blades with NACA 0018 profiles mounted to two circular end plates. The aluminum blades have a chord length of 0.06 m and a 0° preset pitch angle. The turbine has a diameter of 0.51 m and a height of 0.31 m. The test setup is similar to that used by the two-bladed cross-flow turbine, except the bottom load cell is an ATI Industrial Automation Nano25 rather than a Mini40. For some experiments using this turbine, flume dimensions precluded mounting the ADV $5D$ upstream of the turbine's axis of rotation, and the ADV was mounted $3D$ upstream instead.

The axial-flow turbine shown in Figure 3.1 (c) has three variable-pitch NACA 44xx aluminum blades, a rotor diameter of 0.45 m, and a hub diameter of 0.11 m. The blades were fixed at a pitch angle of 0°. A six-axis load cell (ATI Industrial Automation Mini45) mounted between the drive shaft and hub was used to measure the forces and torque. The speed of the rotor was regulated by a stepper motor (Parker Automation LV233), and the rotor position was measured with an optical encoder (Applied Motion ZAA). Turbine performance data were collected at approximately 50 Hz. The free-stream velocity was measured with an ADV (Nortek Vector) located $3D$ upstream of the rotor plane and sampled at a frequency of 64 Hz. The turbine and ADV measurement volumes were centered laterally between the channel walls and vertically in the dynamic water column. Custom Matlab scripts were used for data acquisition. Further information about the turbine blade geometry is given by Barber et al. [7].

3.2 Experimental Facilities

Experiments were conducted in three different testing facilities: the Alice C. Tyler flume in the Harris Hydraulics Laboratory at the University of Washington (UW), the flume in the Fluid Dynamics Laboratory at the Bamfield Marine Sciences Centre (BMSC), and the tow

tank at the Jere A. Chase Ocean Engineering Laboratory at the University of New Hampshire (UNH). The UW flume has a rectangular test section that is 0.76 m wide and 3.7 m long with a maximum fill depth of 0.60 m. Two variable-frequency pumps operating in parallel can achieve a range of free-stream velocities, with a maximum flow speed of approximately 1.0 m/s at a fill depth of 0.60 m. A pool heater and chiller enable the water temperature to be controlled to within ±0.1°C of a target. The turbulence intensity is between approximately 2 and 4% under most operating conditions.

The BMSC flume is 2.0 m wide and 12 m long with a maximum fill depth of 1.0 m. The flow is driven by four pumps operating in parallel. One of the pumps is connected to a variable-frequency drive, so a range of flow speeds can be achieved. This flume has a maximum free-stream velocity of approximately 0.7 m/s at a fill depth of 0.60 m. A chiller connected to the BMSC flume allows the water temperature to be controlled to within ±0.5°C of a target. The turbulence intensity varies between approximately 3 and 5% depending on the specific operating conditions.

The UNH tow tank is roughly 3.7 m wide, 36 m long, and 2.4 m deep. Turbines are mounted below a carriage that travels the length of the tank. Tow speeds above 1.0 m/s can be achieved, depending on the size of the turbine. The water is room temperature, between 20 and 22°C. The turbulence intensity is approximately 0%. Further details about the UNH facility are provided by Bachant and Wosnik [3].

3.3 Performance Characterization

Turbine performance was characterized by quantifying the power and thrust coefficients over the range of tip-speed ratios that produced net power. Desired tip-speed ratios were achieved by controlling the angular velocity of the turbine while maintaining an approximately constant free-stream velocity. Under this type of control, the measured torque was equal to the hydrodynamic torque produced by the rotor [59]. At each nominal operating point (i.e., tip-speed ratio), performance data were collected for at least 30 seconds, and the time series were trimmed to yield an integer number of turbine rotations. To calculate C_P, C_T, and λ

according to the equations presented in Table 2.2, instantaneous values of $\tau\omega$, T, and ω were averaged over each complete turbine rotation. Instantaneous values of V_0, V_0^2, and V_0^3 were averaged over the entire sampling period for each operating point. The free-stream measurements were averaged in this way to minimize uncertainty introduced by the convection of turbulence from the sampling location to the rotor plane and by asynchronous acquisition. These averaging methods produced a set of cycle-average performance coefficients and tip-speed ratios for every nominal operating point. The median of each set of cycle-average values was taken as the representative C_P, C_T, or λ, and the interquartile range was taken to be representative of the uncertainty.

3.4 Wake Measurement

Several of the experiments involved collecting data in the wake of the turbines. Three-dimensional velocity data were collected downstream of these turbines using a pair of ADVs (Nortek Vectrinos). The ADVs have a sampling rate of 100 Hz and were mounted on a motorized gantry with three degrees of freedom. A picture of the gantry operating in the UW flume is given in Figure 3.2. For every experiment that involved collecting wake data, the gantry was mounted on the flume and aligned such that its axes traversed the streamwise (X), lateral (Y), and vertical (Z) directions. The gantry followed a predefined grid and paused at each specified location to collect data for 30 s.

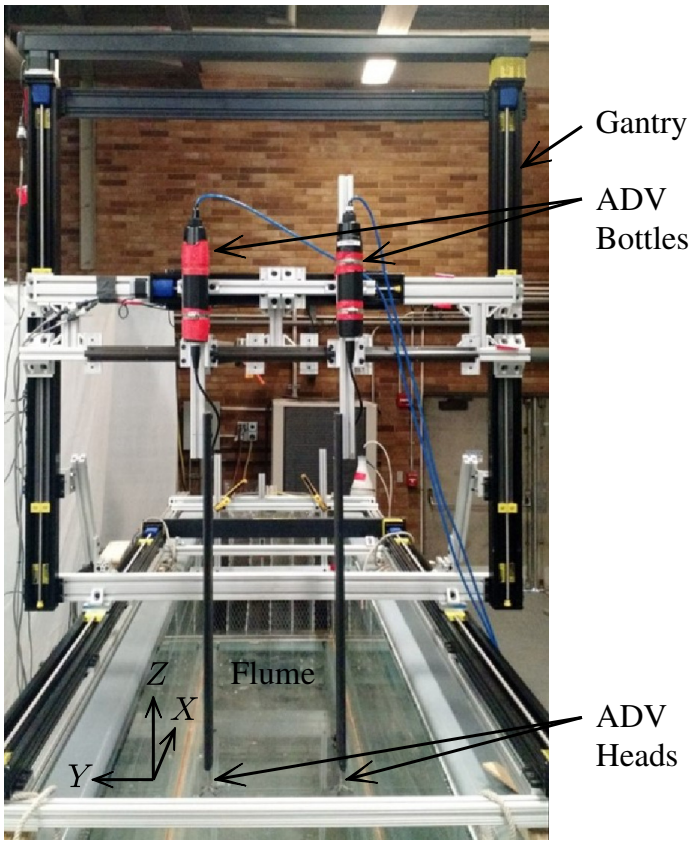

Figure 3.2: Two Nortek Vectrino ADVs mounted on a motorized gantry at the UW flume. The gantry has three degrees of freedom and was used to move the ADVs to specific measurement locations in the wake.

Chapter 4

BLOCKAGE, REYNOLDS, AND FROUDE EFFECTS ON PERFORMANCE

This chapter contains content from Ross and Polagye [63], which is in preparation. The objective of this chapter is to compare the effects of the blockage ratio, Reynolds number, and Froude number on the performance of a cross-flow current turbine to illustrate the importance of controlling these parameters within experiments.

4.1 Introduction

As discussed in Sections 1.2 and 2.4, the blockage ratio, Reynolds number, and Froude number all affect turbine performance, but achieving full-scale values of these parameters at reduced geometric scales can be challenging. Furthermore, because they are derived from common dimensional variables, changing one parameter can affect the others, making it difficult to hold them all constant within experiments. Prior studies have demonstrated the challenge of isolating blockage, Reynolds, and Froude effects from one another. An experimental study conducted by Birjandi et al. [15] investigated the influence of blockage and free surface proximity on cross-flow turbine performance in a laboratory flume. The experimental procedure consisted of incrementally decreasing the channel depth. The authors concluded that, as long as the turbine remained fully submerged, decreasing the channel depth improved its performance. They attributed the performance increase to blockage effects and free surface proximity. However, reducing the channel depth convolves blockage and Froude effects if no other variables are adjusted (i.e., both parameters increase). Therefore, it is not possible to differentiate the relative impacts of the blockage ratio and Froude number on turbine performance from these results. A similar numerical study by Kolekar

and Banerjee [41] varied channel depth to investigate the effects of blockage on a turbine's performance. The authors attributed improved performance to an increased blockage ratio but did not consider attendant changes in Froude number. The authors also investigated Reynolds effects. The Reynolds number was varied by increasing the free-stream velocity, and the authors concluded that the turbine became independent of the Reynolds number above a certain inflow speed. However, changes in the free-stream velocity also affect the Froude number, and a failure to consider Froude effects could lead to incorrect conclusions about when the turbine reached Reynolds independence. Other prior studies have similarly convolved blockage and Froude effects by varying only the channel depth [47] or Reynolds and Froude effects by varying only the free-stream velocity [4, 47]. Bachant and Wosnik [4] acknowledged that both the Reynolds and Froude numbers changed in their study but assumed that Froude effects were negligible. Although the blockage ratio, Reynolds number, and Froude number are often varied simultaneously, the significance of each parameter in determining a turbine's performance is not fully understood [4]. Past work has evaluated the effects of blockage [23, 30, 34, 37, 70], Reynolds number [4, 50], and Froude number [23, 37] on turbine performance, but to our knowledge no prior studies have isolated each parameter and assessed its effects relative to the others. Therefore, the objective of the work described in this chapter is to systematically vary the blockage ratio, Reynolds number, and Froude number of a model cross-flow current turbine and evaluate the impact of each parameter on turbine performance and flow dynamics. In addition to quantifying the relative importance of each parameter, a better understanding of these effects should improve the fidelity of laboratory-scale current turbine testing.

4.2 Methods

To evaluate and compare the effects of the blockage ratio, Reynolds number, and Froude number on turbine performance and flow dynamics, a laboratory-scale cross-flow turbine was tested in an experimental flume. The turbine's performance was characterized with a set of baseline parameters. Blockage ratio, Reynolds number, and Froude number were

then independently increased, and the performance was characterized again. Free surface deformation was measured upstream and downstream of the turbine to assess the impact of each parameter on flow dynamics. Details of the experimental procedure, performance characterization, and flow characterization are given in Sections 4.2.1-4.2.3.

4.2.1 Experimental Procedure

These experiments utilized the turbine and test rig illustrated in Figure 3.1 (a). Experiments were conducted in the UW flume, described in Section 3.2. Baseline performance was first characterized at a relatively low blockage ratio, Reynolds number, and Froude number. Subsequent experiments varied only one of these parameters, and the others were maintained at their baseline values by adjusting dimensional variables. The blockage ratio, Reynolds number, and Froude number were controlled by simultaneously varying the rotor height, free-stream velocity, channel depth, and fluid kinematic viscosity which, as mentioned in Section 2.2, is a function of temperature. Varying the rotor height and channel depth controlled the blockage ratio, varying the channel depth and free-stream velocity controlled the Froude number, and varying the free-stream velocity and water temperature controlled the Reynolds number. The experiments were conducted using an iterative approach, where the blockage ratio, Reynolds number, and Froude number were varied incrementally until the peak power coefficients approximately matched across all three cases, allowing the turbine's relative sensitivity to each parameter to be quantified. The values of H, V_0, d_0, and $\mathcal{T}$ for each final case, and the resulting values of β, Re, and Fr, are given in Table 4.1. Notably, the Reynolds number was increased from 29,000 to 35,000 by varying the temperature of the water less than 10°C with all others variables held constant. This illustrates the sensitivity of the Reynolds number to changes in water temperature and the importance of controlling this variable in experiments. This topic is discussed further in Appendix B.

Because the rotor diameter was not varied, changing its height affected the aspect ratio of the turbine in addition to the blockage ratio. However, concurrent work has shown that varying the aspect ratio within the range tested here does not affect performance, at least

	H (m)	V_0 (m/s)	d_0 (m)	$\mathcal{T}$ (°C)	β	Re	Fr
Baseline	0.2106	0.60	0.60	27.9	0.080	29,000	0.25
Blockage	0.2340	0.52	0.45	34.9	0.117	29,000	0.25
Reynolds	0.2106	0.60	0.60	37.5	0.080	35,000	0.25
Froude	0.1638	0.84	0.47	13.2	0.079	29,000	0.39

Table 4.1: Dimensional variables and dimensionless parameters for the baseline and variable blockage ratio, Reynolds number, and Froude number test cases.

for this specific turbine geometry and support structure configuration [39]. Changing the free-stream velocity and channel depth can also affect the turbulence intensity of the flow, which has been shown to impact turbine performance [16, 53]. For the tests conducted in this study, the turbulence intensity varied only slightly, between 2.3 and 4.4%. Therefore, we believe that variations in turbulence intensity had a negligible effect on observed turbine performance.

4.2.2 Performance Characterization

The turbine's power and thrust coefficients were measured at each of the operating conditions detailed in Table 4.1. For each case, turbine performance was characterized over the range of tip-speed speed ratios that produced net power according to the process described in Section 3.3. For these experiments, data were collected for 60 s at each tip-speed ratio.

As illustrated by Bachant et al. [5] and Strom et al. [75], drag on the rotating components of a turbine's support structure can significantly degrade its performance. To determine if the performance effects caused by the blockage ratio, Reynolds number, and Froude number were primarily a result of increased lift on the blades or decreased drag on the support structure, the turbine was tested with blades removed at each of the operating conditions detailed in Table 4.1. Performance curves for the bladeless turbine were calculated as described

in Section 3.3, using the median of the cycle-average values at each tip-speed ratio. The resulting $C_{\mathrm{P}}(\lambda)$ curves were subtracted from the $C_{\mathrm{P}}(\lambda)$ curves of the full turbine, yielding the blade performance. Due to small fluctuations in the free-stream flow, actual tip-speed ratios varied from the nominal values. Therefore, the full turbine and support structure performance curves were collected at slightly different tip-speed ratios. To directly subtract the support structure C_{P} from the full turbine C_{P}, both sets of curves were interpolated at set tip-speed ratios within the original measurement range using a piecewise cubic polynomial interpolator.

4.2.3 Flow Characterization

To characterize the influence of the blockage ratio, Reynolds number, and Froude number on flow dynamics, the free surface deformation was measured using an array of four acoustic free surface transducers (Omega LVU30). The transducers were mounted above the free surface and centered between the channel walls, such that they were aligned laterally with the turbine. Transducers were mounted $2D$ upstream, $1D$ upstream, $1D$ downstream, and $2D$ downstream of the turbine. An additional transducer was placed $7D$ upstream of the turbine to record the reference free-stream depth. Figure 4.1 gives a top view of this layout, including the turbine swept area and free surface transducer locations, which are denoted by red 'x' markers. The ADV location is marked with a blue circle. The transducers sampled at a rate of 10 Hz, and the data were upsampled to match the 1 kHz sampling frequency of the rest of the instruments. Raw time series were cleaned by discarding samples with a target strength less than 100% and despiked using a thresholding method and the algorithm of Goring and Nikora [33]. Removed points were replaced with nearest neighbor interpolation. The transducers measured the distance from the instrument face to the free surface. Therefore, the channel depth was calculated by subtracting the transducer measurements from the total distance between the instrument face and the bottom of the channel. Similar to the turbine performance data, instantaneous values were averaged over each complete turbine rotation, yielding a set of cycle-average values at each tip-speed ratio. The median of each set was taken

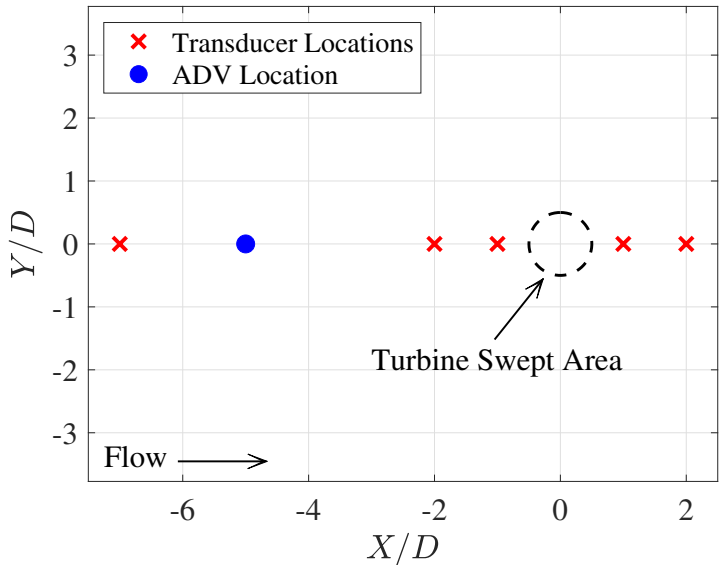

Figure 4.1: Top view of the turbine swept area, free surface transducer mounting locations denoted by red 'x' markers, and ADV location marked by a blue circle.

as the local channel depth (d), and the interquartile range was taken as the uncertainty. As detailed in Table 4.1, the free-stream channel depth varied between experiments. Therefore, to compare the free surface deformation between cases, the local channel depth at each measurement location was normalized by the time average of the free-stream channel depth at each tip-speed ratio.

4.3 Results

The effects of increasing the blockage ratio, Reynolds number, and Froude number on turbine performance are illustrated in Figures 4.2 and 4.3. The power coefficient for each case is plotted as a function of tip-speed ratio in Figure 4.2, and the thrust coefficients are plotted in Figure 4.3. All four cases are initially compared, then the effects of the blockage ratio, Reynolds number, and Froude number are shown individually. The shading indicates the interquartile range (i.e., measurement uncertainty) at each tip-speed ratio. All three

parameters increased the turbine's power coefficient over the majority of its operating range, although each parameter changed the shape of the $C_{\mathrm{P}}(\lambda)$ curve in a different way. The parameters had a similar effect on the turbine's thrust coefficient.

Figure 4.4 presents another way to visualize the effects of these parameters on turbine performance. Figure 4.4 (a) gives the difference between the $C_{\mathrm{P}}(\lambda)$ curves for the blockage, Reynolds, and Froude cases and the baseline case. Figure 4.4 (b) presents analogous results for the $C_{\mathrm{T}}(\lambda)$ curves. The dashed line on each plot indicates the tip-speed ratio corresponding to the peak power coefficient of the baseline case, and the solid line emphasizes the point of zero C_{P} or C_{T}. This figure clearly illustrates that the three parameters affected the turbine's performance differently over the range of tip-speed ratios tested.

The operating conditions outlined in Table 4.1 were intentionally chosen, through iteration, such that the peak power coefficients for the blockage, Reynolds, and Froude cases would be approximately equal (Figure 4.2 (a)). This allowed the turbine's relative sensitivity to changes in each parameter to be evaluated. The peak C_{P} of the blockage case increased by 14.3% from the peak C_{P} of the baseline case. The Reynolds and Froude cases increased by 14.0% and 12.2%, respectively. To achieve this, the blockage ratio was increased by 38.4%, the Reynolds number by 21.2%, and the Froude number by 58.9%, indicating that the turbine's performance was most sensitive to changes in the Reynolds number and least sensitive to changes in the Froude number. Further discussions of the specific effects of each parameter are presented in Sections 4.4.1 - 4.4.3.

The relative influence of the support structure on turbine performance is illustrated in Figure 4.5, which presents the power coefficient as a function of tip-speed ratio for the full turbine and blade-only cases. The $C_{\mathrm{P}}(\lambda)$ curves shown in Figure 4.5 (a) are identical to those presented in Figure 4.2 (a) and are shown for comparison. As concluded by Strom et al. [75], drag on rotating support structure components decreases a turbine's performance. Therefore, the blade-only performance is elevated relative to the full turbine. The peaks of the blockage, Reynolds, and Froude curves are offset by a similar amount relative to the baseline case for both the full turbine and blade-only experiments.

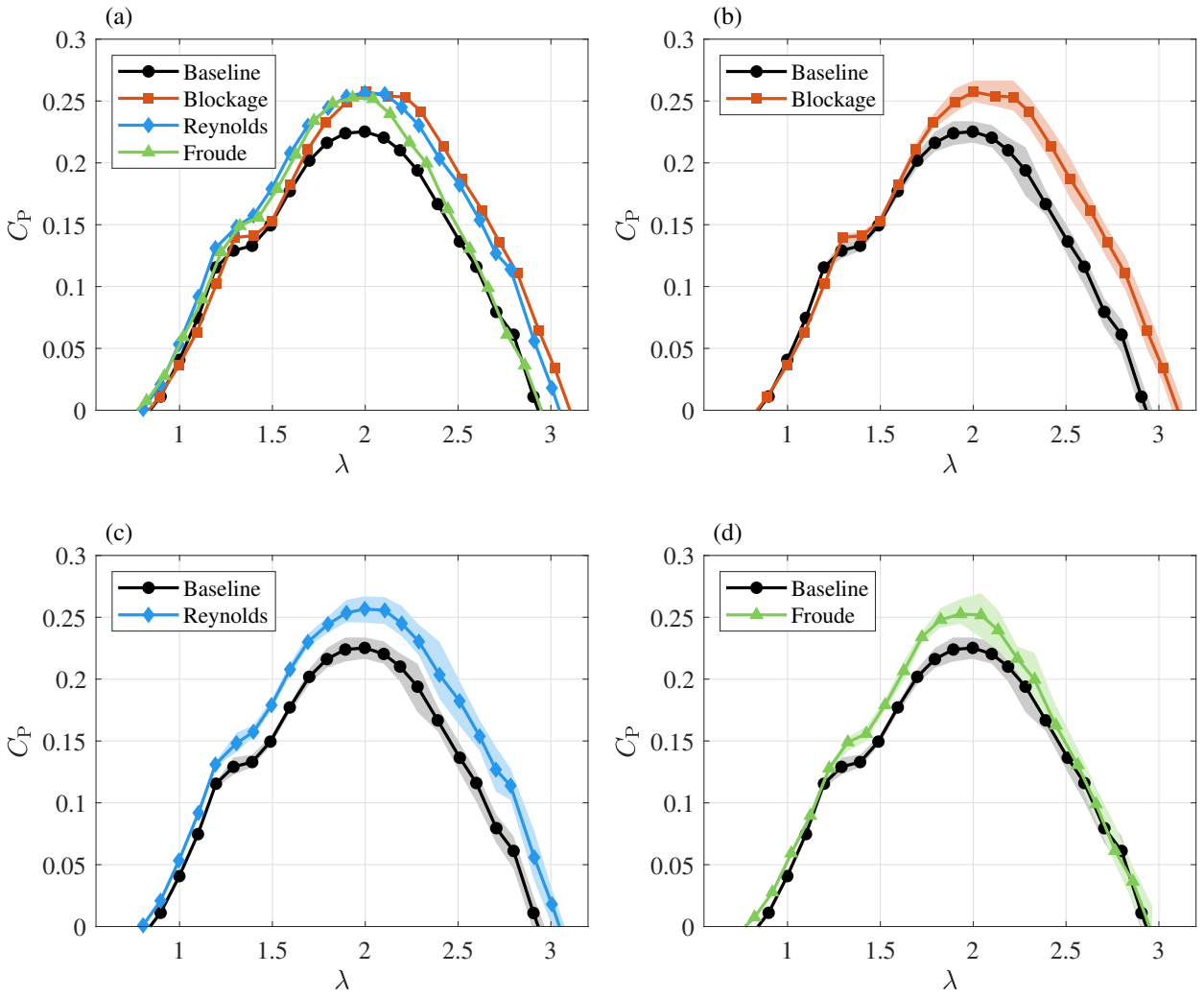

Figure 4.2: $C_P(\lambda)$ curves for each of the operating conditions outlined in Table 4.1. Similar increases in maximum C_P were obtained for a 21.2% increase in the Reynolds number, 38.4% increase in the blockage ratio, and 58.9% increase in the Froude number.

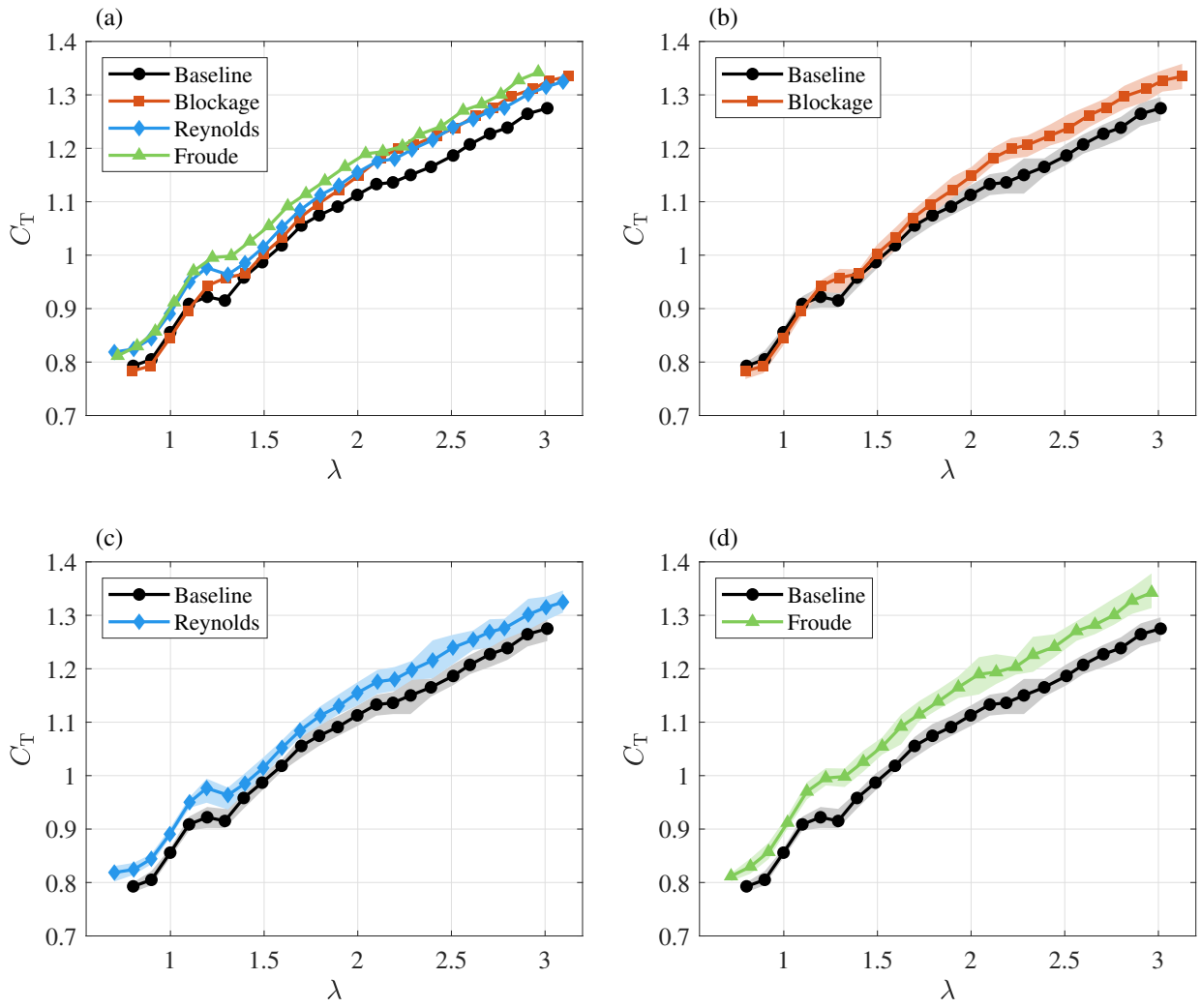

Figure 4.3: $C_T(\lambda)$ curves for each of the operating conditions outlined in Table 4.1. The Reynolds number increased by 21.2% relative to baseline, the blockage ratio increased by 38.4%, and the Froude number increased by 58.9%.

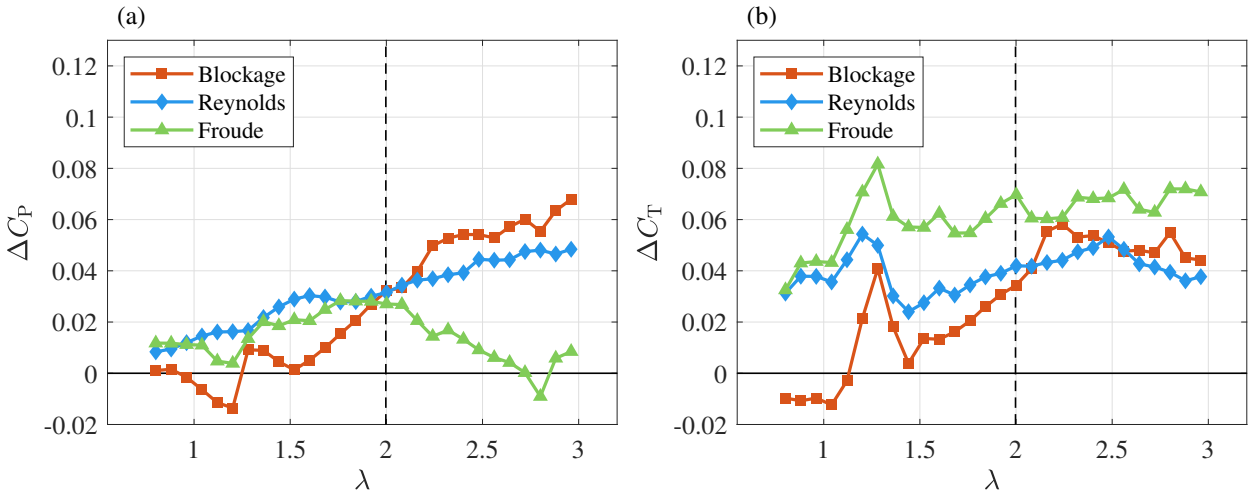

Figure 4.4: Difference between the power coefficients (a) and thrust coefficients (b) of the blockage, Reynolds, and Froude cases and the baseline case.

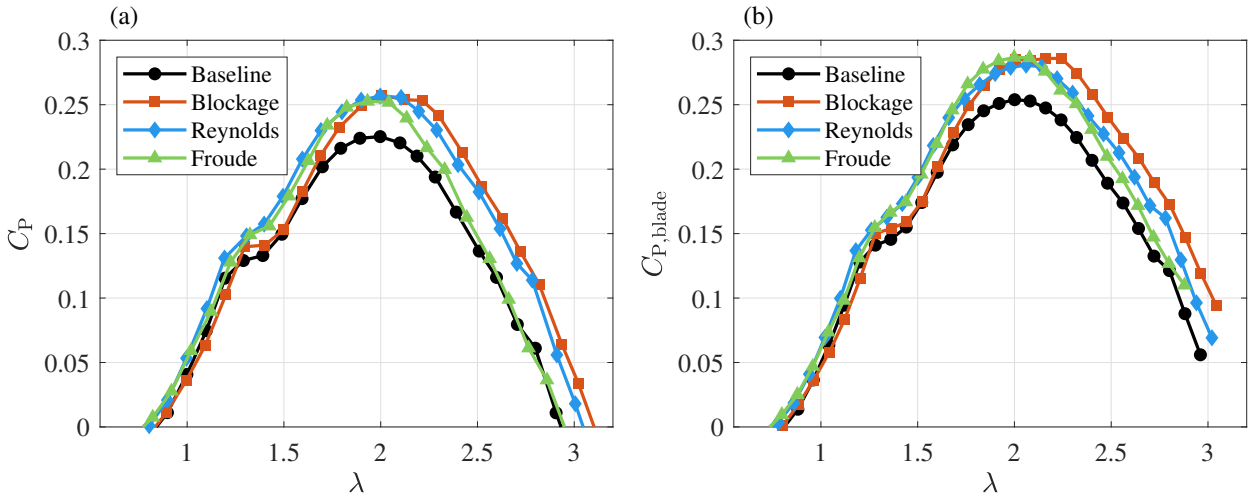

Figure 4.5: $C_P(\lambda)$ curves for each of the operating conditions outlined in Table 4.1 for the full turbine (a) and blades only (b).

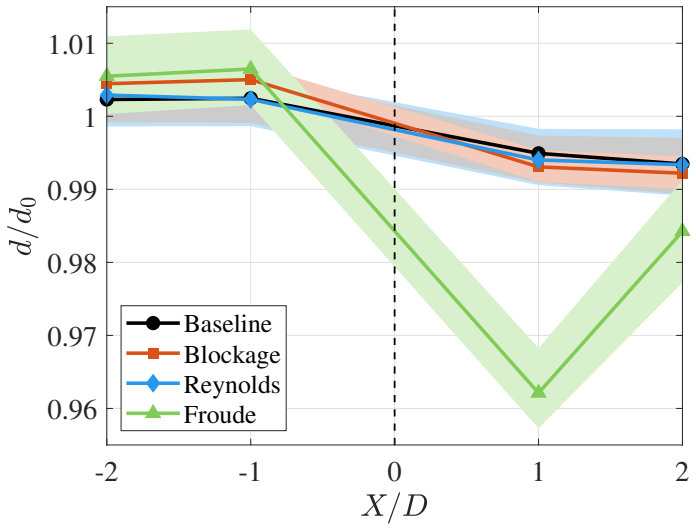

Figure 4.6: Local channel depth normalized by free-stream channel depth. Data were collected at the tip-speed ratio corresponding to peak C_P for each case. The turbine's axis of rotation is located at $X/D = 0$, denoted by a dashed line.

Free surface deformation in the streamwise direction provides additional insight into the underlying fluid dynamics. Figure 4.6 shows the local channel depth measured upstream ($X/D = -2$ and $X/D = -1$) and downstream ($X/D = 1$ and $X/D = 2$) of the turbine at the tip-speed ratio corresponding to peak C_P for each case, normalized by the free-stream depth. The dashed line at $X/D = 0$ denotes the turbine's axis of rotation. The shading represents the measurement uncertainty at each location. These results indicate that increasing the blockage ratio and Reynolds number had a negligible effect on the free surface, but increasing the Froude number caused significantly more free surface deformation around the turbine.

4.4 Discussion

The performance curves presented in Figures 4.2 and 4.3 indicate that the blockage ratio, Reynolds number, and Froude number have distinct effects on a turbine's power and thrust coefficients. For the turbine geometry and test conditions investigated in this study, turbine

performance was most sensitive to changes in the Reynolds number and least sensitive to changes in the Froude number. Because the influence of all three parameters is evident in the blade power coefficients presented in Figure 4.5 (b), we can conclude that their effects are related primarily to increased lift on the blades rather than decreased drag on the support structure, which is consistent with our physical intuition. The local channel depth measurements presented in Figure 4.6 indicate that free surface deformation changes substantially for the Froude case but is negligible for the remaining cases. We now discuss the specific effects of each parameter on the turbine's power and thrust coefficients, as well as the flow dynamics.

4.4.1 Blockage Ratio Effects

Prior work has explored the effects of blockage on the power and thrust coefficients of current turbines, and multiple studies have established the theoretical basis for increased turbine performance caused by blockage [23, 30, 34, 37, 70]. Flow in a channel is more constrained at high blockage, causing the flow speeds through and around the turbine to increase relative to an unconfined case [23, 40, 41, 48]. These higher flow speeds cause increased forces and torque acting on the turbine rotor and, therefore, increased power and thrust coefficients. Our work aligns with these past results. As shown by Figures 4.2 (b) and 4.3 (b), higher blockage increased the turbine's peak C_{P} and corresponding C_{T}. Furthermore, the turbine produced net power over a larger range of tip-speed ratios. However, as illustrated by Figure 4.4 (a), the effects of blockage were negligible below a tip-speed ratio of approximately 1.5. The latter two effects have been observed previously for cross-flow turbines [23, 40] and can be explained, at least in part, by considering the blade kinematics. Cross-flow turbines experience a range of angles of attack throughout a single revolution. At the lowest tip-speed ratios, the angles of attack undergo larger fluctuations, which can lead to dynamic stall and decreased performance. At the highest tip-speed ratios, the angles of attack undergo smaller fluctuations that are less advantageous for lift production, and hydrodynamic drag increases. As blockage increases, the flow speed through the rotor tends to increase as well, decreasing

the effective tip-speed ratio. This allows the turbine to produce net power over a larger range of tip-speed ratios. However, because this exacerbates dynamic stall at lower tip-speed ratios, any gains in C_P caused by higher flow speeds through the rotor are negated in this performance region.

Prior numerical work by Consul et al. [23] has also shown that increasing blockage shifts the peak C_P to a higher tip-speed ratio and causes increased free surface deformation downstream of the turbine. Our results do not reflect these trends. As shown by Figures 4.2 (b) and 4.6, peak C_P occurred at the same tip-speed ratio for the baseline and blockage cases, and there were no significant differences in local channel depth between the two cases. We believe that these discrepancies are a consequence of the relatively small increase in blockage used here, as we were only able to vary the blockage ratio from 0.080 to 0.117, whereas Consul et al. [23] quadrupled the blockage ratio from 0.125 to 0.50. The experiments detailed in Chapter 5 vary the blockage ratio from approximately 0.03 to 0.36. In this work, the peak C_P does shift to a higher tip-speed ratio as blockage is increased.

4.4.2 Reynolds Number Effects

As discussed in Sections 2.3 and 2.4, the Reynolds number represents the ratio of inertial to viscous forces in a fluid and is commonly used to indicate whether a flow is laminar or turbulent. Below a certain threshold, varying the Reynolds number changes the nature of the boundary layer on a turbine's blade, affecting lift production and, consequently, the turbine's performance. Studies by Bachant and Wosnik [4] and Miller et al. [50] found that the Reynolds number can significantly affect the power output of both laboratory-scale and field-scale turbines and that performance becomes independent of the chord-based Reynolds number for values on the order of 10^5 to 10^6 [4, 50]. In this study, the chord-based Reynolds number is $O(10^4)$ and, as illustrated by Figure 4.4, increasing the Reynolds number influenced the turbine's C_P and C_T across the range of tip-speed ratios tested. The Reynolds effects shown in Figures 4.2 (c) and 4.3 (c) are qualitatively similar to those observed in past work. Increasing the Reynolds number had an increasingly significant impact on C_P at higher

tip-speed ratios and a fairly constant effect on C_T across all tip-speed ratios.

Reynolds and blockage effects are caused by two fundamentally different fluid mechanisms. Reynolds effects are related to changes in the blade boundary layer, and blockage effects are caused by increased flow speeds through the turbine. However, when operating in a Reynolds dependent regime at high blockage, the increased flow speeds through the turbine simultaneously increase the local Reynolds number, convolving the performance effects of the two parameters. Therefore, in Reynolds dependent regimes, it is challenging to entirely isolate the effects of Reynolds number and blockage from one another.

As illustrated by Figure 4.6, increasing the Reynolds number had a negligible impact on local channel depth in these experiments. To our knowledge, no prior experimental or numerical studies have reported the influence of Reynolds number on free surface deformation.

4.4.3 Froude Number Effects

The effects of Froude number on turbine performance are less well understood than the effects of the blockage ratio and Reynolds number. In simulation, Consul et al. [23] concluded that the Froude number has a relatively small influence on turbine power and thrust coefficients and a significant impact on free surface deformation. These results are consistent with our findings, which suggest that turbine performance is less sensitive to changes in the Froude number than changes in the other two parameters. Furthermore, as shown by Figure 4.6, the free surface deformation downstream of the turbine was observable, though negligible, for the baseline, blockage, and Reynolds cases, but significant for the Froude case. Consul et al. [23] suggested that increasing the Froude number improves turbine performance because the additional drop in channel depth downstream of the turbine acts to increase the blockage. This explanation assumes that Froude and blockage effects are caused by the same underlying fluid mechanisms. Given this reasoning, the Froude number and blockage ratio should have similar effects on a turbine's $C_P(\lambda)$ and $C_T(\lambda)$ curves. However, as illustrated by Figures 4.2 and 4.3, the Froude number and blockage ratio had distinctly different influences on turbine performance. The Froude number affected the power coefficient mainly near the peak of the

curve and the thrust coefficient consistently across tip-speed ratios, whereas blockage effects were magnified at higher tip-speed ratios for both coefficients. An alternative hypothesis is that the larger free surface deformation improves performance by increasing the hydrostatic pressure difference across the turbine. The increase in thrust coefficient across all tip-speed ratios is consistent with an increased pressure differential, but this does not explain why the power coefficient only increases for a subset of tip-speed ratios. The underlying fluid mechanisms that cause changes in the Froude number to affect turbine hydrodynamics clearly warrant further investigation.

Consul et al. [23] also concluded that free surface deformation is more significant at higher tip-speed ratios, and these effects become more pronounced as both the Froude number and blockage ratio increase. Figure 4.7 shows that this trend was observed for our Froude case but not for the other cases. We expect that this trend was not measurable for the blockage case because the blockage ratios tested were relatively small. Free surface deformation likely becomes more significant at higher tip-speed ratios because the rotor appears more solid to the incoming flow, increasing the thrust. Again, this explanatory hypothesis is not entirely satisfactory, as the thrust coefficient was similar for all three parameters at high tip-speed ratio, but a significant free surface deformation was only observed when the Froude number was increased.

4.5 Conclusions

Varying the blockage ratio, Reynolds number, and Froude number all affected turbine performance, although each parameter changed the shape of the $C_{\mathrm{P}}(\lambda)$ and $C_{\mathrm{T}}(\lambda)$ curves in a different way. The impact of each parameter on turbine performance is grounded in its connection to turbine hydrodynamics. Increasing the blockage ratio increases the flow speeds through and around a turbine, resulting in higher forces and torque. These increased flow speeds modify the angles of attack experienced by the blades, allowing the turbine to produce net power over a wider range of tip-speed ratios and exaggerating performance effects at higher tip-speed ratios. Increasing the Reynolds number changes the nature of the boundary

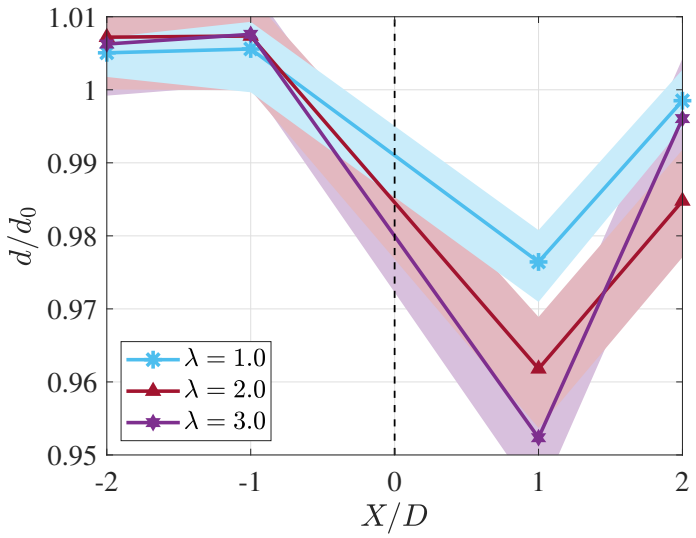

Figure 4.7: Channel depth near the turbine normalized by free-stream channel depth for the high Froude number case for three different tip-speed ratios. The turbine's axis of rotation is located at $X/D = 0$ and denoted by a dashed line.

layer on the blades, augmenting lift forces that affect both the power and thrust coefficients. Reynolds effects increased with tip-speed ratio for the power coefficient and were fairly consistent across tip-speed ratios for the thrust coefficient. Increasing the Froude number caused the largest increase in C_{T} and most significant free surface deformation. Both effects are likely associated with a larger hydrostatic pressure drop across the turbine. Varying the Froude number affected the turbine's power coefficient most significantly near its peak value and, like the Reynolds number, affected the thrust coefficient consistently across tip-speed ratios. However, as discussed, there are inconsistencies in explanations of the Froude number effect that require further investigation.

Although the effects of each parameter are distinct, some are interrelated. For example, higher flow speeds through the rotor that occur with increased blockage can simultaneously increase performance due to Reynolds effects if the turbine is operating in a Reynolds dependent regime. These complicated relationships highlight the importance of understanding

how each parameter affects turbine performance. We concluded that the power coefficient was most sensitive to changes in the Reynolds number and least sensitive to changes in the Froude number for the turbine geometry and test conditions considered in this study. However, because varying all three parameters was found to significantly affect the turbine's power and thrust coefficients, the blockage ratio, Reynolds number, and Froude number should all be given due consideration in experimental design.

Chapter 5

ASSESSMENT OF ANALYTICAL BLOCKAGE CORRECTIONS

This chapter contains content from Ross and Polagye [62], which has been published in *Renewable Energy*. Portions of the article have been edited to avoid redundancy. The objective of this chapter is to assess the effectiveness of analytical models designed to correct for the effects of blockage, improving the extrapolation of model results to larger scales.

5.1 Introduction

Experimental investigations of model current turbines often take place in confined flows, such as flumes and water tunnels. Flow confinement, or blockage, can significantly alter the mechanical performance of a turbine, relative to operation in an unconfined flow. Higher blockage increases streamwise flow speeds through and around the rotor [23, 40, 41, 48], increasing the turbine's torque and thrust. However, the flow velocity far upstream of the turbine remains relatively unchanged. Therefore, increasing the blockage augments a turbine's power and thrust coefficients.

Blockage effects were first examined in the context of wind tunnel testing of propellers in the early 20th century by Wood and Harris [84] and Glauert [32]. More recently, analytical [30, 37], numerical [23, 34, 40, 41, 54, 69, 70], and experimental [6, 11, 15, 25, 31, 48, 67] studies have explored the effects of blockage on wind and water current turbines. The magnitude of these effects is related to the blockage ratio, defined here as

$$\beta = \frac{A_\mathrm{t} + A_\mathrm{s}}{A_\mathrm{c}}, \tag{5.1}$$

where A_s is the projected area of the support structure. Multiple studies have demonstrated that turbine performance changes appreciably when the blockage ratio exceeds 0.05-0.10 [25,

41, 48, 69].

The effects of blockage on turbine models can make it difficult to extrapolate results to larger scales. To accurately model full-scale conditions, the influence of blockage on performance data collected at smaller scales must be accounted for. Over the past century, multiple analytical methods have been developed for this purpose. These methods are often referred to as "blockage corrections" and are the focus of this study. The first such correction was developed by Glauert [32] for propellers tested in wind tunnels. Glauert's method is based on axial momentum theory applied to an actuator disk (i.e., linear momentum actuator disk theory) in a closed tunnel. The most common form of this correction is an approximation based on the assumption that the blockage ratio is less than 0.15. Glauert's approximate correction can be applied to turbines, but it has a limited range of applicability due to a singularity as the thrust coefficient approaches unity [11]. Subsequent studies, following Glauert's approach, have derived corrections specifically for wind and current turbines. Here, we focus on the corrections presented by Barnsley and Wellicome [8], Mikkelsen and Sørensen [49], Werle [81], and Houlsby et al. [38]. All are derived from axial momentum theory applied to an actuator disk in a flow confined either by rigid walls (e.g., a tunnel) or by rigid walls and a free surface (e.g., a channel). These corrections have seen widespread application to performance data from experiments and simulations [2, 6, 31, 41, 48]. However, uncertainty remains as to which corrections, if any, effectively account for blockage [2, 29, 40].

Several previous studies have attempted to address the question of correction efficacy. Kinsey and Dumas [40] simulated a cross-flow turbine and an axial-flow turbine operating in a water tunnel and applied the correction of Barnsley and Wellicome [8]. By comparing the corrected results to simulations conducted in an unconfined domain, they concluded that Barnsley and Wellicome's method worked well for the axial-flow turbine and was adequate for the cross-flow turbine. Similarly, Segalini and Inghels [71] simulated blockage effects on an axial-flow turbine using a vortex model and compared power and thrust corrections estimated from this model to those given by the actuator disk method of Mikkelsen and Sørensen [49]. Results from the two methods agreed reasonably well, providing encourag-

ing validation of actuator disk corrections applied to realistic turbines. Experimentally, Ryi et al. [67] applied Barnsley and Wellicome's correction to an axial-flow turbine tested in a closed-section wind tunnel and found that corrected results agreed well with the same turbine's performance in an open-jet wind tunnel. Using similar methods, Dossena et al. [25] conducted experimental wind tunnel tests of a cross-flow turbine at a blockage ratio of 0.10 and under conditions of negligible blockage. They compared an empirical correction based on experimental data from the two conditions with an analytical correction using Mikkelsen and Sørensen's method. They concluded that the analytical method predicted the trend of the empirical correction but significantly underestimated its magnitude. The authors recommended improving analytical blockage corrections specifically for cross-flow turbines.

Several recent studies [11, 40, 65, 72, 83] have also examined the effectiveness of blockage corrections originally derived for bluff bodies [46, 60], when applied to turbines. For example, Whelan et al. [83] and Kinsey and Dumas [40] determined that Maskell's correction performs better than actuator disk methods when the turbine rotor is heavily loaded.

Overall, previous research has concluded that actuator disk corrections are adequate for axial-flow turbines and give mixed results for cross-flow turbines. However, prior studies have evaluated only one or two of the multiple blockage corrections proposed in the literature. Because the effectiveness of a blockage correction depends on the specific conditions under which it is applied (e.g., turbine and support structure design and tunnel or channel geometry), the relative accuracy of these corrections remains an open question. To our knowledge, no systematic experimental validation that considers both turbine archetypes and multiple analytical corrections has been reported in the archival literature. This lack of validation may be a consequence of the difficulty of undertaking such experiments, which require varying blockage while controlling the Reynolds number [4, 21, 50] and, in the case of a free surface, the Froude number [41, 80]. For experiments conducted at transitional Reynolds numbers, this can only be achieved by changing the physical dimensions of a tunnel or the width of a channel. Therefore, the objective of the present study is to experimentally evaluate blockage corrections for a cross-flow turbine and an axial-flow turbine by varying the blockage ratio

with other significant parameters held approximately constant.

5.2 Experimental Methods

To establish a baseline for the analytical corrections, a cross-flow turbine and an axial-flow turbine were characterized under high blockage and negligible blockage by testing the turbines at experimental facilities of different size. The turbines used for this study are shown in Figure 3.1 (b) and (c) and described in Section 3.1. The testing facilities were the UW flume and UNH tow tank, described in Section 3.2. The performance of both turbines was characterized as described in Section 3.3. Section 5.2.1 describes the dimensionless parameters that were controlled in this study, and Section 5.2.2 details the wake characterization.

5.2.1 Dimensionless Parameters

The dimensions of the UW flume resulted in a blockage ratio of 0.36 for the cross-flow turbine and 0.35 for the axial-flow turbine. The larger cross-section of the UNH facility yielded a blockage ratio of 0.03 for the cross-flow turbine and 0.02 for the axial-flow turbine. Consequently, the blockage effects at the UNH facility were assumed to be negligible [69]. We will refer to data taken in the UW flume as "confined" and data taken in the UNH tow tank as "unconfined". To measure only the effects of a change in blockage, we attempted to hold the Reynolds and Froude numbers approximately constant. Under test conditions, both turbines were operating at transitional Reynolds numbers: 31,000 for the cross-flow turbine and 14,000 for the axial-flow turbine. To maintain a constant Reynolds number, all tests were conducted at a free-stream velocity of 0.5 m/s, and the temperature of the UW flume was controlled to match the temperature of the UNH tow tank. However, the variation in free-stream channel depth from 0.60 m in the flume to 2.4 m in the tow tank resulted in a change in the Froude number from 0.2 to 0.1. Given that these are relatively low Froude numbers, it was assumed that this variation had a negligible effect on performance compared to the changes in blockage [23].

Furthermore, as detailed in Section 3.2, there was a small difference in turbulence intensity

between the two facilities. Past studies have shown that decreasing the turbulence intensity increases a turbine's power and thrust coefficients [16, 53]. However, based on the magnitude of performance change observed in these studies, it is assumed that the impact of a decrease in turbulence intensity from approximately 2% to approximately 0% is insignificant.

Finally, the aspect ratio of the UW flume resulted in higher lateral blockage for the cross-flow turbine and higher vertical blockage for the axial-flow turbine. However, as discussed in Section 2.3, confinement asymmetry is negligible for CA < 3. As the confinement asymmetry of both turbines in the UW flume was approximately 1.3, we assume performance was relatively unaffected by the channel aspect ratio.

5.2.2 Wake Characterization

One of the blockage corrections considered in this study requires information about the wake structure. Because these data were time-intensive to collect, wake measurements were taken only at the tip-speed ratio corresponding to the peak power coefficient. Wake data were collected using two acoustic Doppler velocimeters mounted on a motorized gantry, as described in Section 3.4. For both turbines, measurements were taken at 0.75, 1.25, 1.75, and 2.25 diameters downstream of the center of the rotor. At each downstream location, the measurement grid consisted of a single lateral traverse in the cross-stream direction, with measurements spaced 0.01 m apart. The traverses were centered vertically relative to the turbine rotor. Figure 5.1 illustrates the wake measurement locations for the cross-flow turbine. A similar grid was used for the axial-flow turbine. Raw measurements were despiked using the method of Goring and Nikora [33], and data points with low correlation values were discarded [66]. These measurements were used to estimate the cross-sectional area of the wake (A_1) downstream of each turbine. The values of A_1 were determined by calculating the position, in the cross-stream direction, of the boundary between the core flow (fluid that passes through the turbine) and bypass flow (fluid that passes around the turbine). This boundary was taken as the point where the velocity in the core flow equaled or exceeded the free-stream velocity. According to theory, A_1 is measured at the streamwise location where

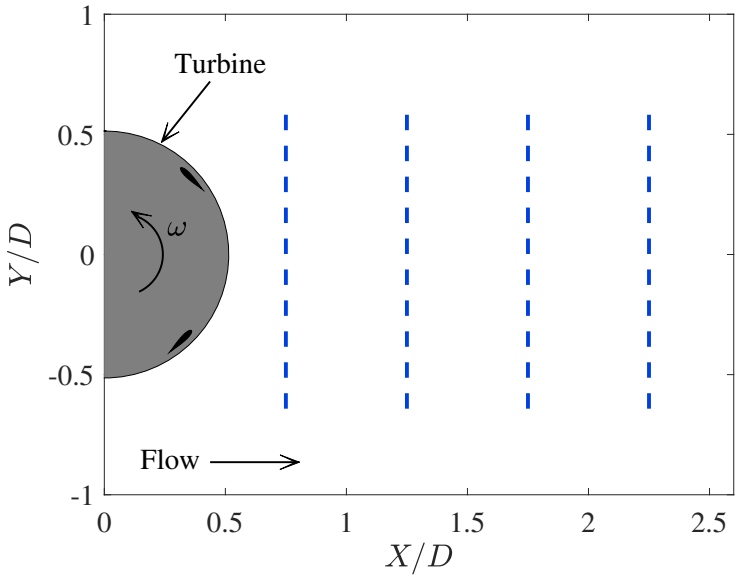

Figure 5.1: Top view of the measurement grid used to collect wake data for the cross-flow turbine. The dashed lines show the location of each cross-stream traverse.

the pressure between the core and bypass flows reaches equilibrium. This point is ambiguous without spatially-resolved pressure measurements, which were not available for these tests. Therefore, the wake area was estimated at each of the streamwise locations shown in Figure 5.1. All four values were used in the analytical correction, and the one which yielded the lowest error was reported.

5.3 Analytical Methods

Blockage corrections applied to confined performance data estimate the equivalent unconfined power coefficient (C'_{P}), thrust coefficient (C'_{T}), and tip-speed ratio (λ'),

$$C'_{\mathrm{P}} = \frac{P'}{\frac{1}{2}\rho A_{\mathrm{t}} V_0'^3}, \tag{5.2}$$

$$C'_{\mathrm{T}} = \frac{T'}{\frac{1}{2}\rho A_{\mathrm{t}} V_0'^2}, \tag{5.3}$$

$$\lambda' = \frac{R\omega'}{V_0'}, \tag{5.4}$$

where the prime denotes an unconfined value. The methods considered in this section are based on axial momentum theory applied to an actuator disk in either closed channel flow (representative of a closed-section wind tunnel or cavitation tunnel with no free surface) or open channel flow (representative of a flume with a deformable free surface). These methods are not suitable for open-jet wind tunnels.

5.3.1 Glauert's Method

Although we do not directly evaluate the original propeller blockage correction developed by Glauert [32], all of the methods considered in this section are based, to a varying degree, on his analysis. The assumptions that underpin Glauert's derivation are that the incoming flow is uniform, the propeller (or turbine) is two-dimensional and has an infinite number of frictionless blades, thrust over the entire rotor is uniform, the wake does not rotate, and the effects of boundary proximity and channel aspect ratio are insignificant.

Given performance data collected at a constant operating condition in confined flow, Glauert's method computes V_0', the free-stream velocity that, in an unconfined flow, would produce the same values of thrust and streamwise velocity through the rotor (u_{t}) at the same

angular velocity, i.e.,

$$T' = T, \tag{5.5}$$

$$u_{\mathrm{t}}' = u_{\mathrm{t}}, \tag{5.6}$$

$$\omega' = \omega. \tag{5.7}$$

Glauert does not specifically address power, but to correct C_{P}, subsequent authors have invoked the definition of power absorbed by an actuator disk,

$$P = T u_{\mathrm{t}}. \tag{5.8}$$

Combining Equations (5.5), (5.6), and (5.8) yields

$$P' = P. \tag{5.9}$$

Dividing Equations (5.2)-(5.4) by the definitions of C_{P}, C_{T}, and λ and using the equalities in Equations (5.5), (5.7), and (5.9) yields expressions for C_{P}', C_{T}', and λ' as functions of V_0':

$$C_{\mathrm{P}}' = C_{\mathrm{P}} \left(\frac{V_0}{V_0'} \right)^3, \tag{5.10}$$

$$C_{\mathrm{T}}' = C_{\mathrm{T}} \left(\frac{V_0}{V_0'} \right)^2, \tag{5.11}$$

$$\lambda' = \lambda \left(\frac{V_0}{V_0'} \right). \tag{5.12}$$

For a turbine, blockage increases u_{t} for a given V_0. Therefore, the free-stream velocity that gives the same u_{t} in an unconfined flow is typically higher (i.e., $V_0' > V_0$). By calculating the equivalent unconfined power coefficient, thrust coefficient, and tip-speed ratio using V_0', Glauert's correction can account for the performance increase that a turbine experiences in confined flow.

The equivalent unconfined free-stream velocity V_0' is estimated by first applying the principles of continuity, conservation of axial momentum, and the Bernoulli equation to an

actuator disk in confined flow. This yields a system of four equations,

$$u_t A_t = u_1 A_1, \tag{5.13}$$

$$u_2(A_c - A_1) = V_0 A_c - u_t A_t, \tag{5.14}$$

$$T = \frac{1}{2}\rho A_t(u_2^2 - u_1^2), \tag{5.15}$$

$$T + \frac{1}{2}\rho A_c(V_0^2 - u_2^2) = \rho A_1 u_1(V_0 - u_1) + \rho(A_c - A_1)u_2(V_0 - u_2), \tag{5.16}$$

where u_1 is the velocity of the core flow and u_2 is the velocity of the bypass flow. It should be noted that Equations (5.13)-(5.16) apply to an actuator disk that extracts energy from the flow (i.e., a turbine). Therefore, the thrust in Equations (5.15) and (5.16) is oppositely signed from the thrust in Glauert's original derivation, which applies to an actuator disk that adds energy to the flow (i.e., a propeller). Assuming u_t has been estimated from Equations (5.13)-(5.16), the unconfined free-stream velocity can then be found by introducing a fifth equation: the expression for thrust in unconfined flow obtained from momentum conservation,

$$T' = 2\rho u_t' A_t(V_0' - u_t'). \tag{5.17}$$

Combining the definition of C_T and Equations (5.5) and (5.6) with Equation (5.17) yields a solution for V_0':

$$V_0' = \frac{V_0((u_t/V_0)^2 + C_T/4)}{u_t/V_0}. \tag{5.18}$$

Once V_0' is known, the unconfined coefficients C_P', C_T', and λ' can be calculated for each operating point using Equations (5.10)-(5.12).

Specific corrections for a turbine operating in closed or open channel flow, as presented by Barnsley and Wellicome [8], Mikkelsen and Sørensen [49], Werle [81], and Houlsby et al. [38] are described separately in the following sections. The correction given by Maskell [46] for bluff bodies is contrasted in Section 5.5.5.

5.3.2 Closed Channel Flow

Several methods have been proposed to account for the effects of blockage in a channel without a free surface. All methods reference the streamtube model shown in Figure 5.2.

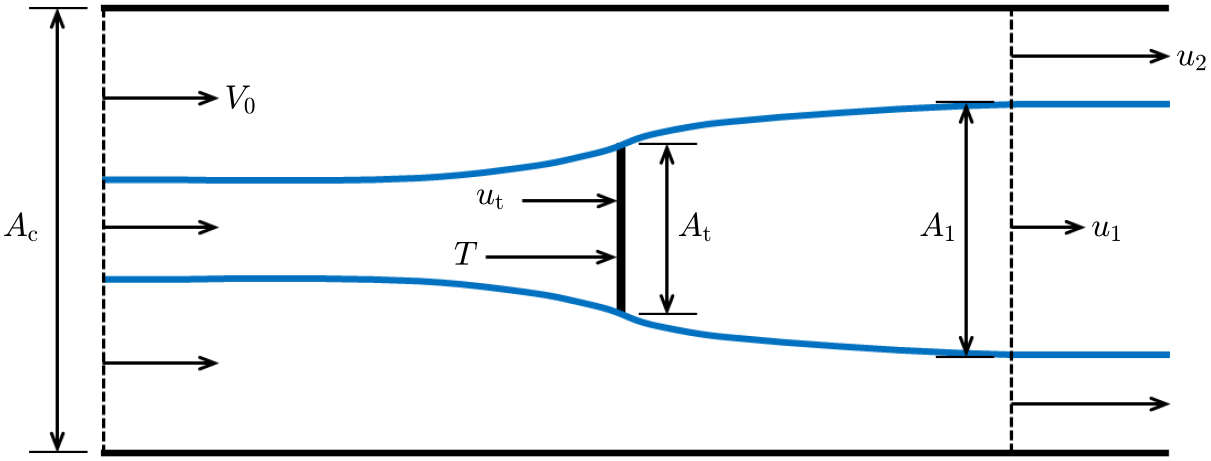

Figure 5.2: Streamtube model of an actuator disk in closed channel flow with no free surface.

The first method, developed by Barnsley and Wellicome [8] and introduced to the marine energy research community by Bahaj et al. [6], applies Glauert's axial momentum theory analysis [32] to a turbine rather than a propeller. A second method, developed by Mikkelsen and Sørensen [49], also follows Glauert's analysis. However, it provides an alternative closure to the correction presented by Barnsley and Wellicome. A third method, derived by Werle [81], applies simplifying approximations to Glauert's theory.

Barnsley and Wellicome's Method

To apply the correction given by Barnsley and Wellicome [8] (BW), measurements of A_t, A_c, V_0, T, and ρ must be available. If so, Equations (5.13)-(5.16) become a closed system with four unknowns: A_1, u_t, u_1, and u_2. Although a compact analytical solution to these equations does not exist, individual solutions can be obtained for certain operating conditions. By rearranging Equations (5.13)-(5.16), an iterative scheme is developed to solve for the ratio

u_t/V_0. This scheme consists of three equations:

$$\frac{u_t}{u_1} = \frac{-1 + \sqrt{1 + \beta((u_2/u_1)^2 - 1)}}{\beta(u_2/u_1 - 1)}, \tag{5.19}$$

$$\frac{V_0}{u_1} = \frac{u_2}{u_1} - \beta\left(\frac{u_t}{u_1}\right)\left(\frac{u_2}{u_1} - 1\right), \tag{5.20}$$

$$\frac{V_0}{u_1} = \sqrt{\frac{(u_2/u_1)^2 - 1}{C_T}}. \tag{5.21}$$

The solution is found by guessing a reasonable value for u_2/u_1 and solving Equation (5.19) for u_t/u_1. Using these values of u_2/u_1 and u_t/u_1, Equations (5.20) and (5.21) can be solved for the ratio V_0/u_1. If the two values of V_0/u_1 do not match, a new value of u_2/u_1 should be selected, and the scheme repeated until the error between Equations (5.20) and (5.21) is minimized. Note that solutions only exist for values of the input variables that yield physical results, e.g., $u_2 > u_t > u_1$, $V_0 > u_t$, and $u_2 > V_0$. With u_t/u_1 and V_0/u_1 known, the ratio u_t/V_0 can be found. Given u_t/V_0, V_0' can be calculated using Equation (5.18), and C_P', C_T', and λ' can be estimated at each operating point using Equations (5.10)-(5.12). A summary of this method is presented by Bahaj et al. [6] and derived by Kinsey and Dumas [40]. While the original technical report [8] does not appear to be publicly available, given limited comments on blockage corrections in subsequent work [9], the primary reference is unlikely to contain more detail than is presented in the secondary sources.

Mikkelsen and Sørensen's Method

Mikkelsen and Sørensen [49] (MS) proposed a correction that presents an alternative closure to Equations (5.13)-(5.16). As with Barnsley and Wellicome's correction, it is assumed that A_t, A_c, V_0, and ρ are known. However, A_1 is measured rather than T. This method rearranges Equations (5.13)-(5.16) to solve for the unknown variables u_t, u_1, u_2, and C_T directly, with no iteration required. Even if measurements of T or C_T are available, they should not be used in conjunction with this method, as the system of equations would become overdetermined.

The correction consists of the following four equations:

$$u_t = \frac{V_0(A_1/A_t)(\beta(A_1/A_t)^2 - 1)}{\beta(A_1/A_t)(3A_1/A_t - 2) - 2A_1/A_t + 1}, \tag{5.22}$$

$$u_1 = \frac{u_t A_t}{A_1}, \tag{5.23}$$

$$u_2 = \frac{A_t(V_0 - \beta u_t)}{A_t - \beta A_1}, \tag{5.24}$$

$$C_T = \frac{u_2^2 - u_1^2}{V_0^2}. \tag{5.25}$$

Once u_t and C_T have been calculated, the unconfined velocity V_0' can be found using Equation (5.18) and the unconfined turbine performance parameters calculated using Equations (5.10)-(5.12). This method highlights the fact that Equations (5.13)-(5.16) can be solved multiple ways, as long as adequate measurements are available to close the system.

Werle's Method

The final closed channel blockage correction considered in this study was developed by Werle [81]. This method is also based on Equations (5.13)-(5.16) but makes several approximations that allow the unconfined parameters C_P', C_T', and λ' to be calculated as functions of the blockage ratio alone, without an intermediate calculation of V_0'. These approximations are given as

$$\frac{C_P'}{C_{P,max}'} \approx \frac{C_P}{C_{P,max}}, \tag{5.26}$$

$$\frac{C_T'}{C_{T,max}'} \approx \frac{C_T}{C_{T,max}}, \tag{5.27}$$

$$\frac{u_t'}{u_{t,max}'} \approx \frac{u_t}{u_{t,max}}, \tag{5.28}$$

where the expressions for $C'_{\mathrm{P,max}}$, $C'_{\mathrm{T,max}}$, and $u'_{\mathrm{t,max}}$ are given by the well-known Betz criterion [14, 42] as

$$C'_{\mathrm{P,max}} = \frac{16}{27}, \tag{5.29}$$

$$C'_{\mathrm{T,max}} = \frac{8}{9}, \tag{5.30}$$

$$u'_{\mathrm{t,max}} = \frac{2}{3}V'_0, \tag{5.31}$$

and the expressions for $C_{\mathrm{P,max}}$, $C_{\mathrm{T,max}}$, and $u_{\mathrm{t,max}}$ are given by Garrett and Cummins [30] as

$$C_{\mathrm{P,max}} = \frac{16}{27}\frac{1}{(1-\beta)^2}, \tag{5.32}$$

$$C_{\mathrm{T,max}} = \frac{8}{9}\frac{(1+\beta)}{(1-\beta)^2}, \tag{5.33}$$

$$u_{\mathrm{t,max}} = \frac{2}{3}\frac{V_0}{(1+\beta)}. \tag{5.34}$$

Substituting Equations (5.29)-(5.34) into Equations (5.26)-(5.28) gives corrections for C_{P}, C_{T}, and u_{t}, which Werle presents as

$$C'_{\mathrm{P}} \approx C_{\mathrm{P}}(1-\beta)^2, \tag{5.35}$$

$$C'_{\mathrm{T}} \approx C_{\mathrm{T}}\frac{(1-\beta)^2}{(1+\beta)}, \tag{5.36}$$

$$\frac{u'_{\mathrm{t}}}{V'_0} \approx \frac{u_{\mathrm{t}}}{V_0}(1-\beta). \tag{5.37}$$

Applying Equations (5.6) and (5.12) to Equation (5.37) yields an expression in terms of the tip-speed ratio,

$$\lambda' \approx \lambda(1-\beta). \tag{5.38}$$

Based on an independent re-derivation of Werle's method, Equations (5.37) and (5.38) appear to contain sign errors and are inconsistent with the rest of the model. If treated consistently, the equations should be given as

$$\frac{u'_{\mathrm{t}}}{V'_0} \approx \frac{u_{\mathrm{t}}}{V_0}(1+\beta), \tag{5.39}$$

$$\lambda' \approx \lambda(1+\beta). \tag{5.40}$$

However, because the purpose of this study is to evaluate blockage corrections as presented in the literature, the tip-speed ratio correction given by Equation (5.38) was applied to our experimental data without modification.

5.3.3 Open Channel Flow (Houlsby et al.'s Method)

An analytical model for an actuator disk in flow with a deformable free surface was first developed by Houlsby et al. [38] (Houlsby). As with Glauert's model for closed channel flow, this model was derived by applying continuity, conservation of axial momentum, and the Bernoulli equation to an actuator disk in confined flow. However, the free surface of the flow was allowed to deform, as shown in Figure 5.3. This yields seven equations, which can be rearranged and expressed as a system of two equations:

$$u_1 = \frac{\mathrm{Fr}^2 u_2^4 - (4 + 2\mathrm{Fr}^2)V_0^2 u_2^2 + 8V_0^3 u_2 - 4V_0^4 + 4\beta C_\mathrm{T} V_0^4 + \mathrm{Fr}^2 V_0^4}{-4\mathrm{Fr}^2 u_2^3 + (4\mathrm{Fr}^2 + 8)V_0^2 u_2 - 8V_0^3}, \tag{5.41}$$

$$u_1 = \sqrt{u_2^2 - C_\mathrm{T} V_0^2}. \tag{5.42}$$

As with the closed channel model, analytical solutions to Equations (5.41) and (5.42) do not exist. However, specific solutions can be found using an iterative method. To apply the correction, measurements of A_t, A_c, V_0, T, ρ, and d_0 are required. The solution method consists of guessing a reasonable value for u_2, solving Equations (5.41) and (5.42) separately for u_1, and iterating until the two values of u_1 are equal. With u_1 and u_2 known, the streamwise velocity through the turbine can be calculated as

$$u_\mathrm{t} = \frac{u_1(u_2 - V_0)(2gd_0 - u_2^2 - u_2 V_0)}{2\beta g d_0 (u_2 - u_1)}. \tag{5.43}$$

The unconfined free-stream velocity and turbine performance parameters can then be found from Equations (5.18) and (5.10)-(5.12).

This open channel flow model is referenced by Whelan et al. [83] and Houlsby and Vogel [37]. Whelan et al. [83] used this model as the basis for a blockage correction that can be applied within a blade element momentum code. Houlsby and Vogel [37] explored solutions

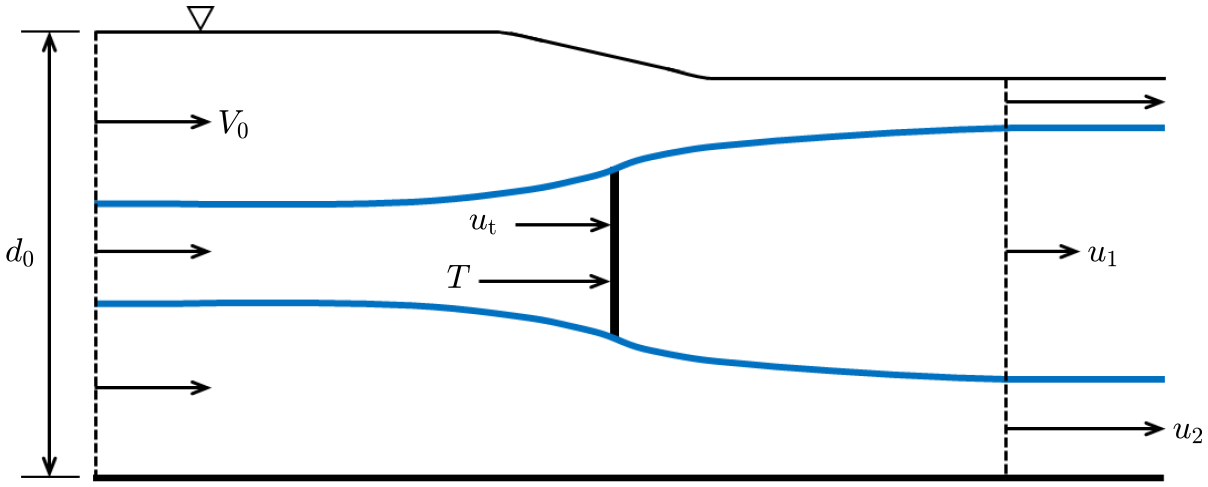

Figure 5.3: Streamtube model of an actuator disk in open channel flow with a deformable free surface.

to this model over a range of operating conditions. However, to our knowledge, it has not previously been cast as an analytical blockage correction.

5.3.4 Summary of Analytical Methods

All of the blockage corrections considered in this section are grounded in Glauert's derivation [32]. In his original work, Glauert presented a set of equations that can be used to solve for V_0' and, therefore, calculate the equivalent unconfined turbine performance coefficients. Glauert also proposed a linearization of this model that provides a simpler method of estimating V_0' when the blockage ratio is less than 0.15. While Glauert's derivation applies to propellers, it can easily be adapted to turbines by reversing the direction of thrust to yield Equations (5.13)-(5.18).

Barnsley and Wellicome [8] and Mikkelsen and Sørensen [49] use measured quantities to solve Equations (5.13)-(5.16) for unknown variables, calculate V_0' using Equation (5.18), and estimate the unconfined performance coefficients using Equations (5.10)-(5.12). The only difference between these two methods is Barnsley and Wellicome's use of thrust to close

the system and Mikkelsen and Sørensen's use of the wake area. The correction presented by Werle [81] uses expressions for the maximum theoretical power coefficient and corresponding thrust coefficient and streamwise velocity through the rotor in confined and unconfined flow. In confined flow, these expressions can be derived from Equations (5.13)-(5.16), following the method of Garrett and Cummins [30]. In unconfined flow, these expressions are given by Lanchester [42] and Betz [14]. Although Werle's correction is based on Glauert's theory, it relies on assumptions that yield a model distinct from the other closed channel corrections. The open channel flow model given by Houlsby et al. [38] is a generalization of Equations (5.13)-(5.16) to allow for a deformable free surface. So, if the free surface does not deform, Houlsby et al.'s correction reduces to the model used by Barnsley and Wellicome and Mikkelsen and Sørensen.

5.3.5 Estimation of Correction Error

The effectiveness of each blockage correction was evaluated by a measure of the difference between the corrected $C_{\mathrm{P}}(\lambda)$ and $C_{\mathrm{T}}(\lambda)$ curves relative to the unconfined performance curves. This error metric was computed as the projection of the Euclidean distance (positive definite scalar quantity) between uniformly sampled points on the corrected and unconfined curves into C_{P}, C_{T}, or λ space. These distances were then normalized by the corresponding values on the unconfined curves to calculate a relative error. The mean of these values, over all operating conditions that produced net power, was taken as an estimate of correction error. Since Mikkelsen and Sørensen's method required wake data, it was applied only at the tip-speed ratio corresponding to the peak power coefficient. Therefore, the error of each method was estimated at this single point as well.

5.4 Results

5.4.1 Performance and Wake Characteristics

The power and thrust coefficients measured under confined and unconfined conditions are shown in Figure 5.4. For both turbines, blockage produces a higher peak power coefficient at an elevated tip-speed ratio. Furthermore, the thrust coefficient at the point of peak C_{P} is increased, and the turbines produce net power over a wider range of tip-speed ratios. These results are in agreement with previous findings [23]. Interestingly, the overall trend of an increased C_{P} at high blockage reverses or becomes negligible at lower tip-speed ratios. As discussed in Section 4.4.1, past studies have reported an insensitivity of C_{P} to blockage at low tip-speed ratios for both cross-flow and axial-flow turbines [23, 40, 41]. For cross-flow turbines, Consul et al. [23] and Kinsey and Dumas [40] attribute this to dynamic stall effects that are magnified by blockage. At low tip-speed ratios, the performance-enhancing effects of blockage are cancelled out by increased dynamic stall. However, as shown in Figure 5.4, we observe that blockage has a negative, rather than neutral, effect on the power coefficient of the cross-flow turbine at low tip-speed ratios. As prior studies are based on numerical simulations, this discrepancy could be explained by the difficulty of accurately modeling dynamic stall.

As described in Section 5.2.2, the cross-sectional area of the wake downstream of both turbines was estimated from velocity measurements. Table 5.1 presents the values of A_1, non-dimensionalized by A_{t}, at each of the four streamwise positions shown in Figure 5.1. These values were used only when applying Mikkelsen and Sørensen's correction.

5.4.2 Application of Blockage Corrections

Barnsley and Wellicome's Method

Figure 5.5 presents the results of applying Barnsley and Wellicome's correction to the confined data. The uncorrected, confined data are superimposed for reference. If the correction

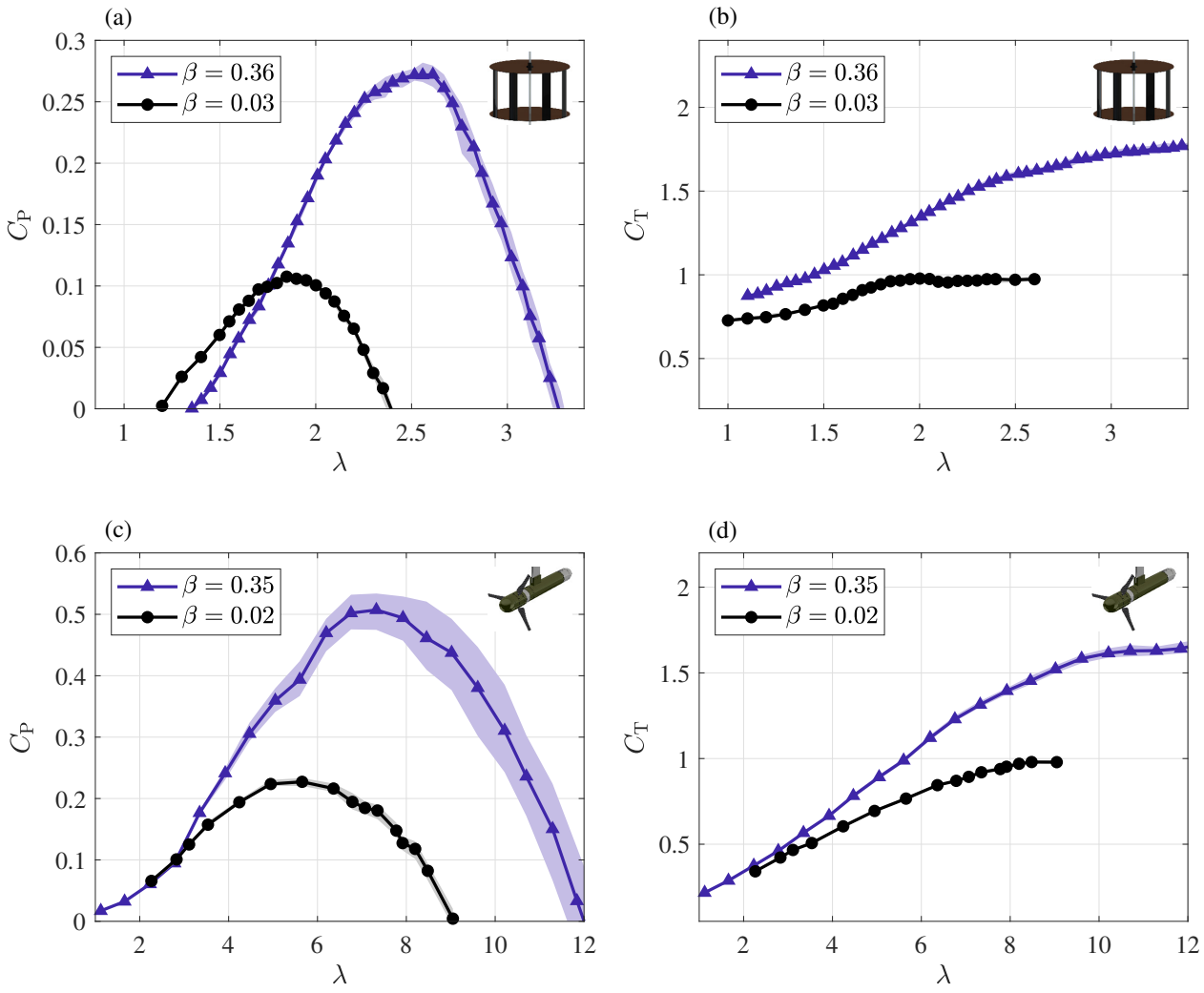

Figure 5.4: Confined and unconfined power and thrust coefficients for the cross-flow (a, b) and axial-flow (c, d) turbines. The shading represents the measurement uncertainty at each tip-speed ratio. In some instances, the uncertainty range is smaller than the plot markers, and therefore not visible.

X/D	0.75	1.25	1.75	2.25
Cross-flow turbine	1.10	1.14	1.16	1.19
Axial-flow turbine	1.11	1.11	1.11	1.06

Table 5.1: Dimensionless wake area (A_1/A_t) at four streamwise locations.

had worked perfectly, the corrected data would have collapsed onto the unconfined performance curve. Although some discrepancies remain, the correction generally accounts for the effects of blockage on the power and thrust coefficients of both turbines.

Werle's Method

Figure 5.6 shows the application of Werle's correction to the confined performance data. Although the correction performs adequately for the magnitude of the power coefficient, it significantly overcorrects the thrust coefficient and tip-speed ratio. As mentioned in Section 5.3.2, the tip-speed ratio correction given by Equation (5.38) is not consistent with the rest of the derivation. However, the modified form given by Equation (5.40) further reduces the corrected tip-speed ratios, increasing the disagreement between corrected and unconfined performance (results not shown).

Houlsby et al.'s Method

Figure 5.7 presents the results of Houlsby et al.'s correction which, unlike the previous two methods, allows for a deformable free surface. The results of this correction are almost identical to those from Barnsley and Wellicome's method (Figure 5.5).

Mikkelsen and Sørensen's Method

Figure 5.8 gives the results of applying Mikkelsen and Sørensen's correction. Unlike the previous methods, a single operating point (peak C_P) was evaluated rather than the full C_P

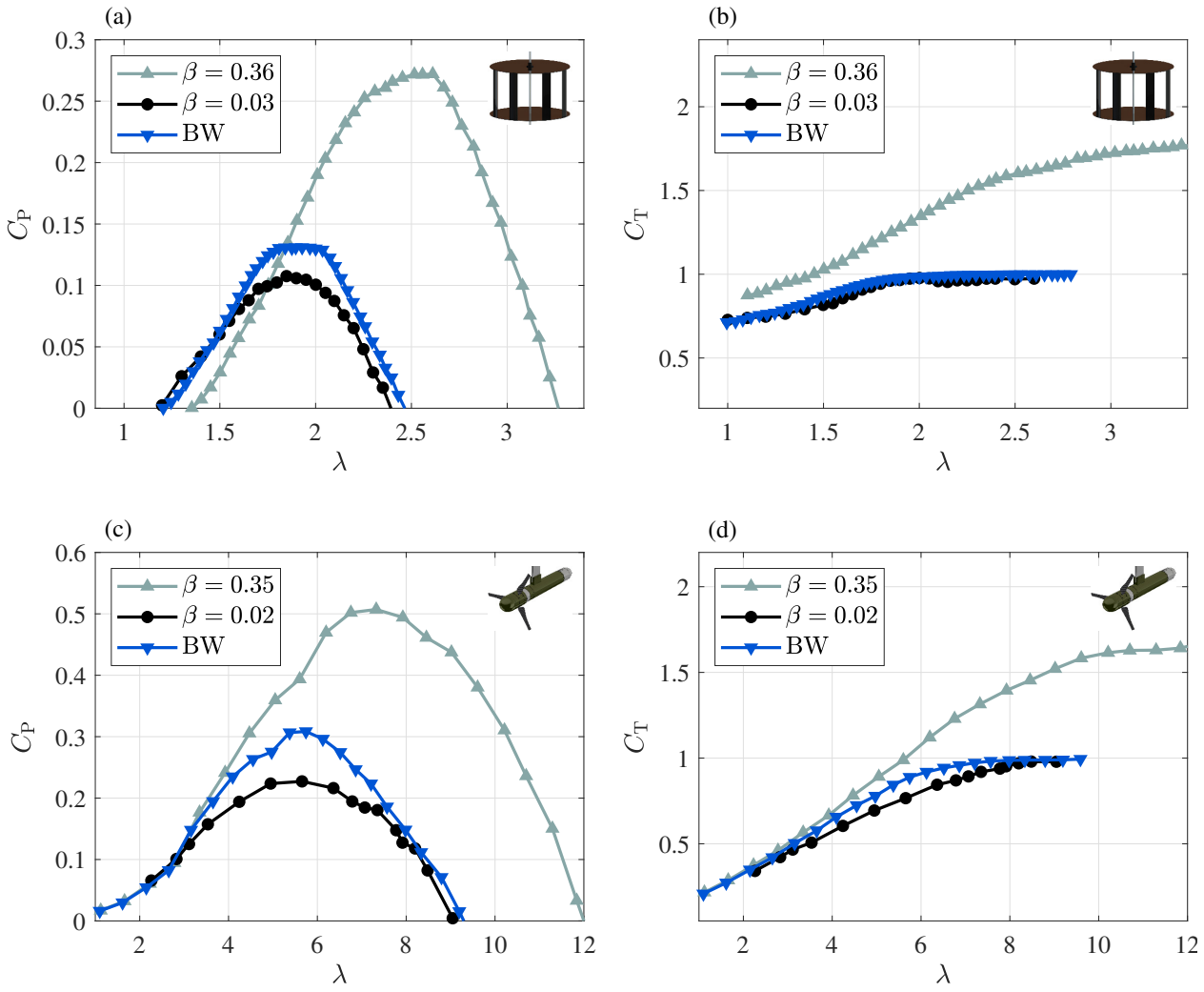

Figure 5.5: Application of Barnsley and Wellicome's correction to the confined performance data from the cross-flow (a, b) and axial-flow (c, d) turbines.

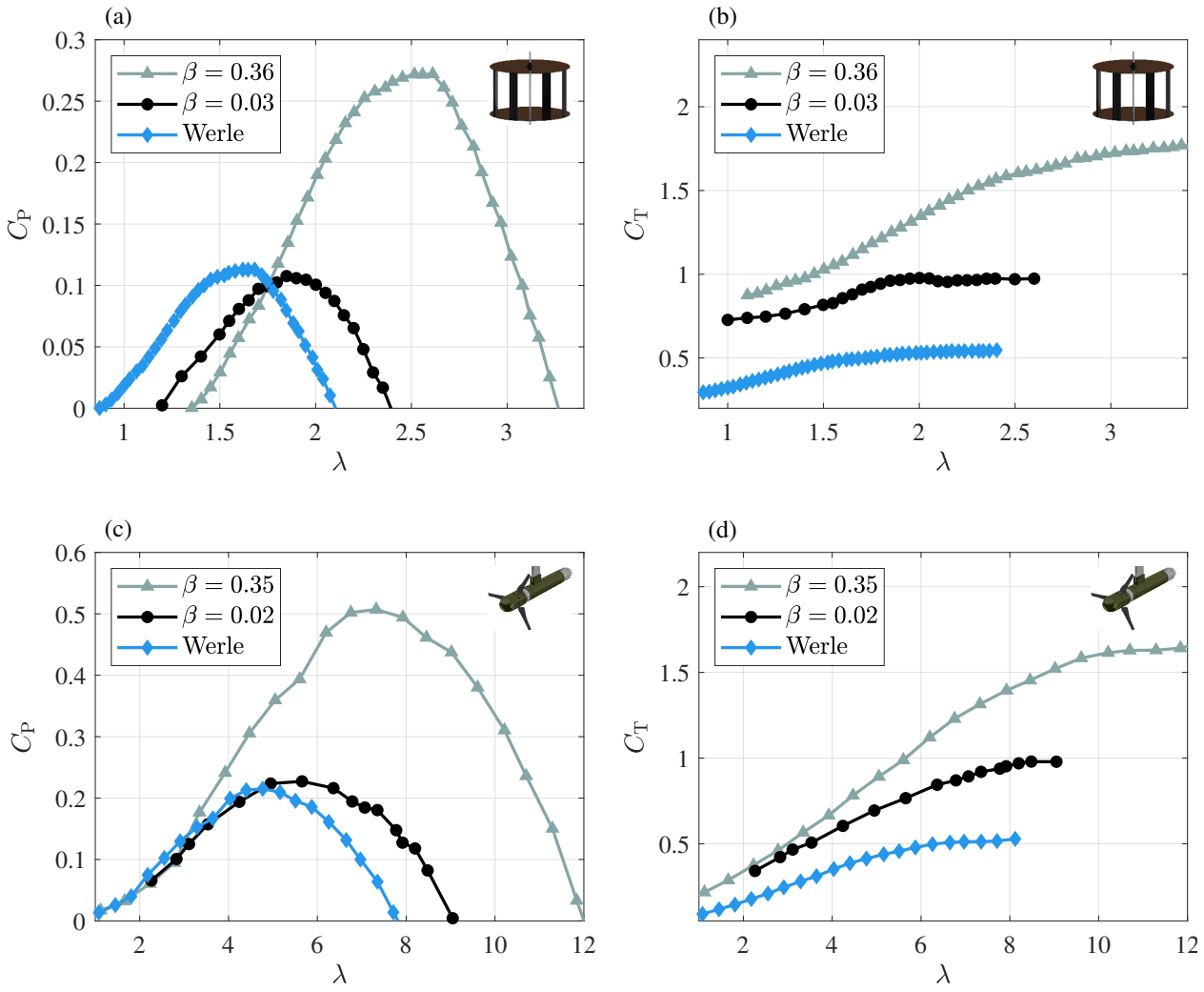

Figure 5.6: The results of applying Werle's correction to the confined performance data from the cross-flow (a, b) and axial-flow (c, d) turbines.

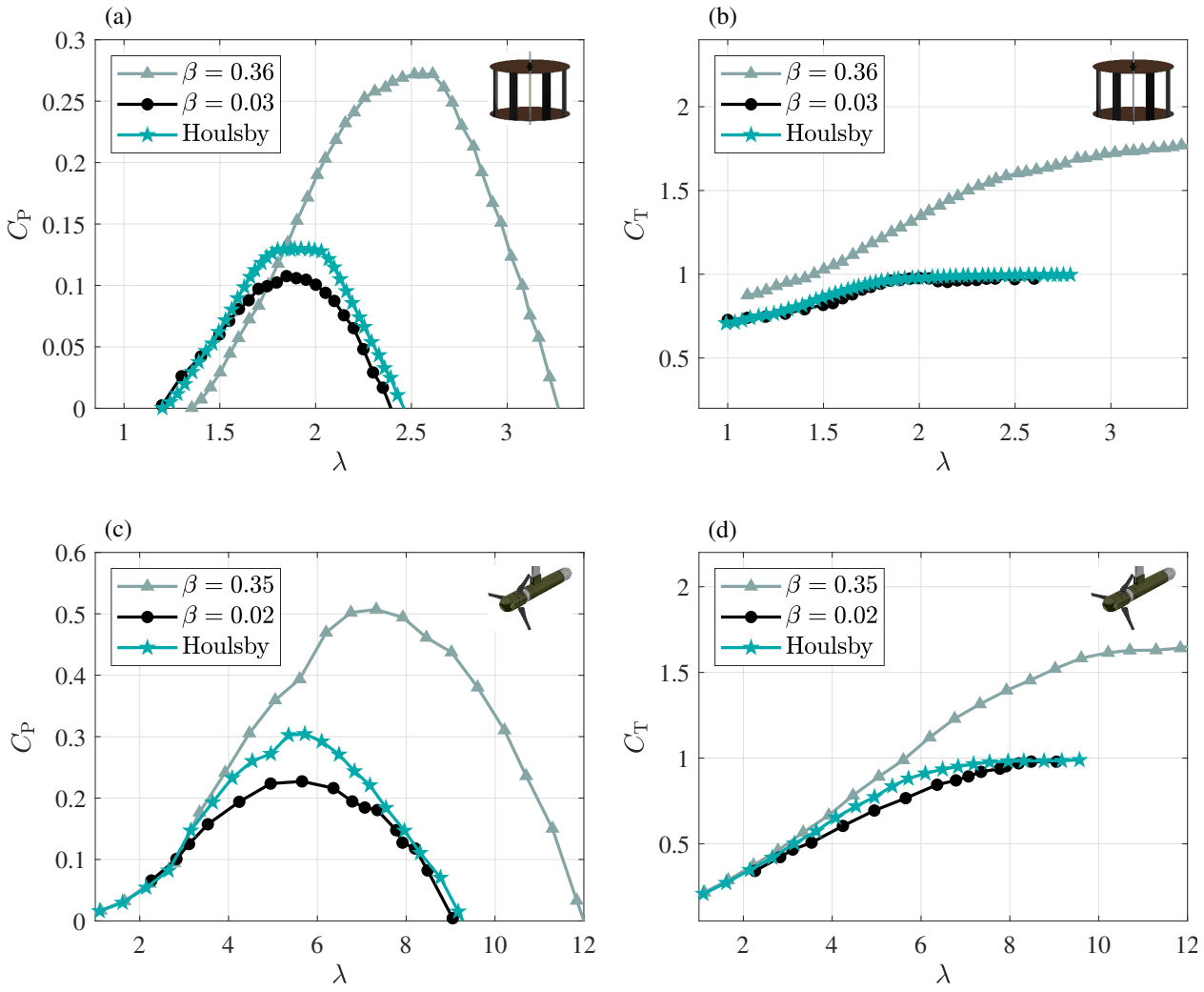

Figure 5.7: Houlsby et al.'s method applied to the confined performance data from the cross-flow (a, b) and axial-flow (c, d) turbines.

and C_T curves, as wake data could not be collected in a timely manner for all operating conditions. All of the values for A_1/A_t presented in Table 5.1 were evaluated, and it was determined that $X/D = 2.25$ gave the least error for the cross-flow turbine and $X/D = 1.75$ gave the least error for the axial-flow turbine. For comparison, the results of applying the other corrections to the peak C_P of each turbine are also shown in Figure 5.8.

5.5 Evaluation of Blockage Corrections

The errors for all blockage corrections applied to both turbines are summarized in Figure 5.9. For reference, the equivalent calculation for the confined, uncorrected data (i.e., performance change as a consequence of blockage) is given as well. The ratio of A_s to A_t was less than 5% under confined conditions for both turbines, so alternative definitions of the blockage ratio, such as $\beta = A_t/(A_c - A_s)$, do not significantly affect the values shown in Figure 5.9.

5.5.1 Full Performance Curve

As quantified in Figure 5.9, Houlsby et al.'s and Barnsley and Wellicome's methods are relatively effective at correcting for blockage over the entire range of tip-speed ratios considered for both turbines. These corrections give almost identical results, with Houlsby et al.'s method performing slightly better overall. This outcome is to be expected, given that Houlsby et al.'s analytical model is a generalization of the one used by Barnsley and Wellicome to allow for a deformable free surface. Since no significant free surface deformation was observed during these experiments, it is unsurprising that the two methods yield similar outcomes.

Werle's method produces mixed results. The C_P correction performs better than or equal to Houlsby et al.'s and Barnsley and Wellicome's for both turbines and the C_T and λ corrections perform significantly worse. These outcomes are consistent with the original derivation [81]. As mentioned in Section 5.3.2, Werle's correction begins with the analytical expressions for $C_{P,max}$, $C_{T,max}$, and $u_{t,max}$ in both confined and unconfined flow [14, 30, 42]. These expressions yield corrections that are applicable only at the peak C_P. To generalize

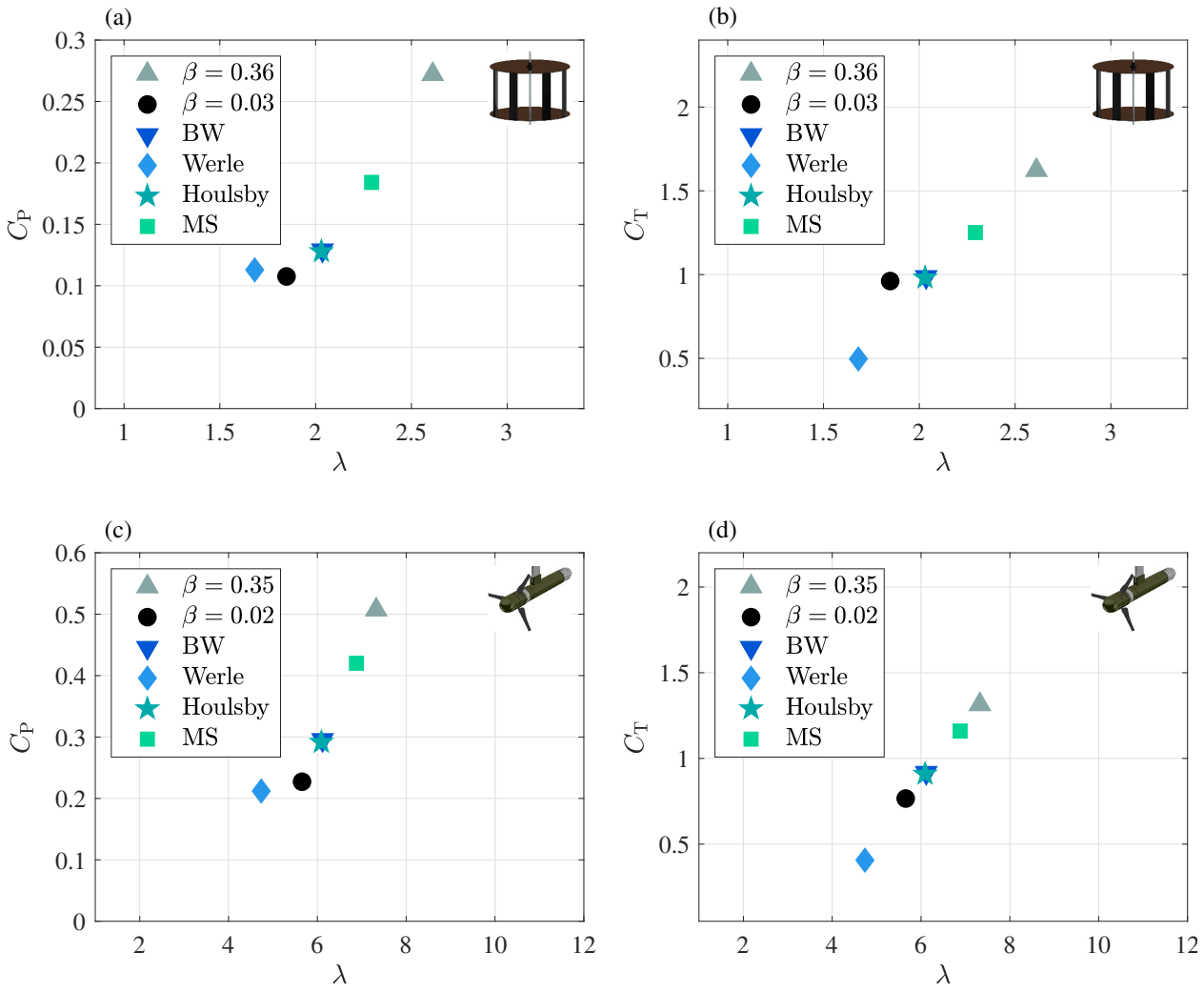

Figure 5.8: Overall correction performance at the tip-speed ratios corresponding to peak C_P for the cross-flow (a, b) and axial-flow (c, d) turbines. Mikkelsen and Sørensen's correction used the downstream wake measurements that gave the closest correction to unconfined data. The closer the corrected performance is to unconfined measurements (black circle), the more effective the correction. Uncorrected performance is shown for reference (gray triangle).

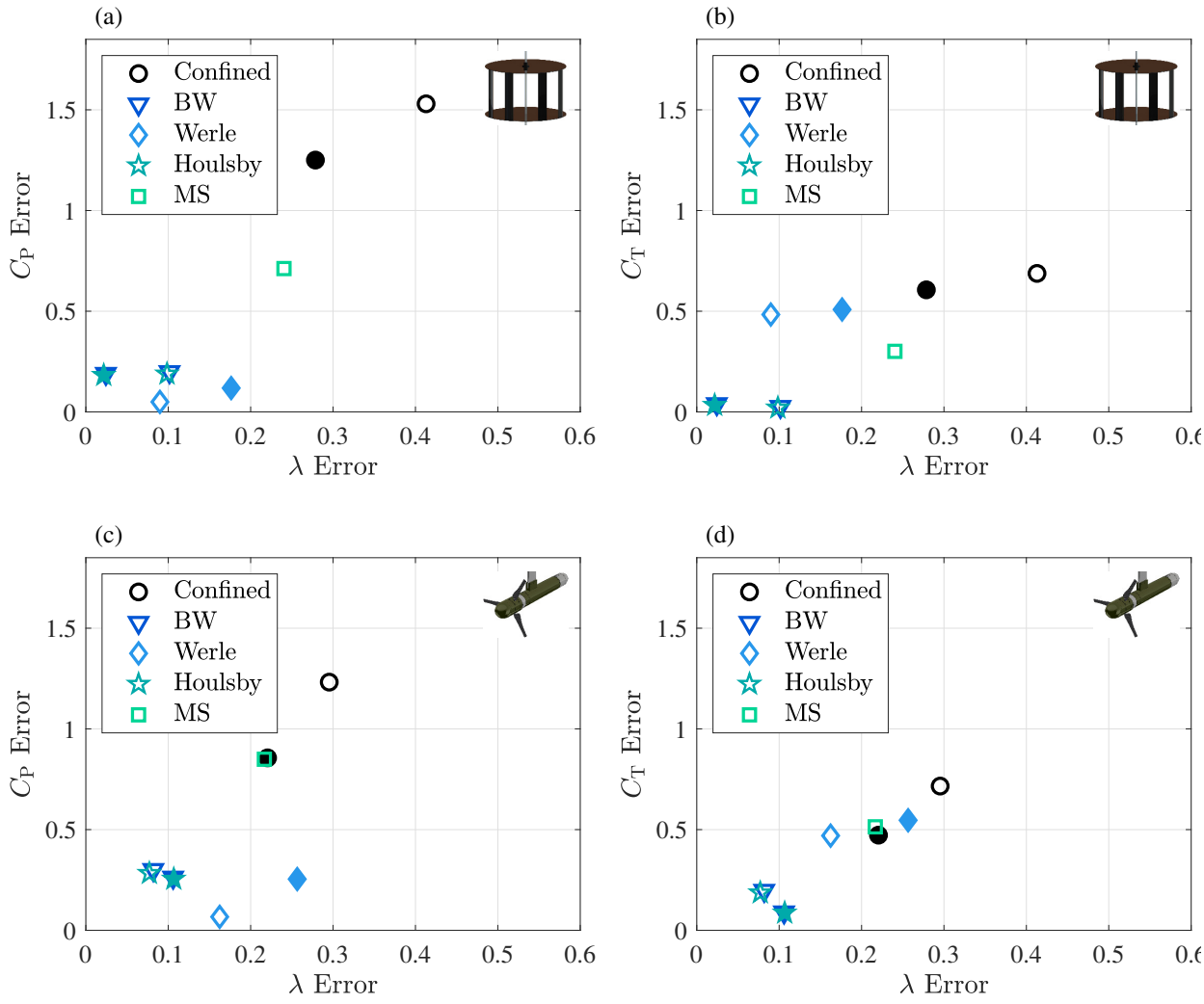

Figure 5.9: Blockage correction error for the cross-flow (a, b) and axial-flow (c, d) turbines, relative to unconfined data. Filled markers indicate error averaged over full curves, while open markers indicate error at peak C_P.

the corrections to other operating conditions, the approximations given in Equations (5.26)-(5.28) are used. However, the approximation for C_P given by Equation (5.26) is the only expression that Werle mathematically justifies in the original derivation. This is done using a "correlation scheme" that is attributed to Werle and Presz [82]. Repeating this method for C_T and u_t reveals that the approximations given in Equations (5.27) and (5.28) are less well justified than Equation (5.26). This could explain why Werle's C_P correction performs better than the C_T or λ corrections.

5.5.2 Peak C_P

Considering only the results for the peak C_P allows a comparison of all four blockage corrections. The errors in Houlsby et al.'s, Barnsley and Wellicome's, and Werle's methods follow the same trends as the full curve error. Mikkelsen and Sørensen's method yields much higher errors than either Houlsby et al.'s or Barnsley and Wellicome's correction. This result is unexpected given that Barnsley and Wellicome's and Mikkelsen and Sørensen's corrections use the same set of equations and differ only in their choice of input variables (thrust versus wake area). The poor performance of Mikkelsen and Sørensen's method is likely due to the difficulty of measuring A_1 in experiment. The lateral traverses shown in Figure 5.1 captured the size of the wakes in only one dimension, while wakes have a higher dimensional structure (e.g., Bachant and Wosnik [3], for cross-flow turbines). Additionally, due to experimental limitations, the wake data were collected at water temperatures of 11°C for the cross-flow turbine and 17°C for the axial-flow turbine, compared to 22°C and 20°C for the performance data. It is uncertain how these changes in temperature, which impact the Reynolds number, would affect the wake, though prior results have suggested that wake structure reaches Reynolds independence sooner than turbine performance [21]. Compounding the difficulty of accurately measuring A_1, the correction is quite sensitive to this variable. An error of $\pm 10\%$ in the value of A_1 produces an error of approximately $\pm 32\%$ in Mikkelsen and Sørensen's C_P correction. By comparison, introducing a $\pm 10\%$ error into the value of T produces an error of $\pm 12\%$ when applying Barnsley and Wellicome's C_P correction to the same data.

Although Mikkelsen and Sørensen's correction did not perform well in this study, its performance should improve if a better estimate of A_1 were available. However, in experiments, it is unlikely that such a measurement would be simpler than measuring the rotor thrust. The fact that Barnsley and Wellicome's and Mikkelsen and Sørensen's corrections give different results, despite solving the same equations, illustrates that the choice of input variables can significantly influence the magnitude of the correction.

5.5.3 Impact of Reynolds Number

Due to experimental limitations, both turbines were operated in a transitional regime, where performance was dependent on Reynolds number [4, 21, 50]. As discussed in Section 4.4.2, because blockage increases the streamwise flow speed through the rotor plane, the turbines experienced an elevated "local" Reynolds number (Re_ℓ, calculated using u_t as the characteristic velocity) under confined conditions, even as the free-stream Reynolds number was held constant. Specifically, momentum theory suggests that, due to blockage, the Re_ℓ of the cross-flow turbine increased by about 9% and the Re_ℓ of the axial-flow turbine by about 7%. Although these increases are relatively small, they can meaningfully change turbine performance, as illustrated in Chapter 4. Because blockage corrections are implicitly Reynolds independent, changes in Re_ℓ are likely to increase the correction error when experiments are conducted below Reynolds independence. This provides two further insights into the accuracy of Houlsby et al.'s and Barnsley and Wellicome's methods reported here.

First, both Houlsby et al.'s and Barnsley and Wellicome's corrections are more effective for the cross-flow turbine than the axial-flow turbine. This is unexpected, considering blockage corrections were originally derived for axial-flow devices. Furthermore, prior work has indicated that Barnsley and Wellicome's correction performs better for axial-flow turbines [40]. This discrepancy may be explained by Reynolds dependence. Although the axial-flow turbine saw a slightly smaller increase in local Reynolds number under confined conditions, it was operating at a lower free-stream Reynolds number ($\mathrm{Re} = 14,000$) than the cross-flow turbine ($\mathrm{Re} = 31,000$) and was likely further from Reynolds independence.

Therefore, the change in Re_ℓ is expected to have a larger effect on the axial-flow turbine. To evaluate this hypothesis, it would be necessary to characterize trends in the performance of both turbines as a function of Reynolds number, which was beyond the scope of this study.

Second, Houlsby et al.'s and Barnsley and Wellicome's corrections are more accurate for the thrust coefficient than the power coefficient. This may also be due, at least in part, to Reynolds number dependency. In unrelated experiments, both turbines were tested in the UW flume at two different transitional Reynolds numbers (see Figure 5.10). The cross-flow turbine's power coefficient changed significantly with Reynolds number around the conditions referenced in this study. However, the thrust coefficient was relatively insensitive to Reynolds number, such that corrections for C_T would not be significantly impacted by the changes in Re_ℓ. The axial-flow turbine performance followed a similar trend.

5.5.4 Impact of Model Limitations

Axial momentum theory applied to an actuator disk is a significant simplification of real turbine dynamics. As noted by Houlsby and Vogel [37], axial momentum theory is not restricted to turbines of a certain shape. However, the assumptions that underpin the theory, discussed in Section 5.3.1, do not hold for most real turbines, either axial-flow or cross-flow. Several past studies have noted that these limitations reduce blockage correction efficacy [2, 31, 40, 71]. Here, we discuss several of these limitations in the context of our experimental results.

With the exception of Werle's method, the thrust coefficient corrections are more effective than the power coefficient corrections. Axial momentum theory does not account for any rotation, either of the turbine or of the wake. While expressions for thrust can be derived without this information, power is equal to torque multiplied by the angular velocity of the turbine. Therefore, power from a real turbine requires rotation and an exchange of angular momentum between the rotor and the flow. Most blockage corrections based on axial momentum theory assume power is the product of thrust and the streamwise flow speed through the rotor. This expression is inaccurate for several reasons. First, the power

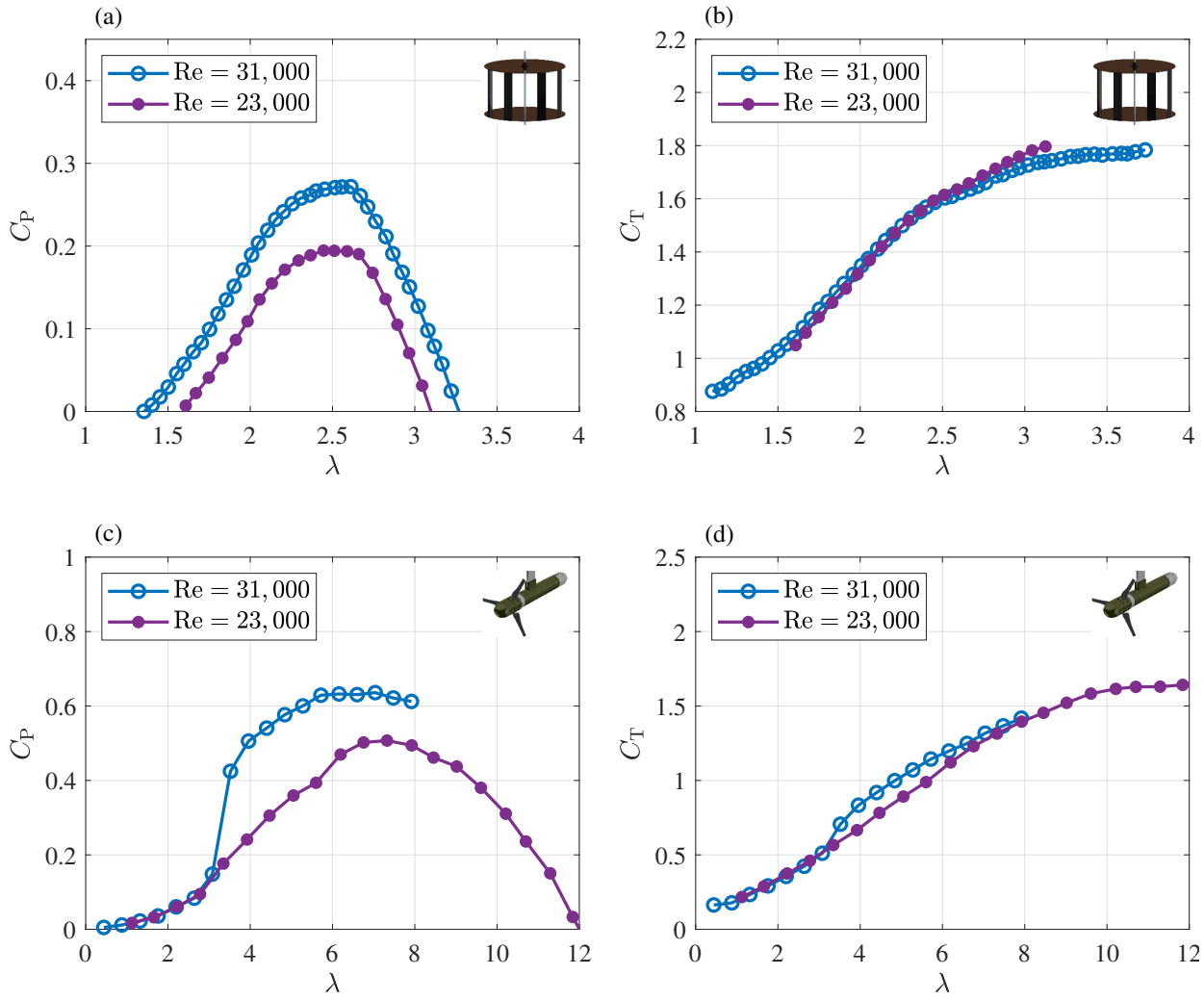

Figure 5.10: Power and thrust coefficient curves for the cross-flow (a, b) and axial-flow (c, d) turbines at multiple transitional Reynolds numbers in the UW flume. The power coefficients are more sensitive to variations in Reynolds number than the thrust coefficients.

absorbed by an actuator disk does not account for the presence of rotational kinetic energy in the wake. Second, although axial momentum theory assumes a frictionless turbine, drag on rotating components reduces the torque produced by the rotor. This is accounted for in measured torque but is not reflected in axial momentum theory. Finally, thrust measurements may include components of the system that do not produce torque, such as the hub or support structure. These factors mean that real power is not generally the product of T and u_{t}. Therefore, because thrust can be expressed directly by axial momentum theory, whereas power can only be estimated, it is expected that corrections based on axial momentum theory would perform better for C_{T} than for C_{P}. This hypothesis is supported by the results of our experimental assessment (Figure 5.9). To overcome this limitation, a blockage correction originating from angular momentum theory would be required.

Examining the limitations of axial momentum theory may also explain why, as shown in Figures 5.5 and 5.7, the C_{P} correction is more effective at lower and higher tip-speed ratios than in the center of the curve. As discussed previously, axial momentum theory neglects wake rotation. Therefore, it is expected that the corrections will perform better at operating conditions with minimal wake rotation. Because wake rotation is a reaction to the torque of the rotor, operating conditions that produce less torque also cause less wake rotation. These operating conditions correspond to lower and higher tip-speed ratios where torque and, consequently, C_{P} are reduced.

The fact that the corrections are based on axial momentum theory also has interesting implications for the tip-speed ratio. Glauert [32] specifies that the angular velocity of the turbine and the flow speed through the rotor remain constant between the confined and equivalent unconfined conditions. With wake rotation neglected, this justifies the assertion that the thrust remains constant as well. However, because the correction is based on axial momentum theory, the calculation of V_0' does not depend on ω. Aside from providing a justification for constant thrust between confined and unconfined conditions, the requirement that $\omega' = \omega$ is used only to derive Equation (5.12), the tip-speed ratio correction. Because axial momentum theory does not directly address rotation, prior work [71] has questioned

whether the equivalent unconfined condition should be that which gives the same angular velocity or the same tip-speed ratio. We chose to assume $\omega' = \omega$ and correct the tip-speed ratio according to Equation (5.12), which is in line with Glauert's statements and gives good agreement with the unconfined results.

5.5.5 Maskell's Bluff Body Correction

Another relevant restriction of axial momentum theory is that it becomes invalid when the unconfined thrust coefficient exceeds unity, as this corresponds to reversed flow in the wake. As shown in Figure 5.4, the unconfined thrust coefficients of the cross-flow and axial-flow turbines tested in this study were within this threshold. However, this is not always the case, motivating the use of a blockage correction based on bluff body theory for highly loaded turbines. As discussed in Section 5.1, two prior studies applied a blockage correction based on the theory of Maskell [46] to an axial-flow turbine [83] and a cross-flow turbine [40]. Both studies found that Maskell's correction performed better than actuator disk methods for highly loaded turbines.

Maskell observed that blockage corrections based on actuator disk theory were inadequate for objects that produced a bluff body wake. Maskell's blockage correction is based on momentum theory coupled with an empirical description of wake behavior. The derivation assumes that the bluff body wake is axisymmetric, the flow is uniform and unidirectional, and the blockage ratio is small, such that higher-order terms of β can be neglected. The correction calculates the free-stream velocity ($V'_{0,\mathrm{b}}$) that, in an unconfined flow, would produce the same flow speed past the object ($u_{2,\mathrm{b}}$). Note that $u_{2,\mathrm{b}}$ is the velocity of the shear layer downstream of the bluff body and is distinct from u_2, the velocity of the bypass flow in actuator disk theory. Given measurements of $u_{2,\mathrm{b}}$, $V_{0,\mathrm{b}}$, C_T, and β, the ratio $u'_{2,\mathrm{b}}/V'_{0,\mathrm{b}}$ can be calculated according to

$$\frac{(u_{2,\mathrm{b}}/V_{0,\mathrm{b}})^2}{(u'_{2,\mathrm{b}}/V'_{0,\mathrm{b}})^2} = 1 + \frac{C_\mathrm{T}\beta}{(u'_{2,\mathrm{b}}/V'_{0,\mathrm{b}})^2 - 1}. \tag{5.44}$$

With $u'_{2,\mathrm{b}}/V'_{0,\mathrm{b}}$ known, the equivalent unconfined thrust coefficient can be estimated as

$$C'_{\mathrm{T}} = C_{\mathrm{T}} \frac{(u'_{2,\mathrm{b}}/V'_{0,\mathrm{b}})^2}{(u_{2,\mathrm{b}}/V_{0,\mathrm{b}})^2}. \tag{5.45}$$

Since $u_{2,\mathrm{b}} = u'_{2,\mathrm{b}}$, Equation (5.45) reduces to

$$C'_{\mathrm{T}} = C_{\mathrm{T}} \left(\frac{V_{0,\mathrm{b}}}{V'_{0,\mathrm{b}}} \right)^2. \tag{5.46}$$

Although this correction is similar in form to Equation (5.11), the unconfined free-stream velocity is that which gives the same value of $u_{2,\mathrm{b}}$ between confined and unconfined conditions, rather than u_{t}. To apply Maskell's correction as presented, it is necessary to have a measurement of $u_{2,\mathrm{b}}$. As for Mikkelsen and Sørensen's correction, it would be difficult to identify an unambiguous location to sample this value in an experimental turbine.

Rather than applying Maskell's method exactly as formulated, past studies have applied a correction inspired by the theory. Whelan et al. [83] assumed that, when operating in a highly loaded condition, a turbine responds primarily to the bypass flow rather than the flow through the rotor plane. This allows C_{T} and λ to be corrected as

$$C'_{\mathrm{T}} = C_{\mathrm{T}} \left(\frac{V_0}{u_2} \right)^2, \tag{5.47}$$

$$\lambda' = \lambda \left(\frac{V_0}{u_2} \right). \tag{5.48}$$

Neither Whelan et al. [83] nor Kinsey and Dumas [40] attempt to estimate C'_{P}. Equations (5.47) and (5.48) are distinct from Maskell's original correction, in that they use the bypass velocity (u_2) as a correction factor, rather than the unconfined free-stream speed ($V'_{0,\mathrm{b}}$). Furthermore, to apply Equations (5.47) and (5.48), Whelan et al. and, subsequently, Kinsey and Dumas estimated u_2 using actuator disk methods, despite assuming the operating conditions are such that actuator disk methods are invalid. Nevertheless, both past studies found that Equations (5.47) and (5.48) were more effective than actuator disk corrections when the rotors were more heavily loaded.

As the bypass flow adjacent to the rotor was not sampled in our experiments, we followed the method of Whelan et al. to correct C_{T} and λ using a Maskell-inspired approach. For

the sake of investigation, we also corrected C_{P} as

$$C'_{\mathrm{P}} = C_{\mathrm{P}}\left(\frac{V_0}{u_2}\right)^3. \tag{5.49}$$

The results of applying Equations (5.47)-(5.49) to our confined performance data are shown in Figure 5.11. The bypass velocity was estimated iteratively according to the method of Houlsby et al. Overall, Maskell's correction performs better at intermediate tip-speed ratios and worse at higher tip-speed ratios, which is in contrast to the results obtained by Whelan et al. and Kinsey and Dumas. Given that $u_2 > V'_0$, this approach makes a larger correction, which reduces some of the error we attribute to Reynolds dependence at the peaks of the C_{P} curves. The poor performance at higher tip-speed ratios is unexpected, as the thrust coefficients for both turbines in confined flow are similar to the values reported in Whelan et al. and Kinsey and Dumas. These mixed results suggest that a bluff body correction may be effective, but is not guaranteed to be more effective, even when the rotor is highly loaded. The physical justification for use is generally weaker than for axial momentum theory, and obtaining a correction factor directly in experiment is likely to be similarly problematic to obtaining the wake cross-sectional data necessary to apply Mikkelsen and Sørensen's correction. Consequently, a Maskell-inspired correction applied to experimental data may have a relatively large unquantified uncertainty. Finally, a Maskell-inspired correction does not resolve the fundamental mismatch between real turbine power and power absorbed by an actuator disk. This being said, prior studies [1, 21] have identified similarities between some turbine and bluff body wakes, suggesting that blockage corrections incorporating elements of bluff body theory could be more effective than those based purely on axial momentum.

5.5.6 Recommended Blockage Corrections

Analytical blockage corrections based on axial momentum theory are imperfect and can only provide estimates of the equivalent unconfined condition for performance data collected at high blockage. Although axial momentum theory solves for thrust directly, an approximate expression for power is required. Here, we demonstrate that for relatively high blockage,

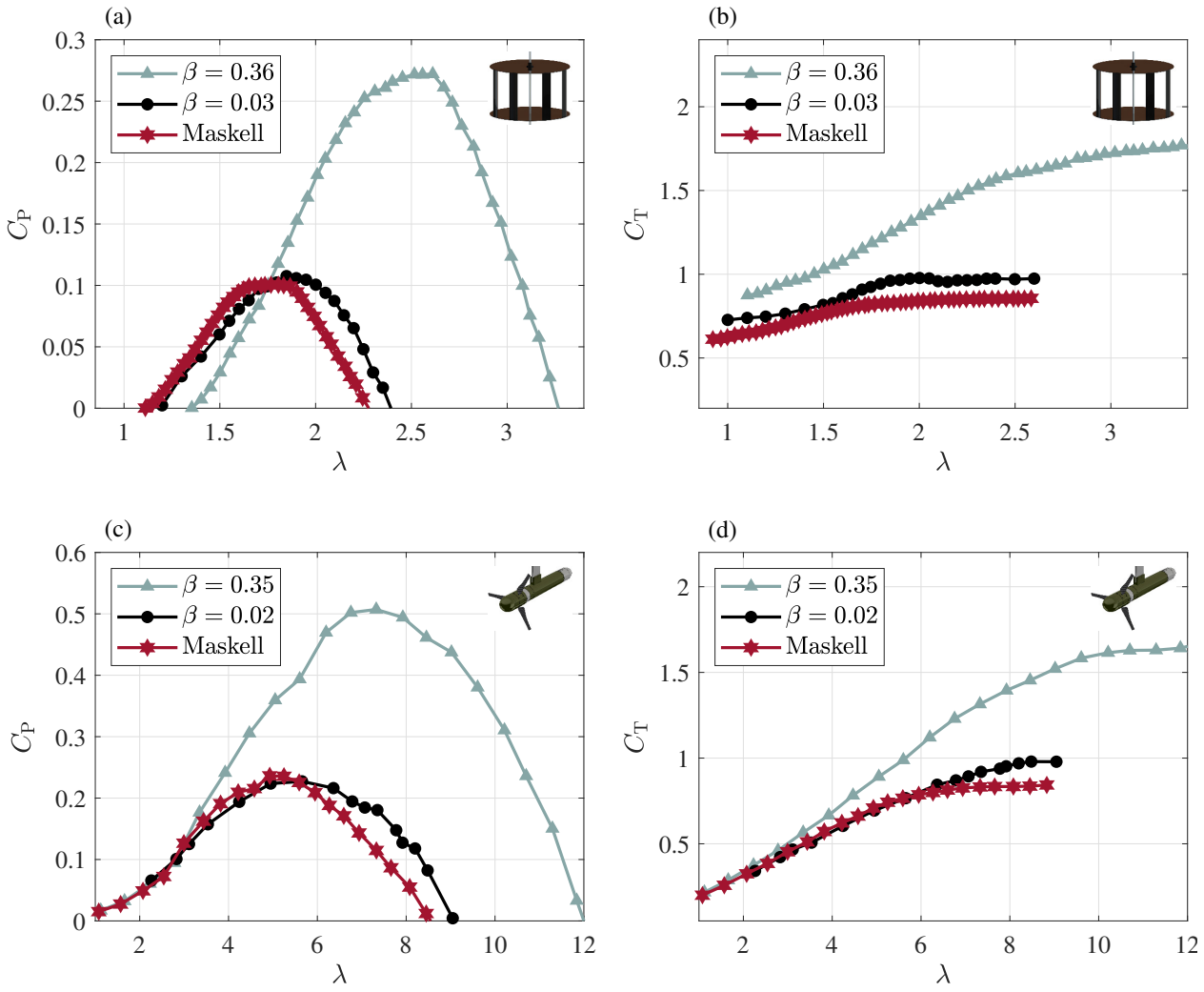

Figure 5.11: Application of a blockage correction inspired by the bluff body theory of Maskell to the confined performance data from the cross-flow (a, b) and axial-flow (c, d) turbines.

this leads to higher error in the C_P correction, which is unfortunate, as the power output of a turbine is often of greater interest than the loading. Despite the limitations of these methods, they do reduce the effects of blockage on performance data. Encouragingly, two of the methods resulted in less than 20% mean percentage error for the power coefficient of the cross-flow turbine tested at a blockage ratio of 0.36, experimental conditions that resulted in a change in the local Reynolds number and likely violated many of the assumptions of axial momentum theory. The same two methods gave less than 30% mean percentage error for the power coefficient of the axial-flow turbine tested at a blockage ratio of 0.35. However, the errors shown in Figure 5.9 are specific to the turbines and test conditions in this study and should not be taken as indicative of the error associated with these blockage corrections for other turbine geometries or test conditions.

Of the corrections evaluated, we recommend the methods presented by Houlsby et al. and Barnsley and Wellicome. Houlsby et al.'s correction allows for a deformable free surface and gave slightly better results for this study, even though no significant free surface effects were observed. If thrust measurements are not available, but detailed wake data are, Mikkelsen and Sørensen's correction may be appropriate. However, given the correction's sensitivity to the wake area, we caution against general use in experiments. Even though Werle's correction performed best for the power coefficient, we do not recommend this method, due to inconsistencies in the underlying assumptions and poor performance for the tip-speed ratio and thrust coefficient. Corrections based on bluff body theory, such as the Maskell-inspired correction applied by Whelan et al. and Kinsey and Dumas, may be appropriate when methods based on axial momentum theory fail to converge but should be used with caution.

5.6 Conclusions

This study experimentally examined the effects of blockage on the performance of a cross-flow and an axial-flow turbine. Both turbines were characterized under conditions of high blockage and negligible blockage, while other significant parameters were held approximately constant.

Overall, the effects of increased blockage on the turbines' power and thrust coefficients were consistent with prior investigations. These data were used to evaluate the performance of analytical blockage corrections for both turbine archetypes. Four of the five blockage corrections considered were based on axial momentum theory applied to an actuator disk in confined flow and followed the original propeller blockage correction presented by Glauert [32]. A correction based on momentum theory applied to a bluff body [46] was also evaluated. Interestingly, and in contrast to some prior results, we observed that the corrections were more effective for the cross-flow turbine than the axial-flow turbine. We hypothesize that this may be a consequence of changes in the local Reynolds number associated with our relatively high experimental blockage. This indicates that additional care should be taken when applying blockage corrections to data collected at transitional Reynolds numbers, which are common in a laboratory setting.

Our results also demonstrate that corrections for the thrust coefficient performed better than corrections for the power coefficient for both turbines. This is likely a combination of Reynolds number dependence and the limitations of axial momentum theory. Glauert's original blockage correction provides a system of equations, based on axial momentum theory, that can be used to calculate the equivalent unconfined free-stream velocity. However, his derivation does not explicitly mention how to apply this correction to measured performance coefficients. Subsequent studies have used his statement that the thrust, angular velocity of the turbine, and flow speed through the turbine remain constant between blocked and unblocked conditions to derive such corrections. However, this requires assuming that the power is given as the product of thrust and the flow speed through the turbine, which is inaccurate for real turbines. So, while thrust is calculated directly from axial momentum theory, power must be approximated, yielding higher error in the corrected power coefficients.

Despite the limitations of axial momentum theory, we have shown that analytical blockage corrections can give acceptable results for experimental data. However, the most effective way to eliminate blockage effects is to characterize turbine performance under approximately unconfined conditions, such that a blockage correction is unnecessary. Unfortunately, the

model scales needed to reduce the effects of blockage are often at odds with the scales needed to achieve Reynolds independence. Large facilities allow testing at both low blockage ratios and high Reynolds numbers but present challenges for collecting well-controlled, high resolution measurements. Due to these limitations, certain experiments will necessarily be conducted in smaller facilities, and corrections will be required to account for the effects of blockage.

Based on our results, in addition to our evaluation of the corrections' ease of application and mathematical robustness, we recommend the methods presented by Barnsley and Wellicome [8] and Houlsby et al. [38]. We also note that the errors shown in Figure 5.9 are specific to this study, and there is no guarantee that these corrections will give satisfactory results for an arbitrary test condition. Our analysis suggests that a new blockage correction that accounts for rotation and better describes highly loaded turbines could be more effective and is an area deserving of future efforts.

Chapter 6

BLOCKAGE EFFECTS ON WAKE

This chapter contains content from Ross and Polagye [64], which has been submitted to the *Journal of Ocean Engineering and Marine Energy*. Portions of the article have been edited to avoid redundancy. The objective of this chapter is to evaluate the effects of blockage on the wake of a current turbine to inform the intentional use of this scaling effect to improve turbine performance.

6.1 Introduction

As discussed in Chapters 4 and 5, flow confinement, or blockage, can significantly augment the power output of current turbines [23, 25, 30, 31, 34, 37, 41, 54, 69, 70]. Chapter 5 focuses on accurately accounting for these effects at model scales to improve the extrapolation of laboratory results to larger scales. However, blockage effects can be used advantageously at full scale to improve the performance of current turbines operating in arrays. Naturally confined flows, such as rivers and tidal channels, are of particular interest for high blockage arrays. There has been significant research conducted on array design, and multiple studies have developed models to predict and optimize the power output from arrays of current turbines operating in confined channels [17, 18, 22, 24, 26, 30, 36, 44, 45, 55, 56, 58, 70, 77, 78, 80].

The effects of blockage on an individual turbine's power output have been explored analytically [30, 37], numerically [23, 34, 40, 41, 54, 69, 70], and experimentally [6, 11, 15, 25, 31, 48, 62, 67]. However, to inform the design of high blockage arrays, the influence of flow confinement on wake dynamics and channel energetics must also be considered. Prior work has indicated that blockage can affect the size of a turbine's wake and alter the streamwise flow

speeds through and around the rotor [11, 23, 30, 37, 40, 41, 48, 69, 70]. The relative speed between the core flow and bypass flow determines the shear in the wake and the magnitude of turbulent kinetic energy (TKE) generated as the two flows mix downstream of the turbine. This TKE is ultimately converted to internal energy via viscous dissipation and represents a loss of upstream mechanical energy [37]. Because blockage affects both turbine power output and viscous dissipation, it influences the total mechanical energy that a turbine or array of turbines removes from a flow. The ratio of useful to total mechanical power removed from a flow is quantified by the basin efficiency (η), defined as

$$\eta = \frac{P}{P_{tot}}, \tag{6.1}$$

where P_{tot} is the total mechanical power removed from the flow, including viscous dissipation in the wake. Wake size, core and bypass flow speeds, and basin efficiency are important considerations in array design, as they affect spacing and overall resource utilization. Therefore, an understanding of blockage effects on wake dynamics and channel energetics is necessary to design high blockage arrays that optimize power output while minimizing the physical footprint and viscous dissipation losses.

Several analytical [30, 37] and numerical [23, 69, 70] studies have explored the effects of blockage on turbine wakes. The analytical model developed by Houlsby et al. [38] and expanded by Houlsby and Vogel [37] provides fundamental insight. This model, discussed in Chapter 5, is based on linear momentum actuator disk theory and quantifies flow confinement in terms of the blockage ratio. The effects of blockage on a turbine's wake can be illustrated with this model by increasing the blockage ratio while holding constant either the thrust on the turbine or the streamwise flow speed through the rotor. First, if thrust is held constant, higher blockage leads to a smaller wake and increased flow speeds through the rotor and in the core and bypass flows. Although the core and bypass flow speeds both increase with blockage, the *relative* velocity between the two flows decreases, decreasing shear and viscous dissipation, as well as increasing basin efficiency. Second, increasing blockage while holding the streamwise flow speed through the rotor constant results in a smaller wake, higher thrust,

and increased flow speeds in the core and bypass flows. Unlike the constant thrust case, the relative velocity between the core and bypass flows increases with blockage, yielding higher shear and more viscous dissipation, as well as decreasing the basin efficiency. It should be noted that although increased viscous dissipation often lowers basin efficiency, and vice versa, the two are not always indirectly correlated. The basin efficiency represents the fraction of total mechanical energy extracted from the flow that is captured by the turbine. Because the turbine power output changes with blockage, both the mechanical energy lost to viscous dissipation and the basin efficiency can increase as blockage increases.

While the analytical model presented by Houlsby and Vogel [37] provides useful insight, a turbine's response to increasing blockage is more complex than the response of an actuator disk. In general, increasing the blockage ratio causes the thrust and flow speed through the rotor to vary simultaneously [69]. The implications for the wake depend on how significantly the thrust changes, which is influenced by a turbine's specific design and operating point. Therefore, numerical and experimental studies of actual turbines are required to capture all the relevant dynamics. For example, a numerical study by Schluntz and Willden [70] investigated the effects of variable blockage and rotor design on turbine wakes. The authors optimized axial-flow turbine performance in an array at different blockage ratios by varying the rotor solidity. To maximize power output, rotor solidity increased with blockage. The streamwise flow speed through the turbines and the basin efficiency decreased with increasing blockage when comparing turbines optimized for specific blockage conditions. However, when comparing a single turbine design operating at peak power under all blockage conditions, the streamwise flow speed through the rotor and the basin efficiency increased with blockage. In both cases, the bypass flow speed increased. The basin efficiency worsened for the turbines optimized for blockage but improved for a single design because the thrust of the optimized turbines increased more significantly with blockage. This caused the relative velocity between the core and bypass flows to increase, with attendant increases in shear and viscous dissipation.

Schluntz and Willden further illustrated that blockage effects depend on a turbine's op-

erating point, defined by its tip-speed ratio, as well as its solidity. The authors found that turbines designed for low blockage conditions achieved peak power at higher tip-speed ratios when operating under highly blocked conditions. Because these turbines had a lower than optimal solidity, operating at higher tip-speed ratios allowed them to exert more thrust on the flow and extract more power. This highlights the fundamental principle that the effects of flow confinement depend on the blockage ratio *and* rotor thrust, which underpins why certain blockage corrections are more effective than others, as discussed in Chapter 5.

Although most of the past work in this area is either analytical or numerical, several studies have explored the effects of blockage on turbine wakes experimentally. McTavish et al. [48] tested an axial-flow turbine at blockage ratios between 0.06 and 0.26 in a laboratory flume and concluded that increasing blockage while operating at a fixed tip-speed ratio produced a smaller wake. Battisti et al. [11] tested a cross-flow turbine in closed and open wind tunnels, resulting in blockage ratios of near 0 and 0.10. They concluded that for a turbine operating at a fixed tip-speed ratio, increasing the blockage ratio increased the flow speeds through and around the rotor. The results of these experimental studies are consistent with the findings of past analytical and numerical work [23, 30, 37, 69, 70] and, notably, the trends are consistent regardless of whether the turbine under consideration is an idealized actuator disk, axial-flow turbine, or cross-flow turbine. However, both experimental studies focus on a single effect rather than comprehensively addressing blockage effects, and neither study addresses channel energetics (i.e., viscous dissipation in the wake). Furthermore, both studies investigate blockage effects at a constant tip-speed ratio, rather than the tip-speed ratio corresponding to peak power for each blockage condition. As demonstrated numerically by Schluntz and Willden [70], understanding how blockage influences a turbine's wake at peak power is likely of greater interest for optimizing array designs. Therefore, the objective of this work is to experimentally characterize the effects of blockage on the wake of a cross-flow turbine operating at peak power, with an emphasis on wake size, core and bypass flow speeds, and viscous dissipation.

6.2 Methods

Turbine performance and wake data were collected for a laboratory-scale cross-flow turbine operating at two different blockage ratios. The turbine used for these experiments is shown in Figure 3.1 (b) and described in Section 3.1. Its performance was characterized according to the process described in Section 3.3. To vary the blockage ratio, the turbine was tested in the UW flume and the BMSC flume, described in Section 3.2. Details of the dimensionless parameters and wake characterization are given in Sections 6.2.1 and 6.2.2.

6.2.1 Dimensionless Parameters

At both test facilities, the free-stream water depth was 0.60 m. The difference in channel width resulted in a blockage ratio of 0.14 in the BMSC flume and 0.36 in the UW flume, where the blockage ratio was defined according to Equation 5.1. The projected area of the support structure accounted for less than 5% of A_t.

To isolate the effects of blockage, it was necessary to hold the Reynolds and Froude numbers constant between experiments [4, 23, 50]. To maintain a constant Reynolds number, the free-stream velocity in both flumes was set to 0.5 m/s, and the water temperature was controlled to approximately 11°C. This resulted in a chord-based Reynolds number of 23,000 in both flumes. A free-stream velocity of 0.5 m/s and water depth of 0.60 m resulted in a Froude number of 0.20 in both flumes. Turbulence intensity, which has also been shown to impact turbine performance [16, 53], was 3% in the BMSC flume and 2% in the UW flume. By varying only the channel width between experiments, the Reynolds number, Froude number, and turbulence intensity were held approximately constant while the blockage ratio increased.

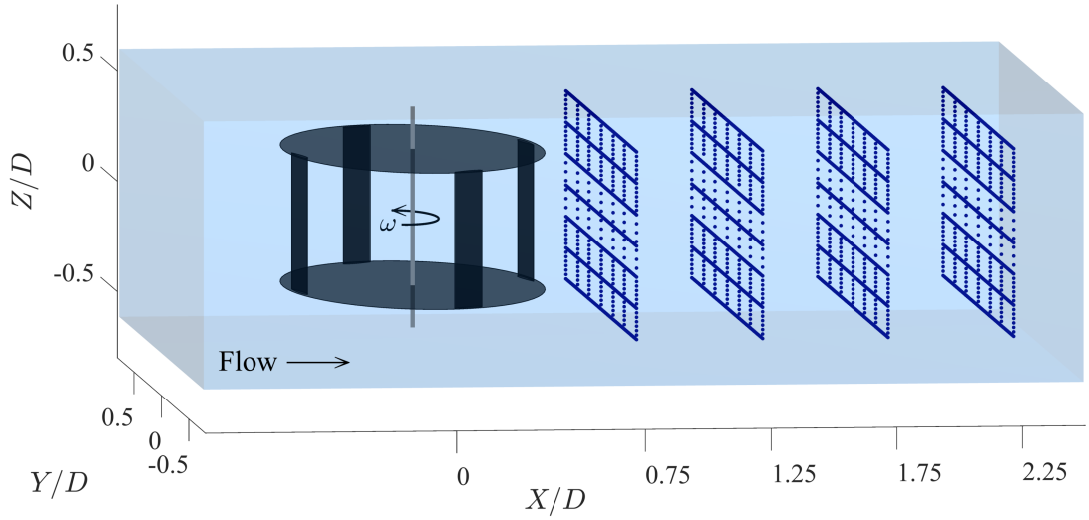

Figure 6.1: Rendering of the measurement grid used to collect wake data downstream of the turbine for the UW flume experiments. Each point on the grid corresponds to a location where velocity measurements were taken. The grid used for the BMSC experiments was similar.

6.2.2 Wake Characterization

Data Collection

For wake characterization, the turbine was operated at the tip-speed ratio corresponding to peak power. Three-dimensional velocity data were collected downstream of the turbine using a pair of ADVs mounted on a motorized gantry, as described in Section 3.4. The grid used for data collection in the UW flume is illustrated in Figure 6.1. In this diagram, the free-stream flow is moving from left to right, and the turbine is rotating in the counterclockwise direction when viewed from above. Variable grid spacing was used to achieve higher spatial resolution in the shear layer between the core and bypass flows. Along the gridlines shown, spacing is 0.01 m in the lateral direction and either 0.01 or 0.02 m in the vertical direction. Gridline separation is approximately 0.10 m in the lateral direction and 0.07 m in the vertical

direction. The first wake profile is $0.75D$ downstream of the center of the turbine, with subsequent profiles spaced $0.5D$ in the streamwise direction. The grid used for the BMSC flume was similar but extended further in the lateral direction to capture the entire wake area. For the BMSC flume experiments, gridlines in the lateral direction were approximately 0.13 m apart. Overall, the grid layouts balanced resolution against total acquisition time.

Data Analysis

Raw velocity time series from the ADVs were despiked using the method of Goring and Nikora [33]. Data points with a low correlation were discarded [66], and the mean values were replaced using a piecewise cubic polynomial interpolator. Less than 4% of wake data points from the UW experiments and less than 2% of wake data points from the BMSC experiments were replaced. The cleaned velocity time series were used to calculate the mean streamwise velocity and TKE and to analyze the effects of blockage on channel energetics. Profiles of the mean streamwise velocity were calculated as the time average of the streamwise velocity component at each wake measurement location. Similarly, the TKE was calculated at each measurement location as

$$\text{TKE} = \frac{1}{2}[\langle(u - \langle u\rangle)^2\rangle + \langle(v - \langle v\rangle)^2\rangle + \langle(w - \langle w\rangle)^2\rangle]. \tag{6.2}$$

As described in Section 6.1, the influence of blockage on channel energetics can be quantified by the basin efficiency, which requires an estimate of viscous dissipation in the wake. Assuming channel boundary friction is negligible, quantifying the basin efficiency requires either measurements of the energy extracted by the turbine and the total viscous dissipation or measurements of the energy extracted by the turbine and the total mechanical energy upstream of the turbine and at a point downstream where the core and bypass flows have fully remixed. In the latter case, viscous dissipation is the difference between the upstream and downstream mechanical energy, less the energy extracted by the turbine [70]. Because the measurement grids did not extend over the entire wake region, the total viscous dissipation could not be calculated. However, the rate of viscous dissipation was estimated at each

wake measurement location according to a theory developed by Kolmogorov that gives the frequency spectrum ($S(f)$) in the inertial subrange as

$$S(f) = \alpha \varepsilon^{2/3} f^{-5/3} \left(\frac{\langle u \rangle}{2\pi} \right)^{2/3}, \tag{6.3}$$

where α is a constant, ε is the rate of viscous dissipation of TKE per unit mass, f is the range of frequencies in the inertial subrange, and $\langle u \rangle$ is the mean streamwise velocity at the point of interest. Because turbulence is isotropic in the inertial subrange, the spectra of the vertical component, which has the least Doppler uncertainty, was used for analysis. The constant α is equal to 0.69 for the vertical spectrum [10, 35]. To estimate ε, each vertical velocity spectrum was multiplied by $f^{5/3}$ to obtain a compensated spectrum with a zero slope in the frequency band corresponding to the inertial subrange. A sliding, windowed polynomial fit was used to identify the frequency range with the minimum absolute slope. Over this frequency range, the rate of viscous dissipation was calculated as

$$\varepsilon = \frac{2\pi}{\langle u \rangle} \left[\frac{\langle f^{5/3} S(f) \rangle}{\alpha} \right]^{3/2}. \tag{6.4}$$

The mean streamwise velocity, TKE, and viscous dissipation rate were interpolated onto a regular grid with 0.001 m resolution within the measurement extent of each wake profile using biharmonic spline interpolation. Interpolated TKE profiles were used to define the wake region for both blockage ratios. Because the core and bypass flows have different bulk velocities, a shear layer develops between them, and mixing begins immediately downstream of the turbine. This shear layer outlines the wake and has a high TKE compared to other areas in the flow. Therefore, a trace of the maximum TKE at each downstream position was used to estimate the size and shape of the wake. Although other methods to estimate the wake size exist, such as choosing a velocity threshold to distinguish between the core and bypass flows, we found the maximum TKE to be more robust.

6.3 Results

The power and thrust coefficients at both blockage ratios are plotted in Figure 6.2 as functions of tip-speed ratio. The performance effects of blockage are consistent with prior investiga-

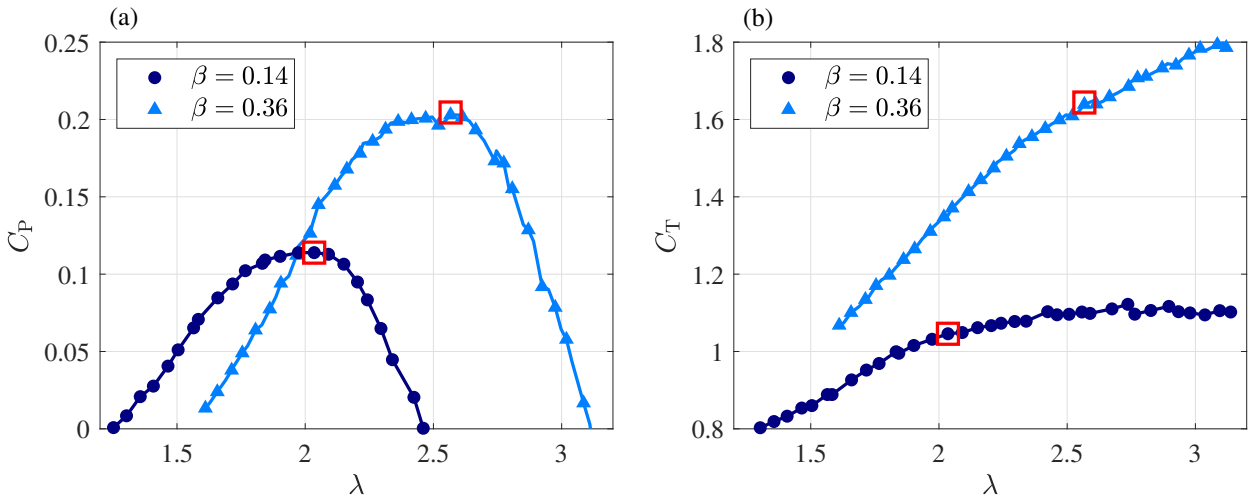

Figure 6.2: Turbine power (a) and thrust (b) coefficients as functions of tip-speed ratio for both blockage ratios. The squares denote peak C_P and the corresponding C_T.

tions [23]. Increasing the blockage ratio from 0.14 to 0.36 resulted in a higher peak C_P at correspondingly higher C_T and λ (red squares in Figure 6.2). Net power is produced over a wider range of tip-speed ratios at higher blockage. Wake data were collected at the tip-speed ratios corresponding to maximum C_P: 2.0 at the lower blockage ratio and 2.6 at the higher blockage ratio.

The interpolated mean streamwise velocity profiles, normalized by the free-stream velocity, are presented in Figure 6.3. The colormap is scaled such that white indicates that the flow speed is equal to the free-stream velocity, blue indicates that the flow is slower than the free-stream, and red indicates that the flow is faster than the free-stream. Although this colormap outlines the slower moving regions of flow, the outlines do not necessarily correspond to the edges of the wake, which are more robustly detected by TKE. The bulk structure of the wake is similar between the two blockage cases, and significant wake recovery is observed in the vertical direction (i.e., reduced vertical extent of the core flow at increasing X/D). In absolute terms, the velocity increases over the entire rotor plane as the blockage

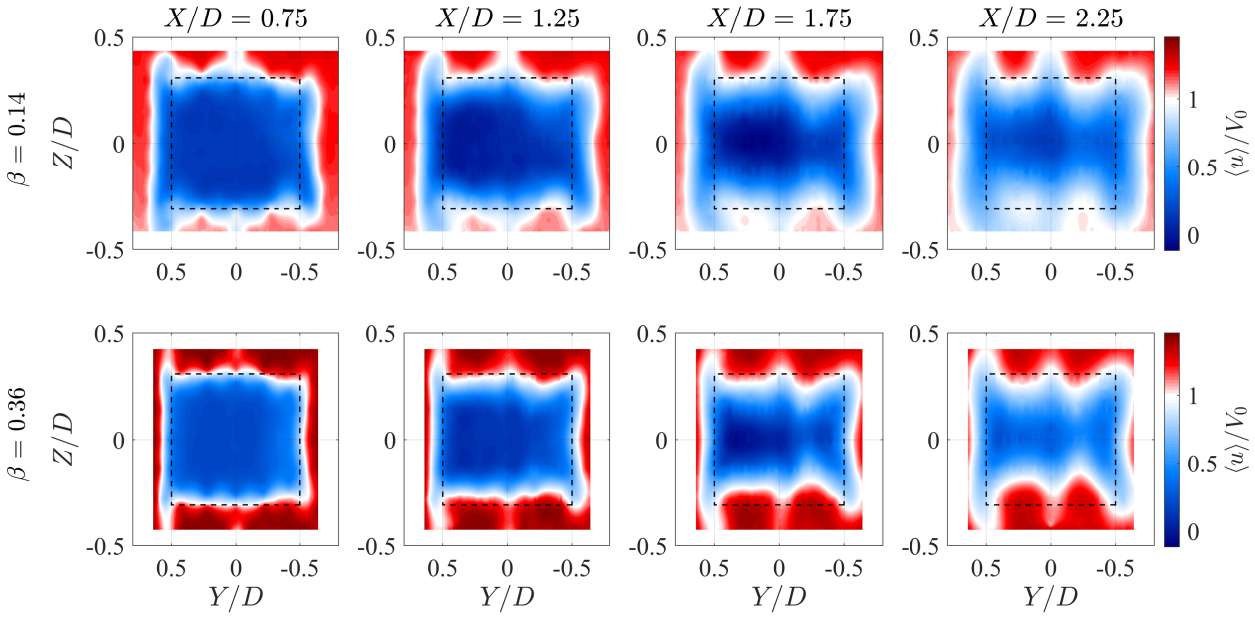

Figure 6.3: Mean streamwise velocity profiles normalized by the free-stream velocity for both blockage ratios. The upper row is the lower blockage case and the lower row the higher blockage case. The leftmost column presents the profile closest to the turbine and the rightmost column the furthest downstream. The dashed black rectangles represent the projection of the turbine location in the streamwise direction.

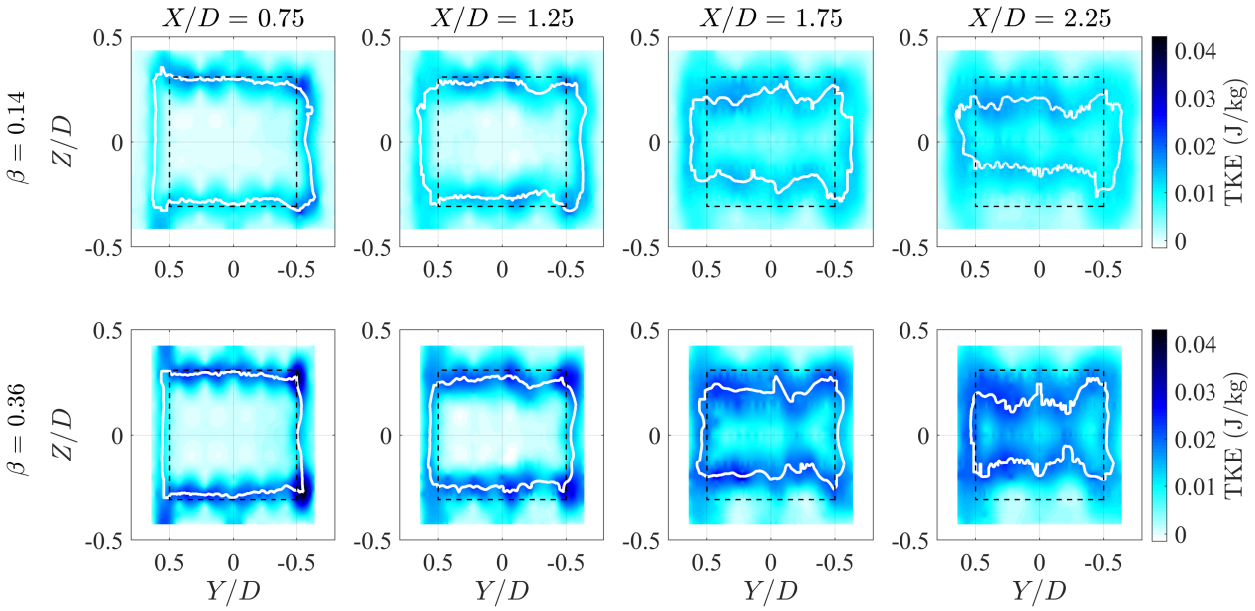

Figure 6.4: TKE profiles for both blockage ratios. The upper row is the lower blockage case and the lower row the higher blockage case. The leftmost column presents the profile closest to the turbine and the rightmost column the furthest downstream. The solid white lines denote the wake extent. The dashed black rectangles represent the projection of the turbine location in the streamwise direction.

ratio is increased. We note that the plot boundaries do not represent the flume walls or free surface and, due to experimental constraints, it was not possible to measure the entire flume cross-section at either blockage ratio.

The equivalent TKE profiles are given in Figure 6.4. The white line overlaying each TKE profile defines the edge of the wake, as identified by a trace of the maximum TKE, and demarcates the core flow from the bypass flow. At both blockage ratios, close to the turbine, the TKE remains relatively low near the center and edges of the measurement region, with a sharp increase in TKE at the shear layer. Further downstream, the shear layer becomes less defined, and the TKE near the center and edges of the profiles increases. There is a pronounced increase in the magnitude of TKE in the shear layer at the higher blockage ratio,

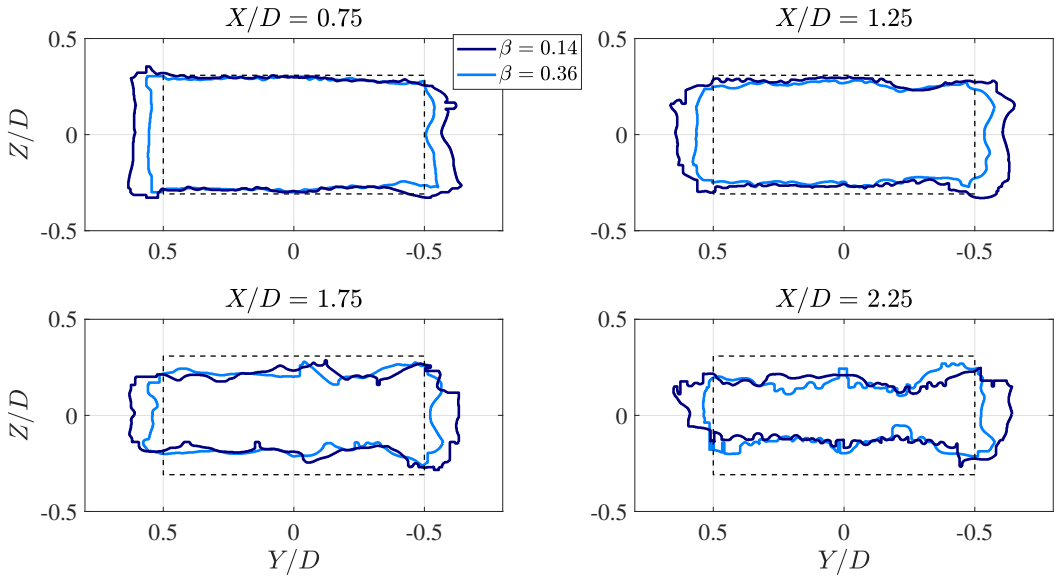

Figure 6.5: Wake extent at both blockage ratios. The darker blue outline corresponds to the lower blockage case and the lighter blue outline to the higher blockage. The dashed black rectangles represent the projection of the turbine location in the streamwise direction.

but the magnitude of TKE outside of the shear layer (i.e., elsewhere within the core and bypass flows) is similar.

The wake extent at both blockage ratios for each downstream position is compared in Figure 6.5. At both blockage ratios, the wake contracts significantly in the vertical direction as the core and bypass flows begin to mix but maintains an approximately constant width. At each downstream position, the wake is smaller for the higher blockage case, but the size difference is primarily observed in the lateral direction, and the vertical extent is relatively independent of blockage.

The viscous dissipation rate is presented in Figure 6.6. The black lines denote the wake extent and are shown for reference. Like the TKE, the dissipation rate is highest in the shear layer at $X/D = 0.75$ and $X/D = 1.25$, but is fairly uniform across the measurement region at $X/D = 1.75$ and $X/D = 2.25$. The magnitude of the dissipation rate increases

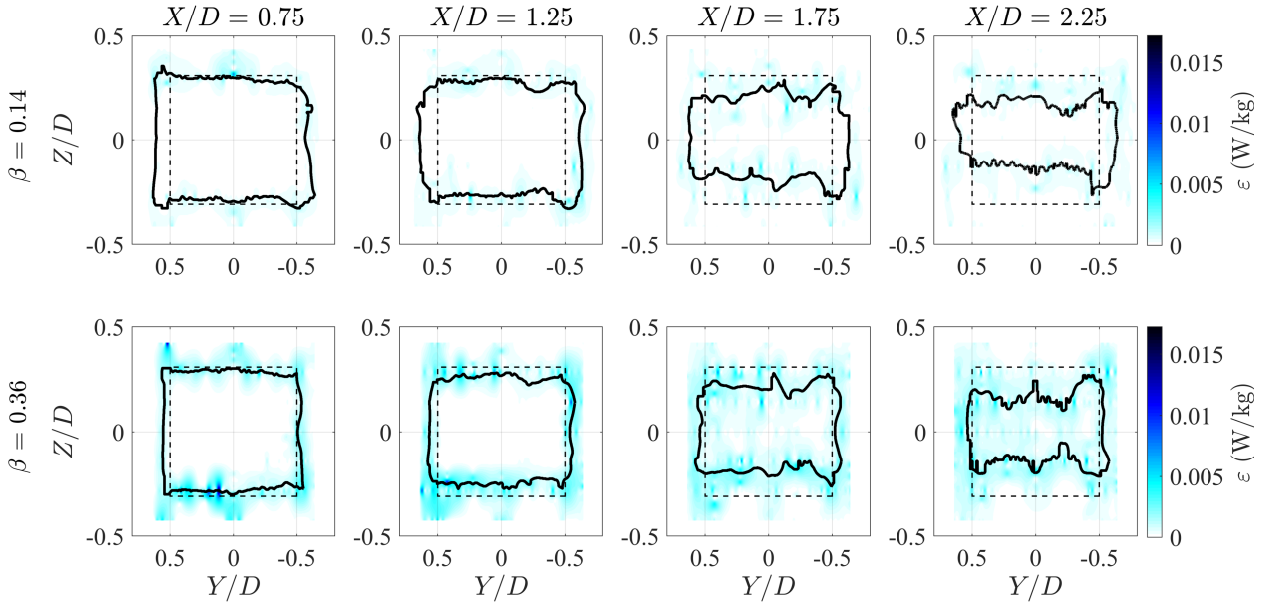

Figure 6.6: Viscous dissipation profiles for both blockage ratios. The upper row is the lower blockage case and the lower row the higher blockage case. The leftmost column presents the profile closest to the turbine and the rightmost column the furthest downstream. The solid black lines denote the wake extent. The dashed black rectangles represent the projection of the turbine location in the streamwise direction.

with blockage. Closer to the turbine, this increase occurs primarily in the shear layer, while at further downstream positions, the dissipation rate increases throughout the measurement region.

6.4 Discussion

6.4.1 Influence of Thrust on Blockage Effects

As discussed in Section 6.1, the effects of blockage on a turbine's wake are determined by the blockage ratio and how significantly the turbine's thrust changes with blockage. Under most operating conditions, including those considered in this study, the thrust and bypass flow speed increase as blockage increases. For a given change in blockage, smaller increases in thrust allow more fluid to pass through the rotor, decreasing the relative velocity between the core and bypass flows and the associated losses due to viscous dissipation [23, 37, 70]. Larger increases in thrust cause more fluid to be diverted around the rotor, increasing the relative velocity between the core and bypass flows and the associated losses due to viscous dissipation [30, 37, 70]. Typically, smaller increases in thrust correspond to a higher basin efficiency and larger increases in thrust to a reduced basin efficiency [23, 37]. However, because basin efficiency also depends on the power extracted by the turbine, the basin efficiency can improve while viscous dissipation losses increase if the turbine power increases by a greater factor.

Changes in a turbine's thrust in response to blockage are affected by its geometry, including the solidity and preset pitch angle, and by its operating point. Prior work for axial-flow turbines demonstrates that if a turbine's geometry and operating point are optimized to extract maximum power from a confined flow, the turbine will have a lower basin efficiency as blockage increases [30, 37, 70]. However, if a turbine's geometry does not change, and the tip-speed ratio is either maintained or optimized for power, the turbine will have a higher basin efficiency as blockage increases [23, 37, 70]. Furthermore, the size of the wake should decrease with increasing blockage [23, 48, 69]. In this study, we used a fixed geometry tur-

bine that was operated at the tip-speed ratio corresponding to peak power for each blockage ratio. Based on prior work, we would expect increasing blockage to reduce the wake extent, increase flow speeds in the core and bypass regions, reduce the mechanical energy lost to viscous dissipation, and improve the basin efficiency. At the higher blockage ratio, we do observe a decreased wake extent and increased flow speeds in both the core and bypass flows. Estimates of the mechanical energy lost to viscous dissipation and the basin efficiency could not be calculated from the measurements. However, we observed that the viscous dissipation rate increased with blockage, consistent with the observed higher relative velocity between the mean core and bypass flows and increased shear. The higher relative velocity, shear, and dissipation rate suggest that the mechanical energy lost to viscous dissipation likely increased with blockage as well. The increase in viscous dissipation rate and likely increase in dissipation losses are not consistent with past studies with fixed turbine geometry, which observed decreased viscous dissipation losses with increased blockage. However, a direct comparison between our work and prior studies requires a similar thrust response as a function of blockage. Therefore, the results of our experiments do not necessarily contradict past work but rather emphasize the influence of thrust on wake dynamics and channel energetics in confined flow.

6.4.2 Implications for Array Design

Flow Speed and Dissipation Rate

As described in Section 6.1 and shown here experimentally, blockage can significantly augment turbine performance, and multiple studies have investigated optimal layouts for arrays of current turbines [17, 18, 22, 24, 26, 30, 36, 44, 45, 55, 56, 58, 70, 77, 78, 80]. For an array with a fixed number of identical turbines, arranging the turbines in a single row produces more power any other layout [26]. However, if this layout is precluded by spatial constraints, turbines are often arranged in multiple rows, such that downstream turbines can be operating in the wake of upstream turbines. In general, placing a second row of tur-

bines directly behind an upstream row is detrimental to the performance of the downstream turbines because of the reduction in inflow velocity [24, 44, 45, 52]. Increased row spacing reduces these impacts, as the flow has more time to recover before reaching the next set of turbines [45, 52]. Additionally, staggering the second row to place the downstream turbines in the bypass flow can increase performance [22, 24, 26, 45, 52, 77] and reduce streamwise spacing [77]. As demonstrated experimentally here, varying the blockage ratio from 0.14 to 0.36 resulted in an approximately 20% increase in the bypass flow speed. Consequently, the benefits of staggered array layouts are likely to increase with blockage. Additionally, past work has demonstrated that when higher blockage results in greater shear between the core and bypass flows, the wake recovers more rapidly [77]. We observed a higher relative velocity between the core and bypass flows and an increased viscous dissipation rate at the higher blockage ratio, indicating that the wake should recover more rapidly and allow closer streamwise spacing.

Wake Size and Shape

We observed that blockage affects the size and shape of the wake. Increasing the blockage ratio from 0.14 to 0.36 decreased the wake size between 10 and 20% at each downstream measurement position. However, increasing the blockage primarily impacted the lateral extent of the wake, with the vertical extent unaffected by blockage (Figure 6.5). We hypothesize that this could be a consequence of the variation in blockage being obtained solely by a variation in channel width. As described in Section 6.2.1, the water depth was held constant to maintain Froude number. This suggests that lateral and vertical blockage may have independent effects on the extent of a turbine's wake. In other words, changes in the lateral blockage may affect the wake only in the lateral direction and changes in the vertical blockage may affect the wake only in the vertical direction. To our knowledge, this independence has not been observed previously and could be useful for informing array design.

We also observed that wake mixing occurred primarily in the vertical direction, regardless of the blockage ratio. As shown in Figure 6.5, the wake remains relatively unchanged in the

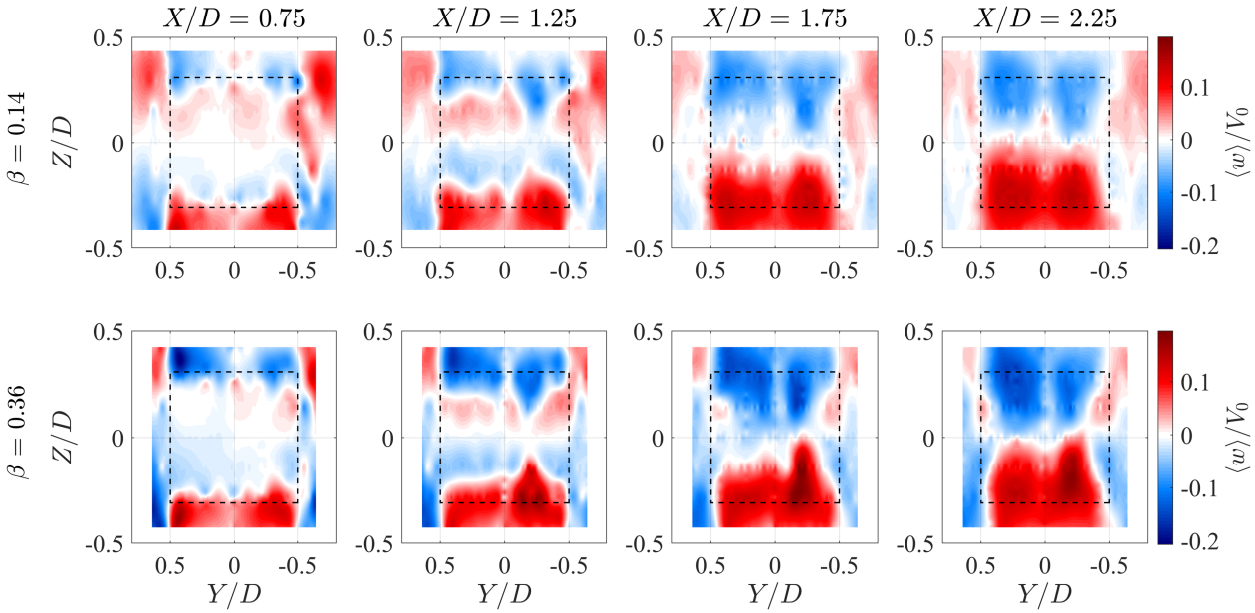

Figure 6.7: Mean vertical (i.e., spanwise) velocity profiles normalized by the free-stream velocity for both blockage ratios. The upper row is the lower blockage case and the lower row the higher blockage case. The leftmost column presents the profile closest to the turbine and the rightmost column the furthest downstream. The dashed black rectangles represent the projection of the turbine location in the streamwise direction.

lateral direction between measurement locations but contracts in the vertical direction at measurement locations further downstream. Relatively strong mixing in one direction has been observed previously in studies of cross-flow turbine wakes and is attributed to tip and dynamic stall vortices shed from the blades that induce flow in the spanwise direction [3, 19, 76, 79]. The mean vertical (i.e., spanwise) velocity profiles, interpolated in the same way as the streamwise velocity profiles and normalized by the free-stream velocity, are presented in Figure 6.7. In this colormap, white indicates a zero velocity, red indicates an upward velocity, and blue indicates a downward velocity. The vertical velocity profiles are roughly symmetrical about the midplane, especially at the further downstream locations. Downward flow from the top and upward flow from the bottom promote mixing of the bypass and

core flows, enabling the wake to recover. Because cross-flow turbines can be oriented either vertically or horizontally, this suggests that faster mixing will not inherently occur in the vertical direction. Rather, the wake will recover more quickly in the direction aligned with the blade span. This has implications for array design, as turbines could be spaced closer together in the direction of more rapid wake recovery.

6.5 Conclusions

Blockage has been shown to increase the power output of current turbines operating in confined flows [23, 25, 30, 31, 34, 37, 41, 54, 69, 70], and this potential for enhanced performance has motivated the design of high blockage arrays [17, 18, 22, 24, 26, 30, 36, 44, 45, 55, 56, 58, 70, 77, 78, 80]. Many array designs involve multiple rows of turbines, with downstream turbines influenced by the wakes of upstream turbines. Therefore, to optimize array layouts in confined flows, it is necessary to understand how blockage affects turbine wakes. We explored this experimentally by characterizing the wake of a cross-flow turbine operating at peak power at two different blockage ratios. To evaluate only the effects of blockage, other parameters that affect turbine performance, such as the Reynolds number, Froude number, and turbulence intensity, were held constant. Increasing the blockage ratio from 0.14 to 0.36 resulted in a higher peak power coefficient that was associated with an increased thrust coefficient and tip-speed ratio. We also observed that increasing the blockage caused higher streamwise flow speeds through and around the turbine, a smaller wake, higher levels of TKE, and an increase in the viscous dissipation rate downstream of the turbine. The increased flow speeds and decreased wake size at higher blockage indicate that increasing blockage could enhance the power output and reduce the physical footprint of an array. However, these benefits should be weighed against the potential disadvantages of removing more mechanical energy from the flow, reducing the basin efficiency. We observed that increasing the blockage ratio only affected the lateral extent of the wake. Because the blockage ratio was increased by changing the flow confinement in the lateral direction only, this suggests lateral and vertical confinement may have independent effects on the wake. Finally, we observed significant

wake mixing only in the vertical (i.e., spanwise) direction at both blockage ratios. Increased mixing in the direction aligned with the blade span has been observed in past work and is attributed to velocities induced by tip and dynamic stall vortices shed from the blades.

Chapter 7

CONCLUSIONS AND FUTURE WORK

7.1 Conclusions

Multiple dimensionless parameters related to the turbine and channel geometry, material properties, and external forces affect the dimensionless performance of current turbines. This work considered three specific parameters: the blockage ratio, Reynolds number, and Froude number, with an emphasis on the blockage ratio. These parameters were the focus of this study because their effects on turbine performance are not fully understood. The emphasis on blockage ratio was motivated by our perception of the most significant gaps in the literature. It can be challenging to achieve full-scale values of these parameters with geometrically scaled models and to hold these parameters constant within experiments. Therefore, our first objective was to better understand the relative effects of each parameter on turbine hydrodynamics and performance to inform experimental design and improve the quality of laboratory-scale testing. Our second objective was to assess the efficacy of analytical models designed to account for the effects of blockage on turbine performance to enable model results to be more accurately extrapolated to larger scales. Furthermore, although scaling effects can present challenges for model testing, they can also provide opportunities to improve turbines performance. Specifically, blockage effects enhance turbine performance and can be used to augment the power output of turbine arrays operating in confined flows. Therefore, the third objective of this work was to characterize the effects of blockage on the wake of a current turbine to inform the design of high blockage arrays.

Chapters 1-3 presented relevant background information and experimental methods used throughout. Chapter 4 focused on the first objective by experimentally characterizing the performance and flow dynamics of a cross-flow current turbine operating under variable block-

age, Reynolds, and Froude conditions. The turbine's baseline power and thrust coefficients were characterized, then each parameter was varied such that the peak power coefficients achieved by increasing only the blockage ratio, Reynolds number, and Froude number were approximately equal. This allowed the relative effects of each parameter to be evaluated, and we concluded that the turbine's power coefficient was most sensitive to changes in the Reynolds number and least sensitive to the Froude number. The free surface deformation across the turbine was also measured, and no significant effects were observed for the baseline, blockage, or Reynolds cases. However, a significant drop in channel depth downstream of the turbine was observed for the Froude case. These results indicate that all three parameters should be closely controlled within experiments to avoid convolving their effects with the hypothesis under consideration (e.g., the effect of turbine geometry on performance). Notably, the Reynolds number was varied by increasing the water temperature, with all other parameters equal to the baseline case. This highlights the sensitivity of Reynolds number to changes in fluid temperature, which is discussed further in Appendix B. Finally, we note that the range of parameters tested in this study was limited by our experimental capabilities, and we expect that larger variations in the parameters will produce more significant performance effects that do not necessarily follow the trends observed in this work, as is the case for changes in characteristic performance at higher blockage ratios.

Chapter 5 focused on experimentally assessing the effectiveness of multiple analytical blockage corrections that have been proposed in the literature. These corrections are intended to account for the effects of blockage on the power and thrust coefficients of current turbines operating in confined flows and are frequently used on data collected at laboratory scales. However, many of the corrections are based on simplified, analytical models, and few have been rigorously validated. This work applied five different blockage corrections to performance data from a cross-flow turbine and an axial-flow turbine operating under highly blocked conditions. The corrected performance curves were compared to data collected under conditions of negligible confinement. To isolate the effects of blockage, the Reynolds and Froude numbers were held approximately constant by testing the same turbines at the

same free-stream velocity and water temperature in facilities of differing size. Of the five corrections tested, the two based on measured thrust performed best and were recommended for future use. These recommendations were made based on the effectiveness of the corrections, in addition to their ease of application and mathematical robustness. Although two corrections outperformed the others, none of the corrections fully accounted for the effects of blockage. This could be due, at least in part, to the fact that the turbines were operated in a Reynolds dependent regime. As the flow speed through the turbines increased with blockage, the local Reynolds number also increased. Therefore, the performance effects of increasing the blockage ratio were likely convolved with some Reynolds effects, which are not accounted for in the analytical theory underlying most blockage corrections. This limitation suggests that blockage corrections may be more effective when applied to data collected in a Reynolds independent regime.

The objective of Chapter 6 was to experimentally characterize the effects of blockage on the wake of a cross-flow current turbine. High blockage arrays of current turbines have the potential to increase power output above that which could be produced by the same number of identical turbines operating in isolation. As most array designs require downstream turbines to operate in the wake of upstream turbines, it is important to understand how blockage affects turbine wake. We concluded that increasing the blockage ratio resulted in higher flow speeds through and around the rotor, increased the turbulent kinetic energy in the shear layer between the core and bypass flows, reduced the overall wake size, and increased the rate of viscous dissipation in the wake. Interestingly, blockage was increased by changing only the width of the channel, and the extent of the wake was reduced only in the lateral direction, indicating that lateral and vertical blockage may have independent effects on wake size. The increased turbulent kinetic energy and viscous dissipation rate suggest that increasing blockage resulted in a greater loss of upstream energy to viscous dissipation. These losses highlight the importance of balancing performance gains with the environmental considerations of extracting more energy from the flow. Furthermore, the fact that these results are not consistent with some prior studies underscores the importance of consider-

ing attendant changes in a turbine's thrust when evaluating blockage effects. Finally, we observed that, regardless of blockage, wake recovery occurred more quickly in the spanwise direction. This recovery was driven by high induced velocities caused by tip and dynamic stall vortices shed from the blades.

7.2 Future Work

The experiments conducted for this work highlighted several potential areas for future research. As discussed in Section 2.3, boundary proximity has been shown to influence turbine performance [41], but its effects are not fully understood. A more detailed discussion of boundary proximity and potential future work related to this topic is given in Appendix A.

Another area of future work related to blockage and boundary proximity is confinement asymmetry, which refers to the ratio of lateral to vertical blockage (or vice versa). As discussed in Section 2.3, prior work [40] concluded that confinement asymmetry affects turbine performance but is negligible for $CA < 3$. However, experimental work on confinement asymmetry is limited and warrants further investigation. Experimentally evaluating confinement asymmetry effects would require holding the overall blockage ratio constant while varying the lateral and vertical blockage ratios. Ideally, confinement asymmetries above and below $CA = 3$ would be investigated in order to compare results to past work. Although possible, this experimental campaign would be complicated, as the relevant geometric parameters, in addition to the overall blockage ratio, Reynolds number, Froude number, and turbulence intensity, would need to be held constant.

An additional topic of future work is related to better understanding the underlying fluid mechanisms that relate changes in the Froude number to turbine performance. In Chapter 4, we demonstrated that the blockage ratio, Reynolds number, and Froude number all affect turbine performance. The mechanisms that cause the blockage ratio and Reynolds number to influence a turbine's power output are fairly well understood. However, our results suggest that each parameter impacts the fluid dynamics differently, and Froude effects have not been explored as thoroughly. Investigating how the Froude number augments turbine performance

could be facilitated by imaging the flow field near the blades to quantify the effects of the Froude number on near-blade hydrodynamics.

A final topic of future work involves developing an improved blockage correction that better accounts for the effects of turbine rotation. In Chapter 5, we concluded that the blockage corrections performed better for the thrust coefficient than for the power coefficient. We hypothesized that this was due, at least in part, to their basis on axial momentum theory, which models the turbine as a stationary, porous plate. Therefore, it assumes that turbine power is the product of the thrust and flow speed through the rotor, which is an idealization that is demonstrably incorrect for real turbines. A blockage correction based on angular momentum theory, which accounts for the rotation of the turbine and the resulting angular induction of the flow, has the potential to better account for blockage effects on the power coefficient.

BIBLIOGRAPHY

[1] D. B. Araya, T. Colonius, and J. O. Dabiri. Transition to bluff-body dynamics in the wake of vertical-axis wind turbines. *Journal of Fluid Mechanics*, 813:346–381, 2017. doi: https://doi.org/10.1017/jfm.2016.862.

[2] P. Bachant and M. Wosnik. Performance measurements of cylindrical- and spherical-helical cross-flow marine hydrokinetic turbines, with estimates of exergy efficiency. *Renewable Energy*, 74:318–325, 2015. doi: https://doi.org/10.1016/j.renene.2014.07.049.

[3] P. Bachant and M. Wosnik. Characterising the near-wake of a cross-flow turbine. *Journal of Turbulence*, 16(4):392–410, 2015. doi: https://doi.org/10.1080/14685248.2014.1001852.

[4] P. Bachant and M. Wosnik. Effects of Reynolds number on the energy conversion and near-wake dynamics of a high solidity vertical-axis cross-flow turbine. *Energies*, 9(2), 2016. doi: https://doi.org/10.3390/en9020073.

[5] P. Bachant, M. Wosnik, B. Gunawan, and V. S. Neary. Experimental study of a reference model vertical-axis cross-flow turbine. *PLoS ONE*, 11(9):e0163799, 2016. doi: https://doi.org/10.1371/journal.pone.0163799.

[6] A. S. Bahaj, A. F. Molland, J. R. Chaplin, and W. M. J. Batten. Power and thrust measurements of marine current turbines under various hydrodynamic flow conditions in a cavitation tunnel and a towing tank. *Renewable Energy*, 32(3):407–426, 2007. doi: https://doi.org/10.1016/j.renene.2006.01.012.

[7] R. B. Barber, C. S. Hill, P. F. Babuska, R. Wiebe, A. Aliseda, and M. R. Motley. Flume-

scale testing of an adaptive pitch marine hydrokinetic turbine. *Composite Structures*, 168:465–473, 2017. doi: https://doi.org/10.1016/j.compstruct.2017.02.051.

[8] M. J. Barnsley and J. F. Wellicome. Final report on the 2nd phase of development and testing of a horizontal axis wind turbine test rig for the investigation of stall regulation aerodynamics. Technical Report E.5A/CON5103/1746, ETSU, 1990.

[9] M. J. Barnsley and J. F. Wellicome. Wind tunnel investigation of stall aerodynamics for a 1.0 m horizontal axis rotor. *Journal of Wind Engineering and Industrial Aerodynamics*, 39(1):11–21, 1992. doi: https://doi.org/10.1016/0167-6105(92)90528-I.

[10] C. Bassett, J. Thomson, and B. Polagye. Sediment-generated noise and bed stress in a tidal channel. *Journal of Geophysical Research: Oceans*, 118(4):2249–2265, 2013. doi: https://doi.org/10.1002/jgrc.20169.

[11] L. Battisti, L. Zanne, S. Dell'Anna, V. Dossena, G. Persico, and B. Paradiso. Aerodynamic measurements of a vertical axis wind turbine in a large scale wind tunnel. *Journal of Energy Resources Technology*, 133:031201–1–031201–9, 2011. doi: https://doi.org/10.1115/1.4004360.

[12] G. Bedon, S. De Betta, and E. Benini. Performance-optimized airfoil for Darrieus wind turbines. *Renewable Energy*, 94:328–340, 2016. doi: https://doi.org/10.1016/j.renene.2016.03.071.

[13] Volker Bertram. Chapter 1 - Introduction. In *Practical Ship Hydrodynamics*, pages 1–39. Butterworth-Heinemann, Oxford, second edition, 2012. doi: https://doi.org/10.1016/B978-0-08-097150-6.10001-6.

[14] A. Betz. Das maximum der theoretisch möglichen ausnützung des windes durch windmotoren. *Zeitschrift für dasgesamte Turbinenwesen*, 26:307–309, 1920.

[15] A. H. Birjandi, E. L. Bibeau, V. Chatoorgoon, and A. Kumar. Power measurement of hydrokinetic turbines with free-surface and blockage effect. *Ocean Engineering*, 69: 9–17, 2013. doi: https://doi.org/10.1016/j.oceaneng.2013.05.023.

[16] T. Blackmore, L. E. Myers, and A. S. Bahaj. Effects of turbulence on tidal turbines: Implications to performance, blade loads, and condition monitoring. *International Journal of Marine Energy*, 14:1–26, 2016. doi: https://doi.org/10.1016/j.ijome.2016.04.017.

[17] P. A. J. Bonar, T. A. A. Adcock, V. Venugopal, and A. G. L. Borthwick. Performance of non-uniform tidal turbine arrays in uniform flow. *Journal of Ocean Engineering and Marine Energy*, 4:231–241, 2018. doi: https://doi.org/10.1007/s40722-018-0118-x.

[18] P. A. J. Bonar, L. Chen, A. M. Schnabl, V. Venugopal, A. G. L. Borthwick, and T. A. A. Adcock. On the arrangement of tidal turbines in rough and oscillatory channel flow. *Journal of Fluid Mechanics*, 865:790–810, 2019. doi: https://doi.org/10.1017/jfm.2019.68.

[19] M. Boudreau and G. Dumas. Comparison of the wake recovery of the axial-flow and cross-flow turbine concepts. *Journal of Wind Engineering and Industrial Aerodynamics*, 165:137–152, 2017. doi: https://doi.org/10.1016/j.jweia.2017.03.010.

[20] S. Brusca, R. Lanzafame, and M. Messina. Design of a vertical-axis wind turbine: How the aspect ratio affects the turbine's performance. *International Journal of Energy and Environmental Engineering*, 5:333–340, 2014. doi: https://doi.org/10.1007/s40095-014-0129-x.

[21] L. P. Chamorro, R. E. A. Arndt, and F. Sotiropoulos. Reynolds number dependence of turbulence statistics in the wake of wind turbines. *Wind Energy*, 15(5):733–742, 2012. doi: https://doi.org/10.1002/we.501.

[22] M. J. Churchfield, Y. Li, and P. J. Moriarty. A large-eddy simulation study of wake propagation and power production in an array of tidal-current turbines. *Philosophical*

Transactions of the Royal Society A: Mathematical, Physical and Engineering Sciences, 371(1985):20120421, 2013. doi: https://doi.org/10.1098/rsta.2012.0421.

[23] C. A. Consul, R. H. J. Willden, and S. C. McIntosh. Blockage effects on the hydrodynamic performance of a marine cross-flow turbine. *Philosophical Transactions of the Royal Society A: Mathematical, Physical and Engineering Sciences*, 371(1985):20120299, 2013. doi: https://doi.org/10.1098/rsta.2012.0299.

[24] T. Divett, R. Vennell, and C. Stevens. Optimization of multiple turbine arrays in a channel with tidally reversing flow by numerical modelling with adaptive mesh. *Philosophical Transactions of the Royal Society A: Mathematical, Physical and Engineering Sciences*, 371(1985):20120251, 2013. doi: https://doi.org/10.1098/rsta.2012.0251.

[25] V. Dossena, G. Persico, B. Paradiso, L. Battisti, S. Dell'Anna, A. Brighenti, and B. Enrico. An experimental study of the aerodynamics and performance of a vertical axis wind turbine in a confined and unconfined environment. *Journal of Energy Resources Technology*, 137:051207–1–051207–12, 2015. doi: https://doi.org/10.1115/1.4030448.

[26] S. Draper and T. Nishino. Centred and staggered arrangements of tidal turbines. *Journal of Fluid Mechanics*, 739:72–93, 2014. doi: https://doi.org/10.1017/jfm.2013.593.

[27] M. El-Samanoudy, A. A. E. Ghorab, and Sh. Z. Youssef. Effect of some design parameters on the performance of a Giromill vertical axis wind turbine. *Ain Shams Engineering Journal*, 1(1):85–95, 2010. doi: https://doi.org/10.1016/j.asej.2010.09.012.

[28] C. S. Ferreira and B. Geurts. Aerofoil optimization for vertical-axis wind turbines. *Wind Energy*, 18(8):1371–1385, 2015. doi: https://doi.org/10.1002/we.1762.

[29] P. W. Galloway, L. E. Myers, and A. S. Bahaj. Quantifying wave and yaw effects on a scale tidal stream turbine. *Renewable Energy*, 63:297–307, 2014. doi: https://doi.org/10.1016/j.renene.2013.09.030.

[30] C. Garrett and P. Cummins. The efficiency of a turbine in a tidal channel. *Journal of Fluid Mechanics*, 588:243–251, 2007. doi: https://doi.org/10.1017/S0022112007007781.

[31] B. Gaurier, G. Germain, J. V. Facq, C. M. Johnstone, A. D. Grant, A. H. Day, E. Nixon, F. Di Felice, and M. Costanzo. Tidal energy "Round Robin" tests comparisons between towing tank and circulating tank results. *International Journal of Marine Energy*, 12: 87–109, 2015. doi: https://doi.org/10.1016/j.ijome.2015.05.005.

[32] H. Glauert. Airplane propellers. In William Frederick Durand, editor, *Aerodynamic Theory: A General Review of Progress Under a Grant of the Guggenheim Fund for the Promotion of Aeronautics*, volume 4, chapter L, pages 169–360. Springer, Berlin, 1935.

[33] D. G. Goring and V. I. Nikora. Despiking acoustic Doppler velocimeter data. *Journal of Hydraulic Engineering*, 128(1):117–126, 2002. doi: https://doi.org/10.1061/(ASCE)0733-9429(2002)128:1(117).

[34] A. Goude and O. Ågren. Simulations of a vertical axis turbine in a channel. *Renewable Energy*, 63:477–485, 2014. doi: https://doi.org/10.1016/j.renene.2013.09.038.

[35] M. Guerra, R. Cienfuegos, J. Thomson, and L. Suarez. Tidal energy resource characterization in Chacao Channel, Chile. *International Journal of Marine Energy*, 20:1–16, 2017. doi: https://doi.org/10.1016/j.ijome.2017.11.002.

[36] V. Gupta and A. M. Young. A one-dimensional model for tidal array design based on three-scale dynamics. *Journal of Fluid Mechanics*, 825:651–676, 2017. doi: https://doi.org/10.1017/jfm.2017.399.

[37] G. T. Houlsby and C. R. Vogel. The power available to tidal turbines in an open channel flow. *Proceedings of the Institution of Civil Engineers - Energy*, 170(1):12–21, 2017. doi: https://doi.org/10.1680/jener.15.00035.

[38] G. T. Houlsby, S. Draper, and M. L. G. Oldfield. Applicaton of linear momentum actuator disc theory to open channel flow. Technical Report OUEL 2296/08, University of Oxford, 2008.

[39] A. Hunt, C. Stringer, and B. Polagye. Effect of aspect ratio on cross-flow turbine performance. In preparation, 2020.

[40] T. Kinsey and G. Dumas. Impact of channel blockage on the performance of axial and cross-flow hydrokinetic turbines. *Renewable Energy*, 103:239–254, 2017. doi: https://doi.org/10.1016/j.renene.2016.11.021.

[41] N. Kolekar and A. Banerjee. Performance characterization and placement of a marine hydrokinetic turbine in a tidal channel under boundary proximity and blockage effects. *Applied Energy*, 148:121–133, 2015. doi: https://doi.org/10.1016/j.apenergy.2015.03.052.

[42] F. W. Lanchester. A contribution to the theory of propulsion and the screw propeller. *Journal of the American Society for Naval Engineers*, 27(2):509–510, 1915. doi: https://doi.org/10.1111/j.1559-3584.1915.tb00408.x.

[43] N. D. Laws and B. P. Epps. Hydrokinetic energy conversion: Technology, research, and outlook. *Renewable and Sustainable Energy Reviews*, 57:1245–1259, 2016. doi: https://doi.org/10.1016/j.rser.2015.12.189.

[44] S. H. Lee, S. H. Lee, K. Jang, J. Lee, and N. Hur. A numerical study for the optimal arrangement of ocean current turbine generators in the ocean current power parks. *Current Applied Physics*, 10(2, Supplement):S137–S141, 2010. doi: https://doi.org/10.1016/j.cap.2009.11.018.

[45] R. Malki, I. Masters, A. J. Williams, and T. N. Croft. Planning tidal stream turbine array layouts using a coupled blade element momentum – computational fluid dynamics model. *Renewable Energy*, 63:46–54, 2014. doi: https://doi.org/10.1016/j.renene.2013.08.039.

[46] E. C. Maskell. *A Theory of the Blockage Effects on Bluff Bodies and Stalled Wings in a Closed Wind Tunnel*. HMSO, London, 1963.

[47] R. A. McAdam, G. T. Houlsby, and M. L. G. Oldfield. Experimental measurements of the hydrodynamic performance and structural loading of the Transverse Horizontal Axis Water Turbine: Part 1. *Renewable Energy*, 59:105–114, 2013. doi: https://doi.org/10.1016/j.renene.2013.03.016.

[48] S. McTavish, D. Feszty, and F. Nitzsche. An experimental and computational assessment of blockage effects on wind turbine wake development. *Wind Energy*, 17(10):1515–1529, 2014. doi: https://doi.org/10.1002/we.1648.

[49] R. Mikkelsen and J. N. Sørensen. Modelling of wind tunnel blockage. In *Global Windpower Conference*, Paris, France, 2002.

[50] M. A. Miller, S. Duvvuri, I. Brownstein, M. Lee, J. O. Dabiri, and M. Hultmark. Vertical-axis wind turbine experiments at full dynamic similarity. *Journal of Fluid Mechanics*, 844:707–720, 2018. doi: https://doi.org/10.1017/jfm.2018.197.

[51] B. R. Munson, D. F. Young, T. H. Okiishi, and W. W. Huebsch. *Fundamentals of Fluid Mechanics*. John Wiley & Sons, Hoboken, N. J., sixth edition, 2009.

[52] P. Mycek, B. Gaurier, G. Germain, G. Pinon, and E. Rivoalen. Numerical and experimental study of the interaction between two marine current turbines. *International Journal of Marine Energy*, 1:70–83, 2013. doi: https://doi.org/10.1016/j.ijome.2013.05.007.

[53] P. Mycek, B. Gaurier, G. Germain, G. Pinon, and E. Rivoalen. Experimental study of the turbulence intensity effects on marine current turbines behaviour. Part I: One single turbine. *Renewable Energy*, 66:729–746, 2014. doi: https://doi.org/10.1016/j.renene.2013.12.036.

[54] T. Nishino and R. H. J. Willden. Effects of 3-D channel blockage and turbulent wake mixing on the limit of power extraction by tidal turbines.

International Journal of Heat and Fluid Flow, 37:123–135, 2012. doi: https://doi.org/10.1016/j.ijheatfluidflow.2012.05.002.

[55] T. Nishino and R. H. J. Willden. The efficiency of an array of tidal turbines partially blocking a wide channel. *Journal of Fluid Mechanics*, 708:596–606, 2012. doi: https://doi.org/10.1017/jfm.2012.349.

[56] T. Nishino and R. H. J. Willden. Two-scale dynamics of flow past a partial cross-stream array of tidal turbines. *Journal of Fluid Mechanics*, 730:220–244, 2013. doi: https://doi.org/10.1017/jfm.2013.340.

[57] C. M. Parker, D. B. Araya, and M. C. Leftwich. Effect of chord-to-diameter ratio on vertical-axis wind turbine wake development. *Experiments in Fluids*, 58(168), 2017. doi: https://doi.org/10.1007/s00348-017-2451-6.

[58] A. Phoenix and S. Nash. Optimisation of tidal turbine array layouts whilst limiting their hydro-environmental impact. *Journal of Ocean Engineering and Marine Energy*, 5:251–266, 2019. doi: https://doi.org/10.1007/s40722-019-00145-8.

[59] B. Polagye, B. Strom, H. Ross, D. Forbush, and R. J. Cavagnaro. Comparison of cross-flow turbine performance under torque-regulated and speed-regulated control. *Journal of Renewable and Sustainable Energy*, 11(4):044501, 2019. doi: https://doi.org/10.1063/1.5087476.

[60] A. Pope and J. J. Harper. *Low-Speed Wind Tunnel Testing*. John Wiley & Sons, New York, 1966.

[61] A. Rezaeiha, I. Kalkman, and B. Blocken. Effect of pitch angle on power performance and aerodynamics of a vertical axis wind turbine. *Applied Energy*, 197:132–150, 2017. doi: https://doi.org/10.1016/j.apenergy.2017.03.128.

[62] H. Ross and B. Polagye. An experimental assessment of analytical blockage corrections for turbines. *Renewable Energy*, 152:1328–1341, 2020. doi: https://doi.org/10.1016/j.renene.2020.01.135.

[63] H. Ross and B. Polagye. Scaling effects on the performance of a cross-flow current turbine. In preparation, 2020.

[64] H. Ross and B. Polagye. An experimental evaluation of blockage effects on the wake of a cross-flow current turbine. *Journal of Ocean Engineering and Marine Energy*, 2020. In review.

[65] I. Ross and A. Altman. Wind tunnel blockage corrections: Review and application to Savonius vertical-axis wind turbines. *Journal of Wind Engineering and Industrial Aerodynamics*, 99(5):523–538, 2011. doi: https://doi.org/10.1016/j.jweia.2011.02.002.

[66] P. J. Rusello. A practical primer for pulse coherent instruments. Technical Report TN-027, NortekUSA, 2009.

[67] J. Ryi, W. Rhee, U. C. Hwang, and J.-S. Choi. Blockage effect correction for a scaled wind turbine rotor by using wind tunnel test data. *Renewable Energy*, 79:227–235, 2015. doi: https://doi.org/10.1016/j.renene.2014.11.057.

[68] A. Sagharichi, M. Zamani, and A. Ghasemi. Effect of solidity on the performance of variable-pitch vertical axis wind turbine. *Energy*, 161:753–775, 2018. doi: https://doi.org/10.1016/j.energy.2018.07.160.

[69] H. Sarlak, T. Nishino, L. A. Martínez-Tossas, C. Meneveau, and J. N. Sørensen. Assessment of blockage effects on the wake characteristics and power of wind turbines. *Renewable Energy*, 93:340–352, 2016. doi: https://doi.org/10.1016/j.renene.2016.01.101.

[70] J. Schluntz and R. H. J. Willden. The effect of blockage on tidal turbine rotor design and performance. *Renewable Energy*, 81:432–441, 2015. doi: https://doi.org/10.1016/j.renene.2015.02.050.

[71] A. Segalini and P. Inghels. Confinement effects in wind-turbine and propeller measurements. *Journal of Fluid Mechanics*, 756:110–129, 2014. doi: https://doi.org/10.1017/jfm.2014.440.

[72] P. Stansby and T. Stallard. Fast optimisation of tidal stream turbine positions for power generation in small arrays with low blockage based on superposition of self-similar far-wake velocity deficit profiles. *Renewable Energy*, 92:366–375, 2016. doi: https://doi.org/10.1016/j.renene.2016.02.019.

[73] B. Strom. *Cross-flow turbine fluid mechanics: Experimental optimization and analysis*. PhD thesis, University of Washington, 2019.

[74] B. Strom, S. Brunton, and B. Polagye. Consequences of preset pitch angle on cross-flow turbine hydrodynamics. In *Proceedings of the 11th European Wave and Tidal Energy Conference*, Nantes, France, 2015.

[75] B. Strom, N. Johnson, and B. Polagye. Impact of blade mounting structures on cross-flow turbine performance. *Journal of Renewable and Sustainable Energy*, 10(3):034504, 2018. doi: https://doi.org/10.1063/1.5025322.

[76] G. Tescione, D. Ragni, C. He, C. J. S. Ferreira, and G. J. W. van Bussel. Near wake flow analysis of a vertical axis wind turbine by stereoscopic particle image velocimetry. *Renewable Energy*, 70:47–61, 2014. doi: https://doi.org/10.1016/j.renene.2014.02.042.

[77] S. R. Turnock, A. B. Phillips, J. Banks, and R. Nicholls-Lee. Modelling tidal current turbine wakes using a coupled RANS-BEMT approach as a tool for analysing power capture of arrays of turbines. *Ocean Engineering*, 38(11):1300–1307, 2011. doi: https://doi.org/10.1016/j.oceaneng.2011.05.018.

[78] R. Vennell. Tuning turbines in a tidal channel. *Journal of Fluid Mechanics*, 663:253–267, 2010. doi: https://doi.org/10.1017/S0022112010003502.

[79] T. Villeneuve, M. Boudreau, and G. Dumas. Improving the efficiency and the wake recovery rate of vertical-axis turbines using detached end-plates. *Renewable Energy*, 150:31–45, 2020. doi: https://doi.org/10.1016/j.renene.2019.12.088.

[80] C. R. Vogel, G. T. Houlsby, and R. H. J. Willden. Effect of free surface deformation on the extractable power of a finite width turbine array. *Renewable Energy*, 88:317–324, 2016. doi: https://doi.org/10.1016/j.renene.2015.11.050.

[81] M. J. Werle. Wind turbine wall-blockage performance corrections. *Journal of Propulsion and Power*, 26(6):1317–1321, 2010. doi: https://doi.org/10.2514/1.44602.

[82] M. J. Werle and Jr. Presz, W. M. Shroud and ejector augmenters for subsonic propulsion and power systems. *Journal of Propulsion and Power*, 25(1):228–236, 2009. doi: https://doi.org/10.2514/1.36042.

[83] J. I. Whelan, J. M. R. Graham, and J. Peiró. A free-surface and blockage correction for tidal turbines. *Journal of Fluid Mechanics*, 624:281–291, 2009. doi: https://doi.org/10.1017/S0022112009005916.

[84] R. M. K. Wood and R. G. Harris. *Some Notes on the Theory of an Airscrew Working in a Wind Channel*. HMSO, London, 1921.

Appendix A
BOUNDARY PROXIMITY EFFECTS

An additional parameter that affects turbine performance is boundary proximity. Changing the blockage ratio requires varying the size of the channel relative to the size of the turbine rotor, so the blockage ratio and boundary proximity are fundamentally related. In other words, it is not possible to change the blockage ratio without changing the actual distance between the turbine and channel boundaries. However, the boundary proximity can be varied while maintaining a constant blockage ratio by moving the turbine closer to one of the channel boundaries. Furthermore, because the lateral and bottom boundaries are solid walls and the top boundary is typically a deformable free surface, lateral and vertical boundary proximity likely affect turbine performance differently and are discussed separately in the following sections. Note that these discussions are relevant to both cross-flow and axial-flow turbines. However, as mentioned in Section 2.1, we assume a vertically oriented cross-flow turbine, and boundary proximity effects would likely change for a horizontally oriented cross-flow turbine.

A.1 Lateral Boundary Proximity

Lateral boundary proximity refers to the minimum distance between a turbine and channel side wall. As mentioned previously, changing the lateral blockage ratio requires changing the boundary proximity. In all of the experiments conducted for this work, the turbine was centered between the side walls. However, a turbine can be moved closer to one wall, varying the boundary proximity while holding the blockage ratio constant. It is not immediately apparent what the appropriate non-dimensionalization is for this variable. The lateral boundary proximity could be taken as the distance between a side wall and the turbine's axis

of rotation or the distance between a side wall and the closest point on the circle swept by the turbine's rotor. Furthermore, this value could be non-dimensionalized by the diameter of the turbine or by the width of the channel. However, the only choice of variables that allows the dimensionless lateral boundary proximity of a centered turbine to remain unchanged while the lateral blockage ratio varies is the distance between a side wall and the turbine's axis of rotation divided by the width of the channel, i.e., d_ℓ/b. Given this parameterization, the dimensionless lateral boundary proximity was 0.5 for every experiment described in this work.

A.2 Vertical Boundary Proximity

Because the top boundary of an open channel flow is a deformable free surface, vertical boundary proximity is distinct from lateral boundary proximity and has been shown to affect performance, even when the blockage ratio and Froude number are held constant [41]. We will refer to the vertical boundary proximity as the distance between the turbine and free surface. As for the lateral case, this could be defined as the distance between the free surface and the midpoint of the blade span or the distance between the free surface and the top of the rotor. This could be non-dimensionalized by the turbine height, turbine diameter, or free-stream channel depth. As for the lateral case, the only parameterization that allows the dimensionless vertical boundary proximity of a centered turbine to remain unchanged while the vertical blockage ratio varies is the distance between the free surface and the midpoint of the blade span divided by the free-stream channel depth, i.e., d_t/d_0. Given this definition, the dimensionless vertical boundary proximity was not held constant during the experiments described in Chapter 5. For experiments at UW and BMSC, the turbine was centered vertically in the channel. However, because the UNH tow tank is several meters deep, it was not possible to vertically center the turbine due to the cantilever distance between turbine and servomotor. Instead, the absolute distance between the free surface and the top of the rotor was held constant between experiments. Notably, non-dimensionalizing the vertical boundary proximity as the distance between the free surface and the center of the blade

span divided by the free-stream channel depth may not capture all of the relevant physics, as a turbine's diameter may affect free surface deformation. The influence of both lateral and vertical boundary proximity, and the proper dimensionless parameters to capture these effects, remain topics worthy of future investigation.

Appendix B

REYNOLDS DEPENDENCE ON TEMPERATURE

As discussed in Sections 2.2, 4.2.1, and 7.1, the Reynolds number and turbine performance are sensitive to changes in the fluid temperature, which affects viscosity. This sensitivity is particularly acute in water, as the viscosity changes rapidly with temperature between approximately 10 and 30°C, the typical operating range for laboratory facilities. The kinematic viscosity of water as a function of temperature is illustrated in Figure B.1, with the typical experimental temperature range highlighted in red.

If a turbine is operating in a Reynolds dependent regime, performance can vary with small changes in water temperature. Figure B.2 shows the power coefficient of a cross-flow turbine that was operated continuously in the BMSC flume over a period of multiple hours during the collection of wake data. The turbine was operating at a chord-based Reynolds number of approximately 23,000. Water temperature in the flume was controlled by a chiller that can hold the temperature to within ±0.5°C of a target. As illustrated by the figure, the target temperature was 10.2°C, and it fluctuated between approximately 9.7 and 10.7°C. Notably, turbine performance visibly tracks the water temperature. Although the performance changes are small, the temperature changes are minimal as well.

The performance effects of water temperature on a larger scale are illustrated by Figure B.3. The left-hand plot shows the power coefficient of a cross-flow current turbine operating at 15°C at two different free-stream velocities. Increasing the free-stream velocity from 0.60 m/s to 0.94 m/s affected the Reynolds number and, to a lesser extent, the Froude number, causing the C_{P} to almost double. The right-hand plot shows the same turbine operating at a free-stream velocity of 0.60 m/s. Here, the water temperature was increased from 15.0°C to 32.9°C. This increase in water temperature affected the turbine's C_{P} almost as much

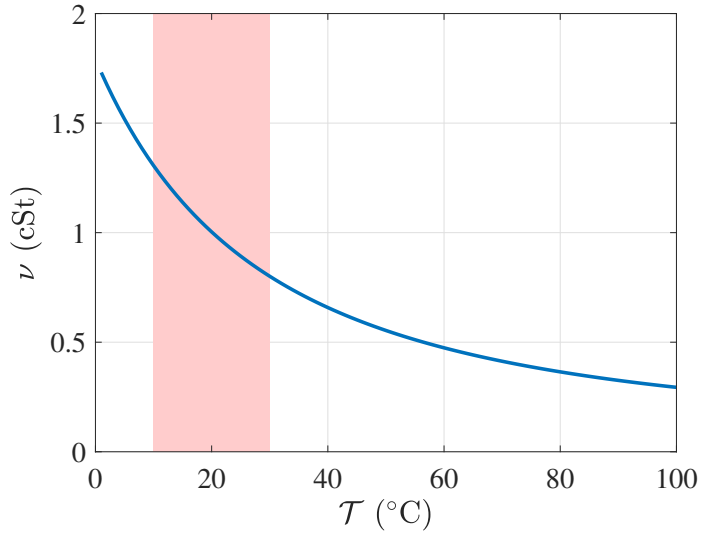

Figure B.1: Kinematic viscosity of water as a function of temperature. The typical temperature range of laboratory facilities is highlighted in red.

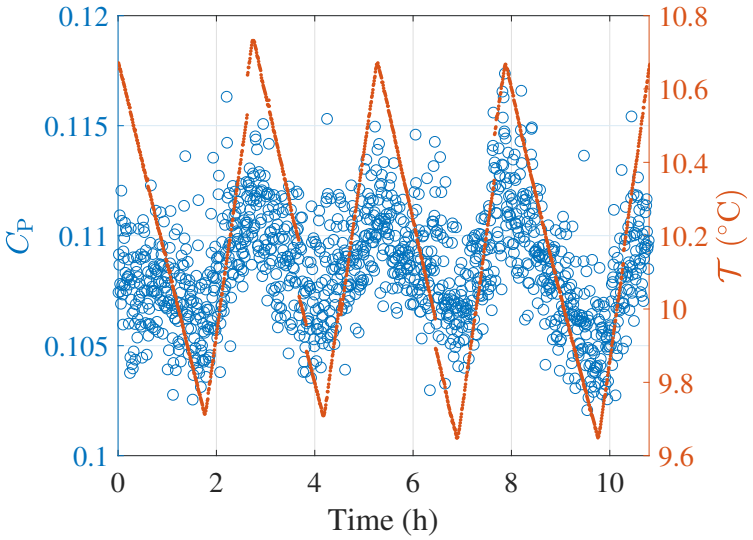

Figure B.2: The power coefficient of a turbine tracking small changes in water temperature.

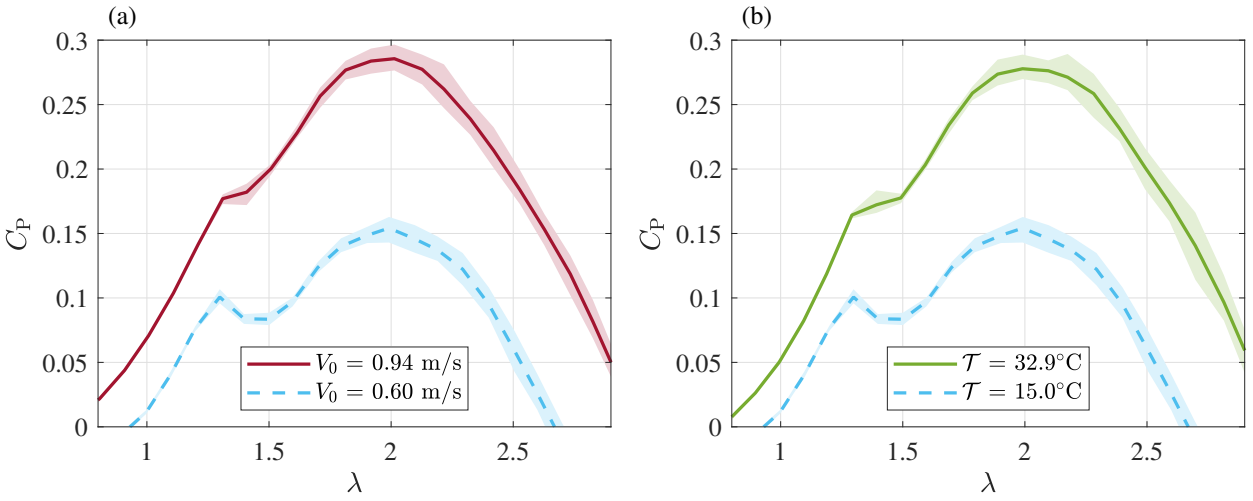

Figure B.3: Power coefficients as functions of tip-speed ratio for a variable free-stream velocity (a) and temperature (b).

as varying the free-stream velocity but, crucially, affected only the Reynolds number. As viscosity does not appear in any other dimensionless parameters, it can be varied without convolving other effects. Furthermore, the ability to increase water temperature gives experimental facilities with a limited range of inflow speeds another method of increasing Reynolds number. While this technique appears infrequently in the recent experimental literature, the construction of "sauna tanks" to increase water temperature to 90°C has been contemplated in the ocean engineering literature [13].

The results presented in this section emphasize the importance of accounting for water temperature when controlling Reynolds number in a laboratory setting. Even small changes in water temperature can significantly affect a turbine's power coefficient and introduce error into performance measurements.